Photobiological studies of a drug delivery system for the treatment of breast and ovarian cancer using 3D *in vitro* models

Layla Mohammad Hadi

A thesis submitted to University College London in fulfilment of the degree of Doctor of Philosophy (PhD)

2018

Division of Surgery and Interventional Science
University College London, UCL

Declaration

I, Layla Mohammad Hadi, certify that the work presented in this thesis is my own. Where information has been derived from other sources, I confirm that this has been indicated in the thesis.

Abstract

Photochemical internalisation (PCI) is a method for enhancing delivery of drugs such as cytotoxins to their intracellular target sites of action through the use of low dose photodynamic therapy (PDT). One of the main applications of PCI is local treatment of solid cancerous tumours. The use of three-dimensional (3D) tissue culture cancer models can provide more physiologically relevant information compared to standard monolayer culture owing to the present of an extracellular matrix. The aim of this study was to examine the effect of PDT and PCI in 3D compressed collagen cancer constructs of breast and ovarian cancer. The use of plastically compressed collagen confers near physiological densities of collagen unlike standard hydrogels.

In the first set of PCI studies, a disulfonated porphyrin ($TPPS_{2a}$) was used as the photosensitiser together with a cytotoxic macromolecule, a ribosome inactivating protein (saporin) to investigate the efficacy of the treatment in spheroid and non-spheroid compressed collagen 3D constructs of breast and ovarian cancer versus conventional 2D culture. Three human cell lines were investigated, a breast cancer cell line (MCF-7) and two ovarian cancer cell lines (SKOV3 and HEY). Using a range of assays including optical imaging, the treatment resulted in significant and synergistic reduction in viability of cells in the 2D and non-spheroid constructs of all 3 cell lines when measured at 48 or 96 hours post-illumination. In a further set of experiments, PCI-induced enhancement in cytotoxicity was observed when Dactinomycin was used as the cytotoxic agent. This is the first time that PCI with Dactinomycin has been investigated. In the larger spheroid constructs of ovarian cancer cells, PCI was still effective but required higher saporin and photosensitiser doses compared to 2D and non-spheroid cultures. PCI treatment was observed to induce death principally by apoptosis in the non-spheroid constructs of ovarian cancer compared to the mostly necrotic cell death caused by PDT. At low oxygen levels (1%) both PDT and PCI were significantly less effective in the constructs compared to 2D models. Using the 3D tumouroid model, where a central cancer mass is surrounded by the collagen matrix populated by fibroblasts to simulate the stroma, PCI was found to be able to both kill ovarian cancer cells within the cancer mass and inhibit their migration to the stroma.

In conclusion, the use of 3D cancer models provides a useful means to assess the efficacy of PCI for the minimally invasive treatment of breast and ovarian cancer prior to *in vivo* studies and could help reduce the number of animals used in animal experimentation.

Impact statement

The use of three-dimensional (3D) cancer constructs provides a model system for researchers which is reproducible and easy to create. Such a model allows different densities and components to be used with the construct and match the purpose of the research better. For future studies within academia such constructs could be used to develop very complex cancer constructs to study cancer behaviour and the effects of various anti-cancer treatments including those which are involve nanoparticles. Outside of academia this model can contribute towards reducing the use of animal models for cancer related studies which in turn could also reduce animal suffering. Furthermore, the cancer models can be developed using tissue samples from the patient to simulate the clinical tumour so that the response of the cancer to different therapeutics can be tested quickly. This allows the use of personalised cancer treatment instead of subjecting the patient to different treatments, with significant benefits to the quality of the patient's life. Immunological factors can also be incorporated into the model to test for any side effects or allergic reactions that may occur as a result of using the therapeutics so that the probability of such side-effects being experienced by patients can be minimised.

Photochemical internalisation is designed to be a minimally invasive technique that is localised and does not induce the photoxicity observed with PDT. This therefore means that the treatment will cause minimal damage to healthy tissues in other parts of the body of the patient and will cause fewer side effects as very small doses of the drugs are required for use. Within academia, this treatment provides the potential for researching the delivery of various therapeutics to their sites of action not only for cancer treatment but also for the treatment of other non-oncological conditions.

List of Abbreviations

Acronym	Definition
2D	2 Dimensional
3D	3 Dimensional
5- ALA	5- Aminolaevulinic acid
ASCS	Adipose-derived stromal cells
AuNPs	Gold nanoparticles
BPD	Benzoporphyrin derivative
CDMs	Cell derived matrices
CNT	Control
CRUK	Cancer Research UK
ECM	Extracellular matrix
EPR	Enhanced permeability and retention
EtNBS	5-ethylamino-9-diethylaminobenzo[a] phenothiazinium
HpD	Haematoporphyrin derivatives
LOC	Lab-on-a-chip
Lu-Tex	Lutetium texaphyrin
MACE	Mono-L-aspartyl chlorin e6
MAME	Mammary architecture and microenvironment engineering
mTHPC	M-tetrahydroxyphenylchlorin
NHS	National Health Service
NIR	Near infrared
PDT	Photodynamic therapy
PCI	Photochemical internalisation
PGA	Polyglycolide
PLA	Polyactide
PLGA	poly(lactic-co-glycolic acid)
PPIX	Protoporphyrin IX

RGO	Reduced Graphene Oxide
SnET2	Ethyl etiopurpurin
SWCNTs	Single-wall carbon nanotubes
$TPCS_{2a}$	Disulfonated tetraphenyl chlorin
$TPPS_{2a}$	Tetraphenyl disulfonated porphyrin
WHO	World Health organisation
ZnPc	Zinc Phthalocyanine

Acknowledgements

First and foremost, I would like to thank God Almighty for giving me the strength, knowledge, ability and opportunity to undertake this research study.

Secondly, I would like to thank my wonderful supervisor Prof. Alexander MacRobert for providing sincere support and direction at all times and giving me invaluable guidance, inspiration and suggestions throughout this journey. He has allowed me to freely pursue my research, whilst ensuring that I stay on track and do not deviate from the core of my research. I would also like to extend my deep gratitude to Prof. Marilena Loizidou and Dr Elnaz Yaghini for being such great inspirations and role models and strongly supporting me through this journey. Moreover, I have great pleasure in acknowledging my gratitude to Dr Bala Ramesh for his constant guidance and assistance.

My acknowledgements would be incomplete without thanking my fellow PhD colleagues for their friendship, help and fun memories. I particularly would like to thank Mrs Helen Tajdivand and Mr Amir Afrashtehpour for their continuous kindness, support and encouragement through the years.

I would like to dedicate this work to my family for their endless love and care and for being the greatest source of strength that God has given me. The blessings of my parents and the love of my sister Maryam M. Hadi have tremendously contributed towards helping me reach this stage of my life. They have patiently held my hand through every stage of my life and motivated me to try and achieve my best in every situation.

Table of Contents

List of Figures

List of Tables

Chapter 1

1. Background and Introduction

1.1 Introduction to breast and ovaries

This thesis addresses a minimally invasive modality with potential applications for the treatment of breast and ovarian cancers. To introduce the thesis, the development of breast and ovarian cancer is summarised together with the current treatment options. The breast is an organ which in females has the special function of producing milk for lactation. This organ is located on top of the pectoral muscle which covers the ribcage. The epithelial parts of the breast tissue include lobules where milk is produced which are connected to ducts that lead out of the nipples. A majority of breast cancers develop from cells that form the lobules as well as the terminal ducts. The lobules and ducts are also found throughout the fibrous and adipose tissues which contribute majorly to the anatomy of the breast. Furthermore, the breast tissue is surrounded by a thin layer of connective tissue known as fascia. The deep layer of this connective tissue sits just on top of pectoral muscle and the superficial layer of it is located below the skin (1).

Blood is supplied to the breast mainly from the internal mammary artery which is found underneath the main breast tissue. This blood supply is responsible for providing nutrients and oxygen to the breast tissue. The lymphatic vessels however run in the opposite direction of the blood supply draining into the lymph nodes. Breast cancers spread to lymph nodes through these lymphatic vessels which mostly flow to the axillary lymph nodes in the underarm while a few of the lymphatic vessels drain to internal mammary lymph nodes which sit deep in the breast. Breast tumours normally first encounter the sentinel lymph node which is the initial lymph node in the series of lymph nodes upon being drained through the lymphatic vessels. Surgeon may sometimes remove this lymph node in order to check for metastases in breast cancer patients (1, 2). Women can also develop breast cysts which are non-cancerous fluid filled sacs (3).

The ovaries are a pair of organs in females that are responsible for producing eggs as well as maintaining the health of the female reproductive system. These organs also secrete two hormones (oestrogen and progesterone) which are crucial for the normal development of the reproductive system and fertility (4).

In terms of anatomy the ovaries are oval in shape (approximately 3-5 cm) and sit on opposite ends of the pelvic wall and are therefore located on either side of uterus. The

ovaries are connected to the very narrow fallopian tubes (also called uterine tubes or oviducts) via a tissue called the fimbria and extend from the ovaries to the uterus (5, 6).

The fimbria is a finger-like projections of the infundibulum which is the funnel shaped peripheral end of the fallopian tube. The fimbriated end of the fallopian tube is not covered by peritoneum, which allows the communication between the fallopian tube and the peritoneal (pelvic) cavity. The currents created in the peritoneal fluid from the beating of the fimbriae, help carry oocytes into the fallopian tube lumen where they may undergo fertilisation in a region within the fallopian tube called the ampulla. The anatomy of breast and ovary has been presented in Figure 1.

The type of diseases and disorders that are normally associated with the ovaries include:

- Osteoporosis which is normally linked with menopause along with other symptoms such as mood swings and hot flushes. Oestrogen is important for protecting bone strength and therefore the drop in oestrogen levels reduces bone density (7).

- Ovarian cancer which has symptoms that typically do not become apparent until the disease has reached a late and developed stage (8).

- Ovarian Cysts which are fluid filled sacs and can occur in women of all ages with those of child-bearing age being more susceptible to this problem. In term of size the cysts can grow up to 10 cm. usually cysts above 5 cm in diameter are removed surgically to prevent them from twisting the ovary that they are affecting and disrupting the blood supply to the ovary (9).

- Polycystic Ovarian Syndrome (PCOS) which is a result of hormonal imbalance and owes most of its symptoms to increased production of androgens such as testosterone. Patients with PCOS suffer from problems such as infertility, irregular menstruation, acne, as well as increased hair growth on the face and body. Other PCOS related issues include obesity, insulin resistance and type 2 diabetes. It is possible for patients to overcome most of the symptoms of PCOS by losing weight (10).

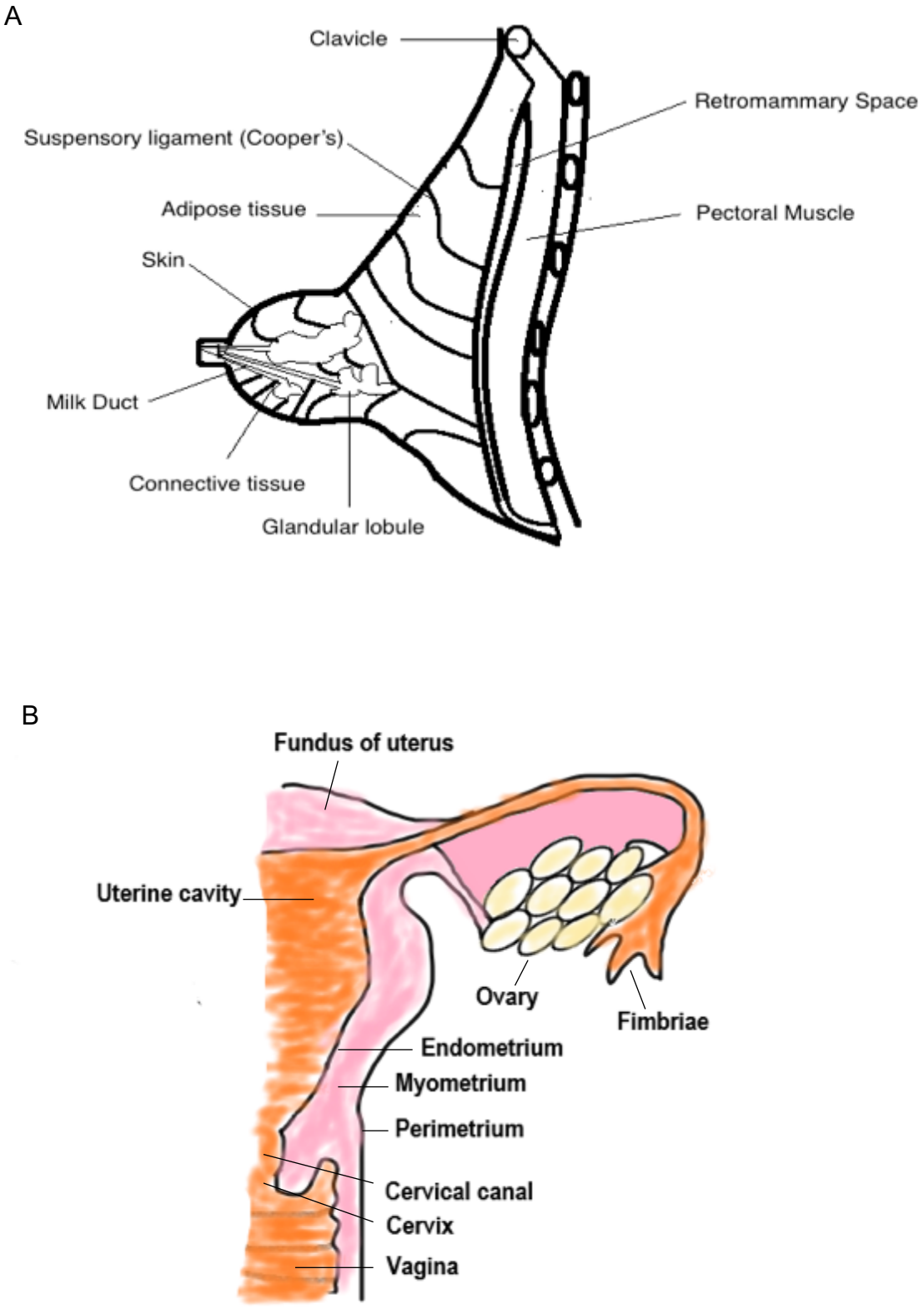

Figure 1: Anatomy of female breast and ovaries. A. Anatomy of the female breast. B. Anatomy of the ovaries.

1.2 Breast and Ovarian cancer

Breast cancer

According to the World Health Organisation, breast cancer is the most common cancer affecting females and affects more than 1.5 million women annually resulting in the highest number of cancer related mortalities amongst women (11). It was reported that in 2015, 570,000 women died from breast cancer which accounted for almost 15% of all the cancer deaths among women (11). Although breast cancer rates are greater in women in more developed countries, an increase in such rates is seen in nearly every region around the world (11).

Almost 54,900 new cases of breast cancer are diagnosed in the UK annually with the most aggressive breast cancers occurring in the upper outer quadrant of the breast (12). It is thought that 1 in 8 females and 1 in 870 males will become diagnosed with breast cancer in their lifetime (13). In 2012 approximately 1.7 million women were diagnosed with breast cancer with UK having the sixth highest incidence rate in Europe (14). The diagnosis of new breast carcinoma *in situ* in UK is about 7,700 cases annually with 30 new cases found in men and 7,900 new cases diagnosed in women in 2015 alone. A majority of the *in situ* breast carcinoma cases are intraductal (15).

With breast cancer being the 4th most frequent cause of cancer death in UK, the total number of deaths from this disease total 11,400 per year. Around 522,000 women died of breast cancer worldwide in 2012 and the UK had the 14th highest mortality rate in Europe (15). Statistics from 2010-2011 found that about 65% of women in England and Wales who are diagnosed with breast cancer survive this disease for 20 years or more. However, the five-year survival rate from breast cancer in women in England, Wales and Scotland is below the European average (16).

Breast cancer is mainly diagnosed through screening with a majority of cases being diagnosed at an early stage. Symptoms of breast cancer include, development of a lump or thickened tissue on either breast, a change in breast size or shape, discharge with blood stains released from the nipples, development of lump or swelling in the armpits, occurrence of dimples on the skin of the breast and/or rash on or surrounding the nipple and change in nipple appearance (17).

Ovarian cancer

Almost 7400 new cases of ovarian cancer are diagnosed in UK every year, making this disease the 6th most common type in females in the UK (18). A CRUK 2014 report found

that nearly 6 out of 10 cancers were diagnosed at a later stage in England and Northern Ireland. Approximately 239,000 females were diagnosed with ovarian cancer worldwide in 2012 with UK being the 9th country in Europe to experience the highest number of incidents (18). Furthermore, ovarian cancer is the 6th most frequent cause of cancer death in UK females making the UK mortality rate from this disease the 16th highest in Europe. Approximately 152,000 women around the world died from ovarian cancer in 2012 (18). If diagnosed at the earliest stage, it gives 9 out of 10 women with the disease a chance survival for 5 years or more, however less than 5 out of 100 women diagnosed with ovarian cancer at the latest stage will experience such survival rate. The 5-year survival rate for ovarian cancer in the UK is below the European average (16).

Ovarian cancer is diagnosed using CA125 (biomarker of ovarian cancer cells) blood test and ultrasound (18). Symptoms of ovarian cancer include: constant feeling of bloatedness, swelling in the tummy, feeling of discomfort in the abdomen or pelvic area, loss of appetite and the urge to urinate more often (19).

1.3 Risk factors of breast and ovarian cancer

Factors that increase the chances of contracting breast and ovarian cancer include being overweight, having a family history of either cancer, inheriting mutated BRCA1 or BRCA2 genes, variations in levels of sex hormones such as oestrogen and testosterone and progesterone with changes in levels of the first two hormones mentioned increasing the risk for breast cancer and exposure to radiation. Age is also another factor influencing the risk of breast and ovarian cancer contraction with women over 50 being more at risk (19). Interestingly, while the use of contraceptive pills slightly increases the risk of breast cancer, it decreases the risk for ovarian cancer. Furthermore, women who have previously had breast cancer are at higher risk of getting both another breast cancer and/or ovarian cancer compared to the general population. Drinking alcohol also puts the risk for breast cancer at an increase (20).

1.4 Treatments available for breast and ovarian cancer

Current treatments for breast and ovarian cancer include surgery, radiotherapy, chemotherapy, hormonal therapy and HER2 targeted therapy.

Surgery:

For breast cancer, surgery involves the removal of the tumour as well as its surrounding tissue. This procedure can also be used for examining the axillary lymph nodes for the spread of cancer. There are two types of procedures: **Lumpectomy** which involves the subtraction of the tumour and a small, margin of the healthy tissue surrounding the tumour

and **Mastectomy** which involves the removal of the whole breast. For cancers treated with lumpectomy if the cancer is invasive then radiation therapy may be applied to the rest of the breast tissue (17).

For ovarian cancer however the 3 mostly applied surgeries include **Unilateral salpingo-oophorectomy** which is the surgical resection of one ovary in addition to one fallopian tube, **Bilateral salpingo-oophorectomy** which is the surgical removal of both ovaries as well as both fallopian tubes and **Total hysterectomy** which involves the removal of the uterus. Chemotherapy may also be recommended after ovarian cancer surgery (21).

Radiation therapy:

Radiation therapy or radiotherapy uses high power X-rays or other particles to destruct cancer cells. This treatment may be given after surgery to destroy the remaining tumour cells as “adjuvant radiation therapy” or prior to surgery as “neoadjuvant radiation therapy” to shrink the size of a large tumour to make it easier to surgically remove (17, 22).

Side effects of such therapy include fatigue, changes in the skin of the treated area (e.g redness, discoloration/hyperpigmentation, pain and burning sensation as well as blistering and peeling), nausea, vomiting and diarrhoea. Vaginal irritation may also occur in patients with ovarian cancer (17, 22).

Chemotherapy:

Chemotherapy uses drugs to kill cancer cells by stopping the cancer cells from growing and dividing. As with radiation therapy, chemotherapy may be given either before surgery to reduce the size of large tumours to make their removal easier (neoadjuvant chemotherapy) or be given after surgery to minimise the likelihood of recurrence (adjuvant chemotherapy) (17, 22).

Side effects of this treatment can vary depending on the drugs used and doses given but normally include tiredness, chance of infection, nausea and vomiting, alopecia, loss of appetite as well as diarrhoea (23).

Hormonal therapy:

Hormonal therapy or endocrine therapy involves effectively targeting tumours that test positive for oestrogen and progesterone receptors (known as ER positive and PR positive) (24). These types of tumours depend on hormones to aid their growth thus blocking the release of such hormones to help cancer growth and recurrence when used on its ownw or in combination with adjuvant or neoadjuvant chemotherapy (24).

Therefore, like chemotherapy and radiation therapy, hormonal therapy can be applied before surgery again for the purpose of shrinking tumour size for easier removal (neoadjuvant hormonal therapy) or after surgery to decrease the risk of cancer recurrence (adjuvant hormonal therapy) (24, 25).

Side effects of hormonal therapy include pain in muscles and joints, hot flushes, vaginal dryness, an increase in risk of developing osteoporosis and bone fractures as well as high cholesterol levels (25).

The following sections introduce other energy-based therapies that can potentially be applied to breast and ovarian cancer as with radiotherapy with potentially fewer side-effects.

1.5 Photodynamic therapy (PDT)

Photodynamic therapy (PDT) is a minimally invasive treatment used for different types of cancer as well as non-malignant lesions (26, 27). PDT requires molecular oxygen and is carried out through the administration of a photosensitiser, which is then activated by light of specific wavelength (e.g blue, red or near infrared (NIR) light) thus resulting in the production of cytotoxic reactive oxygen species (ROS). This treatment method has been clinically approved for treating numerous forms of tumours for example prostate (28),head and neck, skin and oesophagus (29). PDT has also been employed to treat non-cancerous conditions such as age-related macular degeneration, atherosclerosis and bacterial infections (30).

This treatment holds advantages for both the patient and the clinician as it greatly reduces the requirement for major surgery, shortens recovery periods, stimulates good healing and maintains integrity and function of organs with posing very little risk of local and systemic treatment-related morbidity as well as side-effects (31-34). Moreover, PDT can be applied repeatedly and even used after various treatments such as surgery, chemotherapy and radiotherapy without inducing any immunosuppressive or myelosuppressive effects (27, 35). Generally red or NIR light is used for PDT since tissue is relatively more transparent in this wavelength range beyond strong haemoglobin absorption. Very superficial treatment can however be achieved using blue light excitation instead. Although the light delivery can be targeted to the lesion, the degree of selectivity in tumour uptake of the photosensitiser following intravenous administration is generally insufficient to result in tumour-selective treatment. However, the good healing of normal

tissue adjacent to the tumour does offer an important therapeutic benefit in contrast to radiotherapy where normal tissue damage is a major side-effect.

1.6 Mechanism of action of PDT and mode of cell death

The mechanism of action of PDT and the mode of cell death it induces depend on several factors e.g genotype of cells, PDT dosimetry (e.g. light intensity) and the localisation of the photosensitiser (36, 37). As a majority of photosensitisers do not tend to accumulate within the nuclei (38), PDT is not prone to cause DNA related damage, mutations or carcinogenesis (37). Photosensitisers, that predominantly localise within the mitochondria, induce apoptosis (39),whilst photosensitisers that localise within the plasma membrane mainly stimulate necrosis upon exposure to light (40). Overall the mode of cell death triggered shifts from apoptotic to necrotic as the intensity of the damage caused to the cell increases which results in swift cell lysis instead of an orderly programmed type of cell death (41). Photodamage may also lead to a cytoprotective response termed autophagy (42). Figure 2 has been specifically produced for this thesis and shows the possible cell death pathways activated upon treatment with PDT.

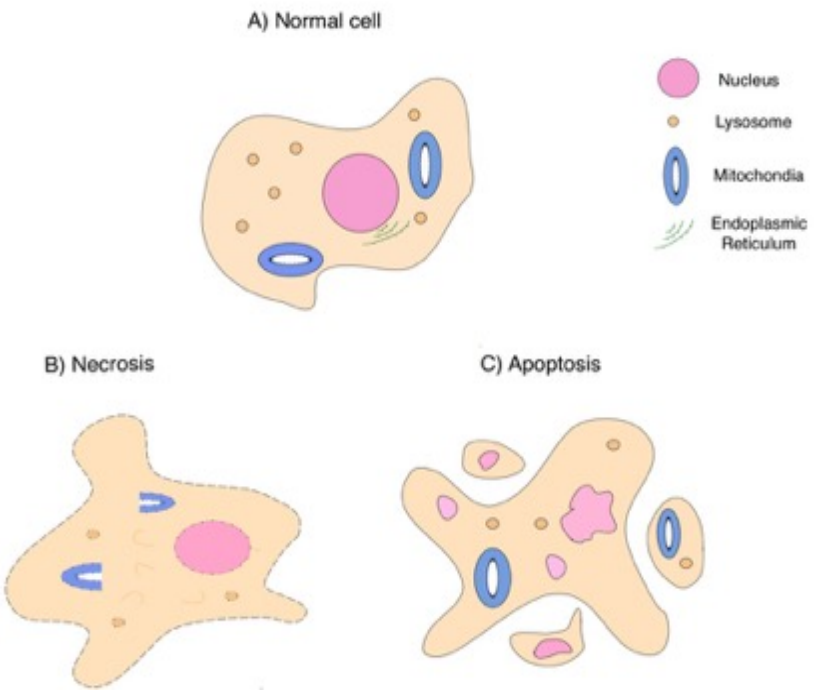

Figure 2: Mode of cell death induced by PDT depending on the localisation of the photosensitiser within the cell. (A) Shows a healthy cell with normal functioning organelles. (B) Necrotic cell death leads to the destruction and rupturing of the cell membrane resulting in non-functional organelles. Apoptosis (C) however, causes shrinkage of the organelles leading to the breakage of the cell into numerous apoptotic bodies, although the organelles are still functioning.

In terms of electronic configuration, photosensitisers possess a stable singlet state (ie no net electronic spin) in their lowest energy level (43). By absorbing a photon of light of a certain wavelength, the photosensitiser molecules are raised to an excited state which is also a singlet state but short-lived (44) (45). The photosensitiser may then return to ground state via internal conversion where the energy is lost as heat or through the emission of a photon as fluorescence which can be used for photodetection purposes in a clinical setting (46). However in order for a therapeutic photodynamic effect to be produced the photosensitiser must undergo conversion to the triplet state via a change in electronic spin, a process known as intersystem crossing (31). This process can be rapid for aromatic photosensitising dyes with comparable or higher efficiencies than fluorescence. Typically, the probability (or quantum yield) of conversion to the triplet state will be > 0.5 for many photosensitisers.

In this case if a sufficient supply of oxygen is available, the triplet excited photosensitiser can either undergo a type I or type II reaction (47) since the triplet state is relatively long-lived. In a Type I reaction the sensitiser reacts with a substrate in a direct manner through proton or electron transfer to produce radicals, which then interact with oxygen molecules to form oxygenated products or reactive oxygen species (ROS) that are damaging to the

integrity of the cell membrane (48). In a type II reaction on the other hand the energy of the sensitiser is directly transferred to the oxygen molecules to generate the singlet oxygen species, which is believed to be one of the most potent reactive oxygen species in PDT (49).

Singlet oxygen is extremely reactive and short –lived with the ability to diffuse approximately 0.01-0.02μm in its short lifetime (50). This therefore means that the reaction occurs within a limited distance and volume resulting in a cytotoxic response being created in a localised manner (50).

1.7 Photosensitisers used in PDT

Ideally a photosensitiser should display chemical, photophysical as well as biological characteristics, which allow it to be uptaken by a tumour, undergo fast clearance and have a large absorption peak at wavelengths of light above of 630nm (50).

First generation photosensitisers:

First generation photosensitisers are known to include haematoporphyrin derivatives (HpD) as well as Photofrin (49). HpD has shown to localise within the tumours and produce a good tumouricidal response upon activation by red light. Porfimer sodium (Photofrin) which is a chemically purified portion of the active component found in HpD was the first photosensitiser to obtain approval for treating recurring superficial papillary bladder cancers using PDT (50) at concentration of 2 mg/kg (51). Porfimer sodium has numerous absorption peaks with the weakest being found at 630nm (52). Despite the display of the weak absorption peak, the light of wavelength 630nm is commonly used in clinical applications for the activation porfimer sodium since lights of a shorter wavelength preclude deep tissue penetration (53). This also means that only light doses ranging from 100-200 J/cm^2 are required for the purpose of tumour treatment (54). Although Photofrin is the most commonly clinically used first generation photosensitier, apart from the relatively short absorption wavelength, its potential has been undermined by a further disadvantage such as long-term photosensitivity of the skin (55), which lasts for a period of 4-12 weeks (50).

Second-generation photosensitisers:

Several second generation photosensitiers have been created to overcome issues related to side effects e.g skin photosensitisation and inadequate tissue penetration that are normally associated with first generation photosensitisers (37) but they must also be as effective in treating tumours as Photofrin (50). In comparison with the first generation molecules, the second-generation photosensitisers are generally more chemically pure,

capable of absorbing light of longer wavelengths and result in considerably less photosensitisation of the skin after treatment (50). Compounds such as benzoporphyrin derivative and temoporfin (mTHPC) are referred to as second generation photosensitisers and have a stronger ability to produce singlet oxygen (48).

An alternative approach is to use 5-aminolavulinic acid (ALA) which is an approved agent used for treating cutaneous lesions in combination with red or blue light. This compound does not have any photosensitising properties per se but it is a natural precursor of haem (56), which is generated by the conversion of protoporphyrin IX (Pp IX), an effective photosensitiser, into haem with the aid of ferrochelatase (57). Since most tumours have a lower level of ferrochelatase activity compared to normal tissue, administering ALA results in a significantly increased amount of PpIX in the tumour cells (57). PpIX has an absorption spectrum close to that of porfimer sodium (50) and can therefore be activated by red light of wavelengths near 630nm (58).

The advantages of PDT with ALA over porfimer sodium PDT are the rapid clearance of PpIX which leads to reduced photosensitivity (normally 1-2 days) (59) (50), its topical and oral applications in the case of treating skin cancer and oral cavity/ digestive tract cancer respectively as well as its ability to attain better tumour selectivity (60) (61). One disadvantage of using ALA however, is that this compound possesses a highly hydrophilic nature and thus cannot penetrate through the cells easily (62). This issue has been resolved through the development of a number of alkyl ester derivatives of ALA that have the ability to enter the cells more efficiently (63).

One of the second-generation photosensitisers that has been approved for use in head and neck cancers in 2001 is mTHPC (tempoporfin, Foscan) (64). This photosensitiser has a higher potency than ALA (50), or porfimer sodium (65) and only requires light dose of 20 J/cm^2 for treating tumours (66). Moreover mTHPC absorbs light at 652nm (67) (68). In comparison to the 630nm absorption peak of both porfimer sodium and ALA which allows it to penetrate deeper into the tissue (50).

The development of new photosensitisers has been a subject of intense interest (69). This has involved development of photosensitising drugs that are more tumour specific, can undergo activation with light of a longer wavelength and result in an overall shorter period of photosensitivity and is still ongoing (70). Other photosensitisers that have been tested in clinical trials are tin ethyl etiopurpurin (SnET2) (71), mono-L-aspartyl chlorin e6 (Npe6) (72), benzoporphyrin derivative (BPD) (73), and lutetium texaphyrin (Lu-Tex) (74). These compounds have absorption peaks at higher wavelengths of 660 nm (75), 664 nm (72),

690nm (54) and 732nm respectively and cause very mild and brief skin photosensitivity (50).

In recent years the term of 'third-generation' photosensitiser has become more widely used, where the photosensitiser can be targeted to the cancer in order to improve treatment selectivity. The use of targeted nanoparticles for PDT has been a particularly active area.

1.8 The use of nanoparticles in PDT

Due to limitations related to the use of current photosensitisers such as poor bioavailability (eg poor water solubility), nanoparticles have been employed to aid the improvement of PDT (76)(77). Photosensitisers can be modified by for example being incorporated into delivery systems such as liposomes, polymer nanoparticles, micelles, gold nanoparticles and ceramic nanoparticles (78). Nanoparticles used for the improvement of PDT efficacy can be categorised in accordance to their functional roles and whether they are actively or passively targeted (79).

The utilisation of targeted nanoparticles has the benefit of improved selectivity by delivering the photosensitiser to the tumour site thus resulting in very minimal harm to the normal tissues. Nanoparticles can be "actively" targeted to the cancer site using surface-conjugated ligands that bind to overexpressed receptors or antigens on the target tissue. The tumour targeting properties of nanoparticles can also be improved through the enhanced permeability and retention (EPR) effect that can enhance selective uptake and retention with respect to normal adjacent tissue, a process called "passive" targeting selectivity. In this case, the targeting of photosensitisers can be made possible via encapsulation or conjugation to nanocarriers (80). These nanoparticles are sub-classified depending on whether their composition is biodegradable or non-biodegradable.

Non-biodegradable nanoparticle-based photosensitisers include for example upconversion nanoparticles, quantum dots and self-lighting nanoparticles where the nanoparticle material has intrinsic photosensitising properties (78).

In the following section some examples of new types of nanoparticles for PDT are reviewed. Since nanoparticle uptake normally takes place via endocytosis this subject is relevant to the theme of this thesis.

Fullerenes and Carbon nanotubes (CNTs)

Fullerenes (C_{60}) consist of 60 carbon atoms arranged in a highly stable spheroidal structure with a diameter of about 2 nm which absorb wavelengths within the visible light spectrum. They also have high triplet yields and an ability to produce to ROS when illuminated (81). The poor solubility of fullerenes in aqueous solutions places these nanoparticles at a disadvantage when considering their use in biological systems. However, such issue may be overcome via methods such as encapsulation in particular carriers, such as undergoing suspension with the aid of co-solvents, introducing hydrophilic attachments or reducing the molecules to water soluble anions (82). One major drawback of fullerenes is that their highest absorption lies in the ultraviolet and blue regions preventing them from penetrating deep into the tissue (83). Therefore, although treatment of cancer using PDT with fullerenes has been demonstrated *in vivo*, it is crucial to develop fullerenes, which can absorb red or in fact near-infrared light, in order to be used successfully for clinical applications with PDT.

Carbon nanotubes (CNTs) are also composed of a lattice of carbon atoms like fullerenes but with a rolled structure in form of a tube (84). CNTs can be categorised into either single-walled nanotubes (SWNTs) or multi-walled nanotubes (MWNTs). Due to the high surface area of the nanotubes, drugs, peptide and nuclei acid molecules can be merged into their walls as well as tips allowing the mammalian cell membrane to be crossed through endocytosis or enabling cancer specific receptors on the surface of cells to be recognised (85). SWNTs are also known as useful fluorescence probe quenchers (86). However, due to limited knowledge regarding the pharmacological and toxicological properties of CNTs, they are not yet being utilised in PDT studies clinically.

Quantum dots (QDs)

Quantum dots (QDs) are nanocrystals typically a few nm in diameter that possess properties such as high fluorescence quantum yields, and photostability (87). Compared to most fluorophores, these nanoparticles have bigger absorption coefficients in addition to size-tunable light emission and greater signal brightness (35). Through specific surface coating modifications, water-soluble and targeted QDs can be developed. Cadmium selenide (CdSe) is the most commonly used material in semiconductor QDs. To reduce their cytotoxicity, Cadmium free QDs have been developed through replacing the cadmium either with nontoxic metals or those with lower toxicity e.g Indium (In) (88, 89). Yaghini *et al*. (2016) recently showed the potential of Indium-based QDs as a better alternative to blue dyes for sentinel lymph node mapping in breast cancer patients using animal models (90). The conjugation of QDs with photosensitisers (QDs-PS) can

significantly enhance their photosensiting properties (91).

Upconversion nanoparticles

Upconversion nanoparticles (UCNPs) are a new generation of fluorophores, which can be activated by near infrared (NIR) radiation through a non-linear optical mechanism (92). The principal material used in the making of UCPs is $NaYF_4$ (93). A type of UCP, $NaYF_4$ nanocrystal with mesoporous silica-loaded zinc phthalocyanine (ZnPc) coating has demonstrated the ability to change NIR light into visible light after becoming excited by a NIR laser. This allows further activation of the photosensitiser resulting in the release of $^1O_2$ and ultimately killing cancer cells. Apart from being resistant to photobleaching, other advantages of UCPs include deeper tissue penetration due to excitation by NIR light, which makes them desirable for use in PDT. Furthermore, the discovery of self-lighting PDT through the utilisation of scintillation luminescent nanoparticle-attached photosensitisers has allowed the enhancement of PDT efficacy without the requirement of an external light source (94).

1.9 Role of nanoparticles as photosensitiser carriers in PDT

Two of the drawbacks of most clinically approved photosensitisers are their poor bioavailability as well as their unfavourable biodistribution (95). This can be resolved by the enhanced permeability and retention (EPR) effect, which results from the irregular tumour neovasculature which is more permeable than normal tissue microvasculature, and the poorer tumour lymphatic drainage that in combination aids both the diffusion and retention processes of photosensitiser carriers within tumours. The EPR effect can be taken advantage of by nanoparticles that function as photosensitiser carriers to improve aspects such as cellular uptake, biodistribution, bioavailability and pharmacokinetics of the photosensitisers systemically. Biodegradable nanoparticles consist of polymers that experience enzymatic hydrolysis within biological environments hence liberating the photosensitisers (96). Nonbiodegradable nanoparticles such as silica are also effective for PDT. In such cases the detachment of photosensitisers from the nanoparticles carriers is not necessarily essential since free oxygen diffusion in and out of the nanoparticles enables generation and release of singlet oxygen (77). These two different classes are now summarised in more detail.

Biodegradable nanoparticles

Biodegradable polymer-based nanoparticles have displayed an enormous potential as photosensitiser carriers owing to their ability to control drug release, their versatile properties in material manufacturing processes and their great drug loading capabilities.

The polymers can be adapted in terms of chemical composition and architecture to suit, various photosensitisers with different hydrophobicity degrees, molecular weights, pH and charges (97). Degradation can be stimulated by the lower tumour pH or enzymatically based on higher tumour expression of the particular enzymes. Surface modifications of nanoparticles can further trigger active targeting to specific sites of actions. The delivery of photosensitisers can be carried out via micelles, liposomes, dendrimers and nanoparticles (98). Nanoparticles are generally composed of natural or synthetic polymers. Even though synthetic polymers are more desirable for utilisation in drug delivery systems, because of their capacity to adjust their mechanical properties as well as degradation kinetics to fit the purpose of different applications, the use of natural polymers such as chitosan has attracted more attention due to their availability, lower costs and potential of being chemically modified (99). Despite the developments made in drug delivery using synthetic biodegradable polymers, natural polymers still continue to be an area of interest in research.

Non-biodegradable nanoparticles

Non-biodegradable nanoparticles function differently in PDT due to their lack of degradability and uncontrollable drug release. Such nanoparticles are not destroyable by treatment processes and are therefore appropriate for repeatable use if activated adequately. Nonbiodegradable nanoparticles hold several advantages in comparison to biodegradable polymeric nanoparticles. These advantages include: 1) the easy management of the particle sizes, shapes, porosities and monodispersibilities of these nanoparticles; 2) the stability of the nanoparticles towards environmental fluctuations; 3) their resistance to microbial attacks and 4) continuous diffusion of oxygen in and out of the particles due to the adjustable pore sizes (99). The majority of non-biodegradable nanoparticles comprise of silica or metallic material. Owing to their unique properties, metallic nanoparticles have been a subject of great research in order to explore their potentially applicable uses in biochemistry as chemical and biological sensors, in nanoelectronics and nanostructured magnetism as systems as well as in medicine as means of drug delivery. In contrast to most silica-based nanoparticles, metallic nanoparticles have to be conjugated with the photosensitisers on their surfaces (100). Gold nanoparticles are an example of metallic nanoparticles that have been intensely investigated because of their inert chemical properties as well as their ability to induce minimal acute cytotoxicity (101).

1.10 Light sources used in PDT

An extensive range of laser and non-laser sources of light can be used in photodynamic therapy (102). Wide spectrum light sources e.g arc lamps that are cost effective and

simple to use can be used to activate photosensitisers (103, 104).The disadvantages of using these lamps include the difficulty behind coupling them to light delivery fibres without having to reduce their optical power, calculating the amount of the efficient dose of light delivered, the limitation of power output to 1W maximum and the requirement of filters to eliminate UV radiation as well as infrared emission which can result in heating (50).

The discovery of lasers with the ability to emit focused beams of light with the exact essential wavelengths proved to be a significant discovery for PDT (105) (106). The additional advancements in the semiconductor diode technology led to the development of more cost-effective systems with high power output, which have the advantage of being compact (107) as well as portable (108). A majority of these systems consist of an internal unit for dosimetric calculations alongside built-in treatment programs that makes them easier to use (109)(104). The one limitation of these laser diodes is their ability to provide one single output wavelength (50). Light emitting diodes (LEDs) may be used clinically (110) as they are small as well as less costly compared to above-mentioned light sources and can offer a maximum power output of 150 mW/cm^2 at wavelengths ranging from 350-1100 nm (45).

Optical fiber technology has become an important means of delivering light to the treatment site to activate the photosensitiser in recent years (111). Optical fibers have the capacity to illuminate at different localisations owing to their ability to convey light to the target site more accurately with a homogenous distribution (112). In the case of treating superficial cancers, optic fibres with a lens on their tips are used to distribute the light across the targeted area (104). For hollow organs e.g bladder and esophagus, illumination is normally carried out using cylindrical diffusers coupled with inflated balloons to aid the provision of uniform light distribution (113)(114)(115). Also black coating a side of the balloon can protect healthy tissue areas by offering shielding (50).

1.11 Clinical trials of PDT in cancer patients

PDT can be applied clinically as a monotherapy or after surgery, chemotherapy and radiotherapy and has been tested in different trials worldwide and received approval for treatment of several solid cancers, eg prostate, head and neck. The numerous trials include treating advanced head and neck cancer, gastrointestinal cancers (oesophagus, stomach, pancreas), pulmonary cancers and ovarian cancer as well as pre-cancerous lesions such as actinic keratoses to prevent its progression to squamous cell carcinoma (28, 71, 116-118).

PDT has also been tested in several trials in patients with breast cancer including one study by Li *et al*. (2011) which coupled PDT with immunotherapy to treat patients with metastatic breast cancer (stage 3 or 4). Out of all patients in this study, one showed a complete response, four demonstrated partial responses, two maintained the disease in stable state and two patients showed disease progression. Furthermore, no serious side effects or deaths as a result of this treatment were observed (27, 119). In another clinical trial study which used Photofrin PDT for the treatment of ovarian cancer in 13 patients, it was found that 2 out of 13 patients did not experience recurrence (118).

Hahn *et al*. (2006) carried out a phase II trial study on the effect of PDT on 33 patients with ovarian cancer using photofrin as a photosensitiser. The results showed an overall survival of 20 months; however, the treatment was not found to lead to significant complete responses or long term tumour control in patients (120).

Banerjee *et al*. (2017) on the other hand carried out a phase I/IIa trial study on the effect of verteporfin (BPD)- PDT on 11 patients with primary breast cancer. In all patients plateau with no diameter increase in the area of necrosis was achieved with increasing light dose. Although the light doses used ranged from 20J- 50J, no information was provided about the minimum light dose that was required for the treatment as the trial is still ongoing (121).

1.12 Photochemical internalisation (PCI)

Although chemotherapy is a commonly used treatment for many metastatic cancers, it is accompanied by side effects as well as likelihood of developing multidrug resistance (122). Improved drug delivery and circumvention of the development of drug resistant are therefore key challenges that need to be overcome to improve treatment response. One factor that degrades the efficacy of immunotoxic and biologic agents is that owing to their size they are generally taken up via endocytosis. Since most therapeutic macromolecules target intracellular components, endocytic uptake presents a barrier against successful intracellular targeting (123) since the agents are not able to reach their target efficiently via diffusion through the cytosol. Entrapment within endosomes and subsequently lysosomes also renders these agents susceptible to degradation by proteolytic enzymes which further limits their efficacy and bioavailability. In some cases even for small molecules the poor bioavailability due to endocytic uptake can also be attributed to low water solubility and/or reduced penetration through cell membrane (124).

Photochemical Internalisation (PCI) is a modification of Photodynamic therapy (PDT) which aids the cytosolic delivery of therapeutic macromolecules and certain small drugs, which are prone to endo-lysosomal entrapment and degradation to their cytosolic sites of action using low-dose PDT (125-128). Like PDT, PCI is spatially selective since the cytosolic release is triggered by light delivered at the target site and not elsewhere in the body. This is achieved through the utilisation of an amphiphilic photosensitiser which localises in the membrane of the endolysosomal vesicle whilst the bioactive agent resides inside the vesicle and causes disruption of the endosomal membrane via the production of reactive oxygen species upon activation by light of a specific wavelength thus releasing the macromolecules into the cytosol (129, 130). Figure 3 demonstrates the mechanism of uptake of the photosensitiser and bioactive agent and the destruction of the cancer cell through PCI.

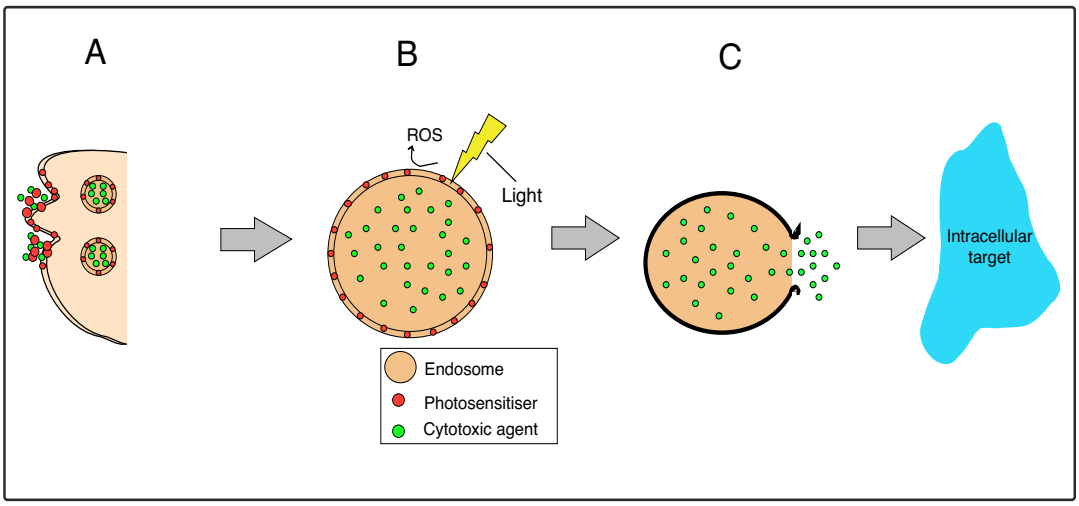

Figure 3: Mechanism of Photochemical Internalisation (PCI) of a cytotoxic agent: Endocytic uptake of photosensitiser (red) and chemotherapeutic drug (green) by cancer cells and the release of endocytosed drug into the cytosol through PCI. (A) Uptake of photosensitiser and chemotherapeutic drug by the cancer cell via endocytosis and their localisation within endosomes and subsequently lysosomes. (B) Localisation of photosensitiser in the membrane of the endosome post washing and the light-induced generation of ROS in the membrane of the endosome containing the chemotherapeutic drugs. (C) Photo-induced rupture of the endo/lysosomal membrane after prolonged irradiation via interaction of ROS with the membrane, leading to the escape of the chemotherapeutic drugs into the cytosol where they can be delivered to their target sites of action to exert their effects.

There are also other types of cytosolic drug delivery systems such as endo/lysosomal pH-responsive drug release systems, redox-responsive drug release systems and lysosomal enzyme-responsive drug release systems (131). However, compared to PCI such systems cannot control the timing of the drug release as well as possible toxicity caused by the delivery system and unlike PCI are not spatially selective.

1.13 Different mechanisms of Endocytosis

There are various mechanisms by which endocytosis occurs. The main pathways include clathrin-mediated endocytosis, caveolin-mediated endocytosis and clathrin- and caveolin-independent endocytosis. In clathrin-mediated endocytosis, the cell surface receptors become bound to appropriate macromolecular ligands and accumulate within specific regions of the plasma membrane called coated pits containing clathrin. The pits then pinch off forming coated vesicles. Once in the cell, the internalised macromolecules are trapped within endo/lysosomal vesicles and eventually undergo degradation by lysosomal enzymes. Caveolae- dependent endocytosis however is a clathrin-independent endocytosis process and involves the formation of bulb shaped plasma membrane

invaginations known as caveolae. In this type of endocytosis, the caveolae pinch off the plasma membrane and whilst some of the caveolae try to fuse back with the plasma membrane most reach early endosome and are then recycled back to the plasma membrane (132, 133).

1.14 Photosensitisers used in PCI

In order to be suitable for use in PCI, photosensitisers are required to localise within the membranes of the endosomes or lysosomes. To assist with this mechanism, carboxylic groups can be incorporated into the photosensitisers, however these groups also allow the photosensitiser to penetrate through the cell membrane. Therefore, by replacing these groups with sulfonate groups which remain negatively charged at physiological pH, the photosensitisers can be taken up by adsorptive endocytosis and do not penetrate through cell membrane or undergo protonation in the acidic environment of the lysosomes (134).

$AlPCS_{2a}$ (aluminium phthalocyanine) has been utilised in many *in vitro* and *in vivo* PCI studies due to its advantages such as having a stable azaporphyrin macrocycle which allows better absorption of light in the far red region (670nm) as well as the two adjacently substituted sulfonate groups that contribute to the amphiphilicity of the sensitiser (135, 136).

Another sulfonated chlorin based sensitiser, disulfonated tetraphenyl chlorin ($TPCS_{2a}$-Amphinex®) was developed as an alternative to $AlPCS_{2a}$ as it can be more reliably synthesised in bulk with relatively few regioisomers. Furthermore, $TPCS_{2a}$ has an enhanced photobleaching rate which is beneficial for the patient as it reduces skin toxicity thus providing $TPCS_{2a}$ with the optimal photobiological and photophysical features required for PCI. Meso-tetra-phenyl porphyrin disulfonate ($TPPS_{2a}$) is the porphyrin equivalent of $TPCS_{2a}$ and is readily available from several commercial sources. $TPPS_{2a}$ is often used for pre-clinical level studies and was the main photosensitiser used in this thesis. Its structure is shown in Figure 4A.

Martinez *et al*. (2017) used $TPCS_{2a}$ and $TPPS_{2a}$ to carryout PDT and PCI studies on 2D and 3D hydrogel models of prostate cancer and not only observed a more superior effect with PCI than PDT in 2D cultures but also found a morphological change in the 3D cultures (137).

1.15 Chemotherapeutic drugs used in PCI

Examples of macromolecular drugs that have been approved for clinical use include CD33-targeted immunoconjugate (Mylotarg), HER2-targeted antibody (Herceptin), (EGFR)- targeted antibody (Cetuximab), IL-2 modified diphteria toxin fusion protein (Ontak) (138).The most commonly used chemotherapeutic agents which have been used experimentally for PCI include saporin, bleomycin, gelonin (137-139), but to date only bleomycin has been used in clinical trials of PCI. One common chemotherapeutic to be used experimentally is Doxorubicin, whose structure is shown in Figure 4. Since this drug is a weak base owing to the presence of the amino group it is susceptible to protonation within acidic lysosomes thus resulting in its entrapment since the ionise form is less likely to pass through the lysosomal membranes into the cytosol.

Saporin: also known as Saporin-S6 is a natural toxin derived from a plant and acts as Type 1 ribosome-inactivating protein (RIP). RIPs function by removing the A4324 adenine residue, in the rat ribosome which then interferes with the interaction between the ribosome and elongation factor 2, which irreversibly damages the ribosome and results in the inhibition of protein synthesis (140). As saporin has a high molecular weight (30 kDa) (141), it is prone to endocytic uptake and subsequent endolysosomal degradation and therefore has limited efficacy when applied alone. The structure of saporin is illustrated in Figure 4B.

Bleomycin: is a glycopeptide antibiotic which acts by causing a break in the double strand of DNA therefore imitating the effects of ionising radiation. Although the exact mechanism by which bleomycin functions is still not fully understood, there has been a suggestion that this drug form complexes with iron ions thus forming a pseudoenzyme which can generate hydroxide and superoxide radicals that can cause breaks in DNA strands. However, the benefits of bleomycin can be limited by its toxic effects in the lung leading to fibrosis (142).

Gelonin: like saporin is also a natural ribosome-inactivating protein derived from a plant. Gelonin therefore functions by removing the base A4324 in 28S rRNA and preventing the association of elongation factor-1 and -2 with the 60 s ribosomal subunit, thus resulting in cell death. Due to its large molecular weight (29 kDa), gelonin is not able to cross the plasma membrane and exert its therapeutic effect when applied alone and therefore displays very limited toxicity under such circumstances (143, 144).

Dactinomycin: is a clinically approved agent which acts as an anti-tumour antibiotic and functions through DNA intercalation as well as inhibition of RNA and protein synthesis. This agent has not been tested for PCI before and based on its high molecular weight (approximately 1255 Da), it should be taken up partly via endocytosis like bleomycin which has a molecular weight of approximately 1400 Da. Furthermore, as Dactinomycin is fluorescent unlike bleomycin, therefore fluorescence imaging can be carried out to show endolysosomal localisation of this drug.

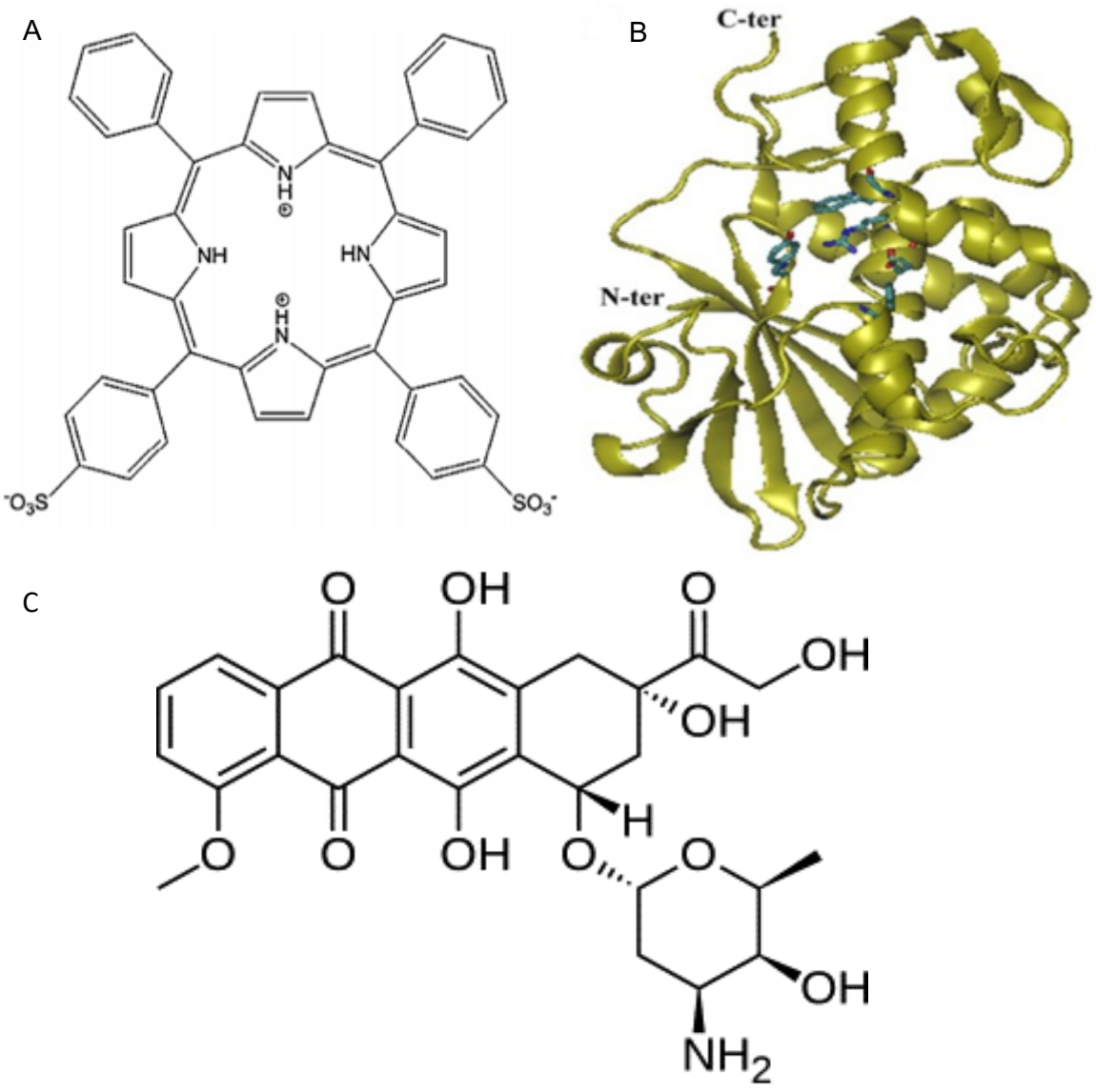

Figure 4: Structure of photosensitiser and chemotherapeutic agents used in PCI. A. Structure of $TPPS_{2a}$ (145). B. Structure of saporin (140). C. Structure of Doxorubicin (146) .

1.16 Three- dimensional (3D) *in vitro* cell culture models

Whilst various non- mammalian *in vivo* models such as fruit fly, zebra fish, amphibians and chicken embryos have also shown potential for use in PDT studies, the development of *in-vitro* three-dimensional (3D) cancer models has attracted considerable interest as it has provides a way of recapitulating key aspects of a solid cancer tissue, including tumour-stromal cell interactions without the use of living species (147-149). 3D models have several advantages over simple two-dimensional (2D) cell culture e.g the enhancement of the expression of differentiated functions, improvement of cell or tissue organisation, anti-apoptotic signalling, multicellular resistance as well as expression of hypoxic conditions and limited drug penetration. Furthermore, the cellular and stromal characteristics of the 3D cultures can be manipulated to provide a more representative model for assessing the therapeutic response as an alternative to animal model testing (150-155).

Various methods can be employed for the development of 3D culture models, for example multicellular aggregates, culturing cells on inserts or embedding cells in an artificial nanofibrous matrix or scaffold developed from natural or synthetic material (156). A summary of the different characteristics of various types of 3D models is presented below.

Spheroids

Spheroids (also called spheres, nodules or micronodules) are well-rounded 3D cancer models that are usually several hundred μm in diameter (157-159). These models can be developed either by growing cells in low adhesion conditions (e.g plates, hanging drop methods etc.) where they adopt a spherical shape through aggregation (160-162) or by embedding cells in a 3D matrix. The closely packed arrangement of cells in spheroids, which provides cell to cell contact as well as reduced rate of drug and oxygen diffusion through the models makes the spheroids comparable to *in vivo* tissues (163). Spheroid 3D models can be used for the assessment of various specific 3D properties such as the development of invasive characteristics, changes in the dependence of cells on growth factors, increased luminal survival because of the stimulation of anti-apoptotic and pro-proliferative signals and the capability to avoid growth arrest because of these pro-proliferative signals (147) (164). Spheroids have also been widely used for a variety of photosensitiser-PDT studies.

Cell derived matrices (CDMs)

CDMs are normally produced by culturing cells that excrete ECM proteins on pre-coated

scaffold surfaces or as a monolayer (2D), or multicellular aggregates (3D) to allow enough ECM to be deposited. Once adequate ECM has been deposited, the cellular component is removed from the ECM using decellularisation processing. Such processing is crucial for minimising the risk of encountering adverse immunological responses (165). Cells that are cultured on CDMs have shown to have similar morphologies to those observed *in vivo* as they are able to form specified 3D matrix adhesions, which are also found within *in vivo* models (166).

Microfluidic devices

The microfluidic technology also called Lab-on-a-chip (LOC) (145) allows the development of 3D cell cultures and cell-based assays in complex microenvironments whilst providing the capability for the environment to be controlled, reproduced and optimised (146). There are several key features possessed by this type of technology: 1) it exhibits micro-scale dimensions which have great compatibility to the microstructures found in the microenvironments of *in vivo* cancer models; 2) It allows small quantities of samples to be used which keeps reagent consumption low therefore reducing the costs of bioanalysis as well as drug discovery and development; 3) Some of the substrates used in microfluidic devices enable high O_2 diffusion which has an important impact on cell proliferation and 4) numerous features such as cell culture and sampling, control of fluids, cell capturing, cell lysis and detection can be integrated on one single microfluidic device (147, 148). The various types of microfluidic devices that have been used in studies involving 3D cell cultures include glass/silicon-based, polymer-based together with paper-based platforms, which have been given their names based on the substrates used in the production of the micro-device (146).

Scaffolds

3D scaffolds consist of a nano-fibrous matrix which allow the creation of an environment that supports the proliferation, growth and migration of cancer cells thus providing the opportunity for such aspects to be investigated (150). In comparison to spheroids, scaffolds hold several advantages particularly the capability of mimicking tumour heterogeneity as well as the control of the 3D dimensions. Furthermore, it is possible to control the extent of migration, proliferation and aggregation of the cells through the surface properties as well as the composition, configuration and the porosity of the scaffolds (150, 151). Such properties also make scaffolds suitable candidates for nanocarrier delivery studies as shown by Lopez *et al.* (2016) who focused on the diffusion properties of liposomes and micelles in a 3D collagen scaffold model (152). Scaffolds can be categorised into natural or synthetic scaffolds depending on the materials incorporated into them (153).

Natural scaffolds are mainly hydrogels that consist of mostly water (167) and natural components such as collagen type 1, Matrigel (a gelatinous complex protein mixture), agarose, elastin, laminin and hyaluronic acid (164) (168). Although the large volume of excess fluid with these models makes them mechanically, the hydrogel models allow the movement and proliferation of cells within a biological environment (169). However the low density of these models does not represent the density observed in the environment surrounding tumour cells *in vivo* (169). This problem can partially be resolved by the remodelling of the hydrogel to assist cell-matrix interaction studies and an increase in matrix density due to contraction (170).

The development of the plastic compression technology has led to production of better biomimetic scaffolds with increased cell and collagen density due to removal of interstitial fluid from the hydrogel model (171). The collagen density in these compressed hydrogels (c. 10% wt/wt) is similar to physiological values. The collagen stiffness and density in these scaffolds not only affects rate of cell growth as well as morphologies (172), but also enables the hypoxic core that is normally observed *in vivo* to be imitated *in vitro* as a result of the reduced oxygen diffusion through the denser matrix (169). Figure 5 demonstrates the stages involved in the formation of the compressed 3D model. Recent studies with compressed collagen hydrogels have used 'tumouroid' models consisting of a cancer mass surrounded by a multi-cellular stroma to investigate the uptake of nanoparticles as well as their use in enhancing drug delivery (173) (155). The construction of tumouroids was originally demonstrated by Nyga *et al*. (2013), who used plastic compression of collagen type I to create a colorectal tumouroid construct (174).

Synthetic scaffolds can also be developed from polymers such as polyactide (PLA), polyglycolide (PGA) and co-polymers (PLGA) (175). Such polymers are biodegradable and can be molded into a variety of structures such as mesh, fibers and sponge (176). In terms of mechanical structure, synthetic scaffolds are stronger than natural scaffolds and are able to specifically replicate biomolecular structures observed *in vivo* (177). However, one disadvantage associated with these polymers is the weaker cell adhesions therefore surface modifications are needed to overcome this issue (169).

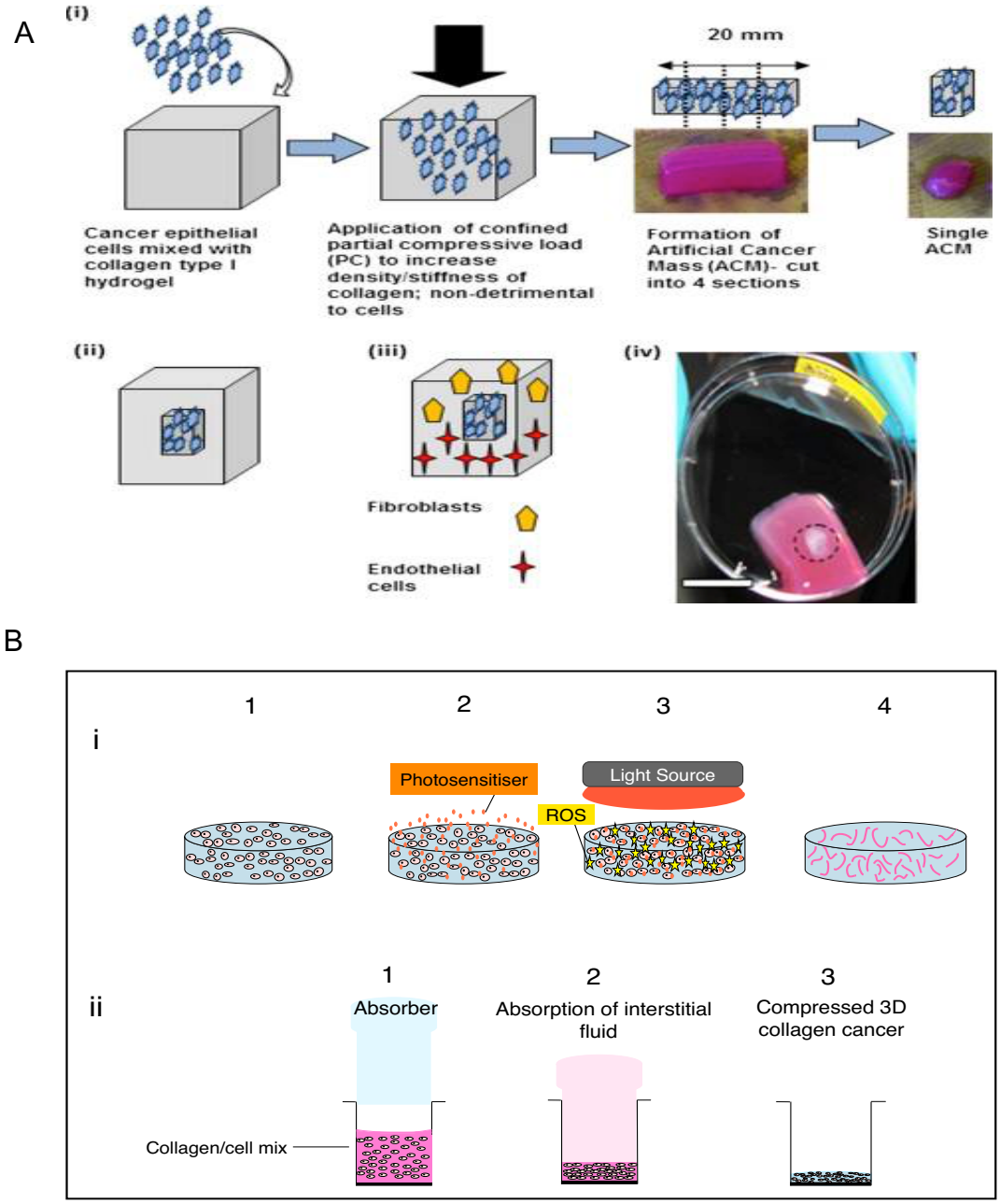

Figure 5: Fabrication of tumouroid constructs.A: The original method of creating simple and complex 3D compressed collagen cancer models (174). B: PDT in 3D compressed cancer constructs and the construction of compressed 3D cancer models (i) PDT using photosensitiser in 3D compressed collagen construct consisting of cancer cells surrounded by a matrix (eg type 1 rat tail collagen) illustrated with sequential procedures (80); Step 1: seeding of cancer cells in the collagen scaffold; Step 2, addition of a photosensitiser for cell uptake followed by washing; Step 3: the irradiation of the 3D model with light of a specific wavelength and generation of ROS. Step 4; the dead cancer cells in the collagen scaffold. (ii) Novel method of constructing compressed 3D collagen cancer models with higher collagen density for therapeutic studies illustrated sequentially. Step 1, the formation of collagen/cell mix before undergoing plastic compression using an insertable absorber to extract fluid from the hydrogel; Step 2 gradual absorption of the interstitial fluid from the collagen/cell mix by the absorber and the slow compression of the model; Step 3 the creation of the thinner (typically 200 μm depth) compressed 3D collagen cancer model following the absorption of the fluid from the model resulting in a ten-fold higher collagen density.

1.17 *In vitro* and *in vivo* studies of PDT

PDT has been used in many *in vitro* studies and *in vivo* studies to examine the effectiveness of various photosensitisers for treating different types of cancer. Some of the *in vitro* PDT studies have included the use of nanoparticles to improve the efficacy of the treatment (178).

There are numerous studies and reviews of PDT using conventional 2D models but in recent years the development and employment of 3D models for cancer studies including PDT has specifically provided many benefits for PDT-related investigations since their use allowed the uptake, localisation and efficacy of the drugs to be studied in more physiologically realistic models. In the following section, the types of 3D models being used are summarised. This section is later followed by a section that summarises PDT studies carried out using 3D models to date. A summary of the PDT studies which have involved the use of 3D models is provided in Table 1.

The studies summarised in table 1 have mainly used spheroid models for their experiments. Spheroids also known as spheres, nodules and micronodules are spheroidal 3D cancer models that can be several hundred μm in diameter. Till *et al*. (2016) employed the 3D spheroid model from human colorectal carcinoma cell line (HCT-116) and human squamous cell carcinoma cell line (FaDu) to investigate PDT efficacy of free pheophorbide photosensitiser (Pheo) compared to the use of encapsulated photosensitiser in crosslinked polymeric micellar self-assemblies and their uncrosslinked micellar counterparts (161). However, in another study Hung *et al*. (2016) used the ovarian cancer spheroid model from OVCAR5 cells to examine whether the dark toxicity of 5-ethylamino-9- diethylaminobenzo[a] phenothiazinium chloride (EtNBS) can be reduced through its encapsulation in PLGA nanoparticle (179). The same cell line was also used in two other studies by Evans *et al*. (2011), and Rizvi *et al*. (2013) to form ovarian cancer spheroids (180, 181). Like Hung *et al*., the study by Evans *et al*. also used EtNBS as a photosensitiser but in this case to study the effect of this photosensitiser on the hypoxic cell populations situated within the 3D spheroids. Rizvi *et al*. (2013) however, focused on the effect of Benzoporphyrin Derivative (BPD)-PDT on the ovarian cancer spheroids.

Photosensitiser	Nanoparticle	Description of 3D cancer model	Cancer cell line	Ref.
Methylene blue	-	Spheres on (poly 2- hydroxyethyl methacrylate) (polyHEMA) coated microwells in a microfluidic device	Human breast carcinoma (T47D)	(182)
Benzoporphyrin Derivative (BPD)	-	Micronodules on Matrigel matrix	Human ovarian carcinoma (OVCAR5)	(183)
5-ethylamino-9-diethylaminobenzo[*a*] phenothiazinium chloride (EtNBS)	-	Nodules on growth factor reduced (GFR) Matrigel matrix	Human ovarian carcinoma (OVCAR5)	(180)
BPD in DMSO	-	Micronodules on Matrigel matrix	Human ovarian carcinoma (OVCAR5)	(184)
BPD	-	Micronodules on Matrigel matrix	Human ovarian carcinoma (OVCAR5)	(181)
5-Aminolevulinic acid (5-ALA)	-	Nodules on Matrigel matrix	Human epidermal carcinoma (A431)	(45)
BPD, mono-N-aspartyl derivative of chlorin e6 (MACE)	-	Mammary architecture and micro-environment engineering (MAME) of breast cancer- Spheroids formed on glass cover slips coated with reconstituted basement membrane	Human breast carcinoma (SUM149, MDA-MB-231, Hs578T)	(185)
Tetraphenyl disulfonated porphyrin ($TPPS_{2a}$), Disulfonated tetraphenyl chlorin ($TPCS_{2a}$)	-	Single cells seeded in hydrogel (collagen) scaffold	Human prostate adenocarcinoma (PC3)	(137)
Tetraphenyl disulfonated porphyrin ($TPPS_{2a}$), Disulfonated tetraphenyl chlorin ($TPCS_{2a}$)	-	Single cells seeded in hydrogel (collagen) scaffold	Human head and neck squamous cell carcinoma (PCI30)	(186)
mTHPC	-	Single cells seeded in hydrogel (collagen) scaffold	Human breast carcinoma (MCF-7)	(187)
BPD	-	Nodules on Matrigel	Human ovarian carcinoma (OVCAR5)	(188)
Hypericin	-	Spheroid on agarose coating	Human bladder carcinoma (RT-112)	(189)
Ruthenium(II) polypyridyl complexes (Ru1- Ru3)	-	Spheroid on agarose coating	Human cervical carcinoma (HeLa)	(190)
Ruthenium(II) polypyridyl complexes (RuL1- RuL4)	-	Spheroid on agarose coating	Human cervical carcinoma (HeLa)	(191)

Fluorinated ruthenium(II) complexes (Ru1- Ru5)	-	Spheroid using liquid overlay method	Human cervical carcinoma (HeLa)	(192)
5- Aminolaevulinic acid (5-ALA) induced PPIX	Gold nanoparticle (AuNPs)	Nodules on microfluidic device	Human breast carcinoma (MCF-7)	(193)
Pheophorbide A (Pheo)	Micelles (poly ethyleneoxide-b-3-caprolactone)	Spheroid on ultra- low attachment well plates	Human colorectal carcinoma (HCT-116), Human squamous cell carcinoma (FaDu)	(161)
m-tetrahydroxyphenylchlorin (mTHPC)	Lipidots	Spheroid using hanging drop method	Human tongue squamous cell carcinoma (CAL-33)	(162)
EtNBS	Poly(lactic-co-glycolic acid) (PLGA)	Spheroid on Matrigel	Human ovarian carcinoma (OvCAR)	(179)
Cis-Bis(2, 2'-bipyridine)dichlororuthenium(II) hydrate	SWCNTs	Spheroid using liquid overlay method	Human cervical carcinoma (HeLa)	(194)
Chlorin e_6 (Ce6)	Reduced Graphene Oxide (rGO)	Spheroid	Human brain carcinoma (U87)	(195)
m-THPC	Liposome (Foslip™ and Fospeg™)	Spheroid using liquid overlay method	Human cervical carcinoma (HeLa)	(196)
Zinc Phthalocyanine (ZnPc)	Liposome	Spheroid on agarose coating	Human cervix adenocarcinoma (HeLa cells) and Mouse Mus musculus colon carcinoma (CT26)	(197)
Photofrin	Liposome	Spheroid using spinner flasks on a stir-plate	Human bladder carcinoma (MGHU3)	(198)
Indocyanine green	PLGA/lipid	Spheroid on agarose coating	Mouse breast carcinoma (4T1)	(199)

Table 1: Summary of PDT studies in 3D in vitro cancer models with or without nanoformulated photosensitisers

1.18 Pre-clinical and clinical studies of PCI

PCI has been studied pre-clinically *in vitro* (137)(186) and *in vivo* (137). The majority of studies have either been in 2D monolayer culture or using experimental tumour models in mice which are now briefly summarised in the following sections. For example, an *in vitro* and *in vivo* PCI study of colorectal adenocarcinoma and murine colon carcinoma models by Berg *et al*. (2005) found that $TPPS_{2a}$ and bleomycin significantly enhanced cytotoxicity by three times compared to bleomycin alone *in vitro*. The *in vivo* studies showed that photochemical internalisation of bleomycin led to delay in tumour regrowth. Furthermore 60% of the animals were found to be tumour free 200 days post PCI treatment, however in the case of PDT treated animals only 10% were found to be tumour free after the same period. None of the animals were found to be tumour free after treatment with bleomycin alone (139).

PCI using bleomycin combined with $AlPcS_{2a}$ lead to a significant delay in tumour growth in comparison to control groups which had not undergone PCI (139). In a different study, Arentsen *et al*. (2014) demonstrated enhanced cell killing in monolayer and multicellular spheroid cultures of bladder and brain cancer also using bleomycin PCI (200).

A clinical study using PCI in patients with local recurrent, advanced, or metastatic cutaneous or subcutaneous malignancies has also been conducted recently using Amphinex as photosensitiser and bleomycin as chemotherapeutic drug and the treatment was found to be safe and tolerable (201).

1.19 Advantages of PCI over PDT

Although both PDT and PCI share some common features, PCI offers several potential advantages over PDT. PCI relies on the use of sub-lethal PDT to trigger cytosolic release of agents entrapped within endolysosomes. Firstly, the lower dose of photosensitiser required for PCI could reduce skin photosensitivity that is normally associated with PDT. Secondly, compared to PDT, PCI may lessen and delay the damage caused to endothelial cells, that in turn leads to vascular shutdown, perhaps due to lower PCI light fluence used (202-204). Consequently oxygenation of the tumour required for production of singlet oxygen may be less affected by PCI thus resulting in greater eradication of the tumour (203). Another advantage of PCI is that the photosensitisers used for this treatment, e.g $TPPS_{2a}$, are not substrates for efflux via ABCG2 transporters which mediate cellular multidrug resistance whilst many of the second generation photosensitisers used in PDT have shown to be subject to efflux by ABCG2 (127, 205-208).

Lou *et al*. (2006) found that PCI was able to overcome doxorubicin resistance in MCF-7/ADR cells and render them nearly as sensitive to the drug as for the MCF-7 cells. Weak-base drugs like doxorubicin are thought to be susceptible to entrapment in endocytic vesicles of multiple drug resistant cells which exhibit increased acidification of the vesicles as well as increased cytosolic pH (209). Bostad *et al.* (2013) on the other hand used PCI to target CD133-positive colon cells (WiDr) using an immunotoxin consisting of mAb CD133/1 bound to ribosome inactivating plant toxin saporin (anti-CD133/1-sap). They found that $TPCS_{2a}$-PCI of anti-CD133/1-sap increased the effect of the immunotoxin. Furthermore, the WiDr cells were found to be resistant to PDT, whereas the use of PCI helped bypass this resistance (210).

1.20 Aims of the thesis

Due to the benefits that 3D cancer models offer over other simpler *in vitro* systems and based on the potential compressed collagen 3D models have in mimicking *in vivo* models, the aim of this thesis was to investigate and evaluate the potential of PDT and PCI in different 3D compressed collagen models of breast and ovarian cancer.

In this work experiments were conducted *in vitro* using monolayer and 3D constructs to serve as templates that could provide guidance for further *in vivo* studies that may be undertaken in the future. The outcomes from the aims set during this project have been presented in different sections within this thesis.

The main hypothesis was that Photochemical Internalisation (PCI) is an efficient means of enhancing the cytotoxicity of a macromolecular toxin when applied to cancer cells grown in a 3D model and could present an improvement in therapeutic efficacy compared to PDT.

Three cancer cell lines were selected for this project. These cell lines included breast cancer cell line (MCF-7) and ovarian cancer cell lines (HEY and SKOV3). MCF-7 cells are luminal A breast carcinoma cells which are oestrogen receptor positive (ER^+) and human epidermal growth factor receptor 2 negative ($HER2^-$) whilst the ovarian cancer cell lines form papillary cystadenocarcinomas and clear cell adenocarcinomas, respectively. The fact that all cancer cell lines used in this study develop in epithelial tissues, makes them suitable for treatment with PDT and PCI.

Drugs used in this study included the photosensitiser meso-tetraphenyl porphine disulfonate ($TPPS_{2a}$) and chemotherapeutic drugs Saporin and Dactinomycin. $TPPS_{2a}$, has two sulfonate groups substituted on adjacent phenyl rings of the porphyrin macrocycle which reside at the aqueous-lipid interface with the hydrophobic portion of the macrocycle inserted into the lipid bilayer. Saporin and Dactinomycin both have high molecular weights over 1000 Da and are therefore relatively large molecules which makes them prone to endolysosomal degradation and therefore suitable for delivery via PCI. Also, due to the fluorescence of dactinomycin, it can be used to show endolysosomal localisation via fluorescence imaging.

The primary objective was to examine the efficacy of PDT and PCI in treating monolayer as well as non-spheroid and spheroid constructs of breast and ovarian cancer cells using $TPPS_{2a}$ as a photosensitiser and saporin as the chemotherapeutic agent. The uptake of the photosensitiser as well as change in oxygen consumption with the growth of ovarian cancer cells in 3D were also investigated using fluorescence staining and microscopy.

The effects of pre-incubating the cells with the drugs prior to seeding as well as applying the treatments without chasing and the modes of cell death stimulated after each treatment were additionally studied using cytotoxicity assays and fluorescence imaging.

The second objective of this project was to test Dactinomycin also known as Actinomycin D as a chemotherapeutic drug in PCI studies in non-spheroid 3D ovarian cancer constructs using viability assays and to confirm the mechanism by which dactinomycin is uptaken by the cells.

The final objective of this project was to study the effect of PDT and PCI (using saporin as toxin) in complex tumouroid constructs of ovarian cancer which also included a stroma with stromal cell consisting of fibroblasts and endothelial cells. Since tumours *in vivo* are more complex than the simple models created *in vitro.* Embedding the original cancer mass in a bigger compressed collagen construct consisting of stromal cells allows the growing cancer cells to invade the stromal environment unlike the spheroid constructs where the cells could only grow within the simple cancer mass model. In this part of the study the invasion of stroma by cancer cells and the effect of PDT/PCI on the cancer cells in the original cancer mass and those that had invaded the stroma as well as stromal cells were examined. The regrowth of cancer cells after PDT treatment was also examined.

Chapter 2

2. Methods and Materials

2.1 Cell culture

Human breast (MCF-7) and ovarian (SKOV3 and HEY) carcinoma cell lines (American Type Culture Collection, ATCC, U.S.) were cultured in Dulbecco's modified Eagle's medium (DMEM/F-12, low glucose, Sigma Aldrich, UK) using aseptic techniques. Human dermal fibroblasts (HDFs) and Human umbilical vein endothelial cells (HUVECS) (both used as cell lines by previous researchers in our group and were available at Division of Surgery and interventional Sciences, UCL) were cultured in high glucose DMEM (Gibco, by Life Technologies, Thermo Fisher Scientific, UK) and endothelial cell growth medium (PromoCell, UK) respectively using aseptic techniques. All cell culture mediums again consisted of 10% heat inactivated fetal bovine serum (FBS, Gibco by Life Technologies, Thermo Fisher Scientific, UK) and 1% penicillin (5000 units/mL) and streptomycin (5000 μg/mL) solution (Gibco by Life Technologies, Thermo Fisher Scientific, UK).

MCF-7 cells are luminal A breast carcinoma cells which are oestrogen receptor positive (ER^+) and human epidermal growth factor receptor 2 negative ($HER2^-$) whilst the ovarian cancer cell lines form clear cell adenocarcinomas and papillary cystadenocarcinomas, respectively.

2.2 Alamar blue cytotoxicity assay

The cell viability in the 2D monolayer cultures and 3D cancer models were measured using the Alamar Blue reagent (Invitrogen, Thermo Fisher Scientific, UK). Alamar blue reagent functions through its active component “resazurin” changing colour from blue to pink upon becoming reduced by the metabolic activity of viable cells. The working solution of this assay was made by the addition of the dye to fresh culture media with the dye making up 10% of the overall solution. The models were incubated with the Alamar blue solution for 4 hours and the solutions were transferred from each well into a corresponding well in a black well plate (TPP, Sigma Aldrich, UK) for measurements. The fluorescence intensities were measured at wavelengths of ($\lambda_{Ex/Em}$ 530nm /620nm) using Fluoroskan ascent FL plate reader (Thermo Labsystems, UK). Treatment-free monolayer cultures and 3D models were also used as controls. The MTT assay based on absorbance was used solely for measuring viability in 2D cultures.

2.3 MTT cytotoxicity assay

The MTT assay was used to measure cell viability in the monolayer cultures. This assay functions through the reduction of the tetrazolium dye by NAD(P)H dependent oxireductase enzymes in viable cells. The MTT reagent (Thiazolyl Blue Tetrazolium Bromide, Sigma Aldrich, UK) was dissolved in cell culture media at concentration 1mg/mL and filtered before being applied to monolayer cultures, which underwent incubation for 2 hours. The MTT solution was then removed and DMSO (Sigma Aldrich, UK) was added to the well plates to dissolve the crystals formed. Absorbance was measured at 562nm using absorbance plate reader (BioTek, ELx800, U.S.).

2.4 Total DNA cytotoxicity assay

In preparation for the Total DNA assay which measures the amount of intact DNA in the samples, media from SKOV3 monolayer cultures were removed from the wells and the cells were washed with PBS at the end of the PCI experiment. The PBS was then removed and replaced with 100µL of distilled water per well. The cells were lysed following 3 freeze thaw cycles where each cycle involved placing the well plates in -80 C and then at room temperature for 30-45 minutes each. A serial dilution (concentrations 0-10 µg/mL) used for generating a standard curve were prepared in duplicates from the cell thymus DNA provided in the total DNA kit (Sigma Aldrich, UK) and 100µL each were added to well in a black well plate. Once the cell lysis process was complete, 100µL of the SKOV3 cell lysates were added to each well plate in a black well plate. (Hoescht 33298) fluorescent dye solution was prepared at (1:100) dilution with assay buffer. 100µL of Fluorescent dye solution was then added to each well containing the SKOV3 cell DNA and the standard DNA resulting in 200µL volume per well and were mixed well. The Fluorescence levels were measured using an excitation wavelength of 360nm and an emission wavelength of 460nm in a Fluorescence microplate reader (Fluorosckan Ascent FL, Thermo Fisher Scientific, UK).

2.5 Fabrication of simple non- spheroid and spheroid 3D cancer constructs

The 3D *in vitro* compressed spheroid and non-spheroid cancer constructs were created following the protocol from RAFT 3D culture systems (Lonza, Slough, UK) (211) (212). The compressed 3D culture system contains a cell-embedded Type 1 collagen matrix that has been subjected to plastic compression through the use of fluid absorbers producing 3D constructs with a thickness of c. 200 µm (collagen density, 9.6%) in wells of a 96 well plate (212).

The hydrogels were prepared from a mixture containing 10% 10x medium essential medium (MEM) (used as colour/ pH indicator) (Gibco by life technologies, Thermo Fisher Scientific, UK), 80% Rat Tail Collagen Type I (First Link UK Ltd. Custom Bio-Reagents) before undergoing neutralisation using neutralising solution made from 1.65 M NaOH and 840 mM HEPES buffer solution (Gibco by Life Technologies, Thermo Fisher Scientific, UK). The cells were seeded separately into each collagen mix at concentrations of 75,000 cells (determined after a cell density gradient experiment) for non-spheroidal models and 50,000 cells for spheroidal constructs at volumes of 240μL per well in 96 well plate (TPP, Sigma Aldrich, UK). The constructs were incubated at 37℃ for 15 minutes to set before being subjected to plastic compression using absorbers (Lonza, UK) at room temperature for a further 15 minutes. After the removal of the absorbers, Fresh media was added to each construct before incubation at 37℃. The cell culture media of the constructs were changed daily.

2.6 Cell seeding and imaging of spheroid formation

The response of larger spheroids, consisting of multicellular aggregates of SKOV3 and HEY cells that grew over a period of 7 days prior to treatment were investigated. As part of the pilot study, cell morphology and spheroid formation at different time points (days 3, 5 and 7) after the initial seeding and compression were investigated using fluorescently labelled Phalloidin to visualise filamentous actin, and the Hoechst 33258 dye to observe the cell nuclei. The constructs were fixed with Formalin (10%) and washed with PBS. They were then permeabilised with 1% BSA and 0.3% Triton X solution and stained with Phalloidin (2.5% in BSA /Triton-X solution) for 90 minutes before washing with PBS (3x) and further staining with Hoechst 33258 ($\lambda_{Ex/Em}$ 352/461 nm), 2 μg/mL in PBS for 10 minutes. Alexa Fluor 488 labelled Phalloidin ($\lambda_{Ex/Em}$ 495/518 nm, Molecular Probes, Life Technologies) and Hoechst 33258 ($\lambda_{Ex/Em}$ 352/461 nm, Sigma-Aldrich) were imaged using an EVOS fluorescence inverted microscope (EVOS FL color, Life Technologies, Thermo Fisher Scientific, UK). The cellular aggregate sizes were measured using image analysis by delineating the boundary and the area was computed by the software. Approximately 20-30 aggregates were measured per construct. The same imaging technique using Phalloidin/ Hoechst 33258 was used in therapeutic studies of spheroids that followed later. Image analysis of the fluorescence images was carried out using the open source ImageJ software (NIH, US). In general, the HEY cells formed a higher population of larger spheroids compared to SKOV3 cells. Although irregular in shape they approximate to a circular shape, with the approximate diameters being estimated using the cross-sectional area. The small (approximately < 50 μm in diameter) and medium (100-150 μm) aggregates predominated (over 50% of total sampled) in the SKOV3 constructs whereas

the medium and large (approximately >150 μm) predominated in the HEY constructs.

2.7 Fabrication of Tumouroid constructs

The tumouroid construct was created using a compressed cancer mass, which was sandwiched between two layers of collagen containing stromal cells (fibroblasts and endothelial cells).

The cancer masses were developed following the same protocol described in section 2.5 using 50,000 cells/construct seeding density. The artificial stroma was then created also following the same steps as above to prepare the hydrogels with HDFs and HUVECS seeded at densities of 25,000 and 50,000 cells respectively (densities-based protocol by Magdeldin *et al*. (2017)) (212) and volumes of other components as instructed by Lonza. First half of the total volume per well (650μL) of the stromal cell/collagen mix was added to each well on a 24 well plate (Corning, Costar) and allowed to set slightly at room temperature for 5 minutes. The cancer constructs were then removed from the 96 well plate and each placed on top of a slightly set stroma hydrogel in the 24 well plate before being topped with an additional 650μL of the stroma cell/collagen mix (totaling 1.3 mL per well) and incubated at 37℃ for 15 minutes to set well. Once set well the tumouroid hydrogels undergo compression using absorbers (Lonza, UK). Upon removal of the absorbers, 200μL of each media (600μL in total) appropriate to the individual cell lines included in the tumouroid construct was added per well. Based on previous experiments on mature 3D constructs, the tumouroids constructs were incubated at 37℃ for 7 days to allow the HEY cells to grow forming spheroid like structures and metastasise prior to undergoing treatment. The cell culture media of the constructs was changed on daily basis. Figure 6 shows partially compressed 3D tumouroid collagen hydrogels. The fully compressed 3D tumouroid collagen constructs are shown in Figure 7.

Figure 6: Partially compressed 3D tumouroid collagen hydrogels. The compressed cancer mass embedded between the two layers of hydrogels containing stromal (fibroblasts and endothelial) cells.

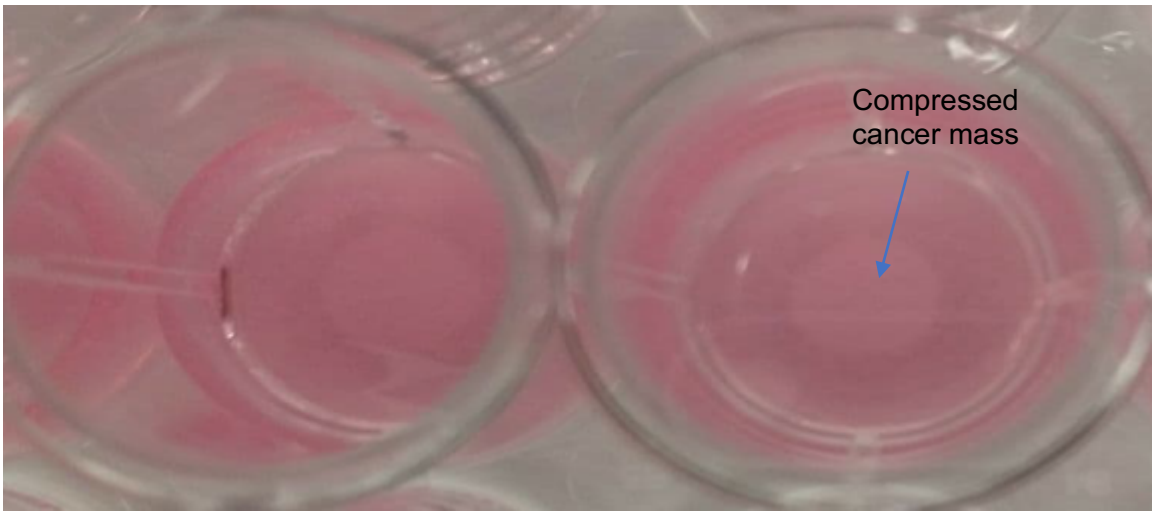

Figure 7: Compressed 3D tumouroid constructs. The construct consists of a compressed cancer mass created in a 96 well plate which is sandwiched between two layers of compressed collagen constructs containing stromal cells in a 24 well plate.

2.8 *In vitro* PDT/PCI phototoxicity studies in 2D monolayer cultures

PDT and PCI treatments were carried out in 2D monolayer cell culture for the purpose of comparing the results to the 3D constructs. HEY, SKOV3 and MCF-7 cells were seeded as well as cultured at a density of (5000 cells/ well) in 96 well plates for 24 hours. Concentrated stock solutions of the photosensitiser, $TPPS_{2a}$ (Frontier Scientific Inc. U.S.), were prepared in dimethyl sulfoxide (DMSO). $TPPS_{2a}$ absorbs across the visible spectrum with its longest wavelength peak at 650 nm but strongest absorption peak at c. 420 nm (Soret band) and emits red fluorescence (600-720 nm). Initial screening studies were carried out with each cell line to determine appropriate concentrations of the $TPPS_{2a}$ and the cytotoxic agent, saporin (Sigma Aldrich). Cells were incubated with $TPPS_{2a}$ 0.4μg/mL (HEY) and 0.3μg/mL (SKOV3 and MCF-7) alone respectively (for PDT only), Saporin (Sigma Aldrich, UK) only (concentrations ranging from 10nM-20nM) or Dactinomycin (1nM) (Sigma Aldrich, UK) and co-incubation of $TPPS_{2a}$ and saporin or $TPPS_{2a}$ and Dactinomycin (for PCI) with all drugs being dissolved in media before addition. Similar drug doses have been used in previous studies in the lab. Figure 8 demonstrates a time- line showing the steps involved in the PDT/PCI treatment of cultures.

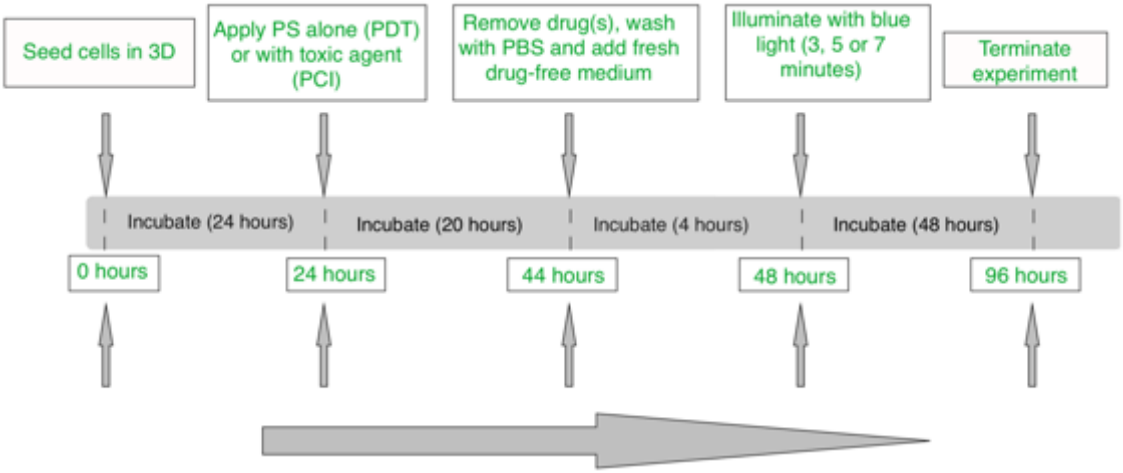

Figure 8: Time- line showing the process of carrying out PDT/PCI experiment in a non- spheroid 3D construct. The process was carried out for cultures that were seeded as monolayer cultures. For the spheroid and tumouroid constructs, the constructs were incubated for 7 days before the addition of drugs. As the time-line shows in this figure, the samples were incubated for 48 hours post illumination however, in some cases, the experiments were terminated 96 hours post illumination.

The cells were then incubated for 20 hours before being exposed to drug removal, thorough washing with phosphate-buffered saline (PBS, PH 7.4, Sigma Aldrich, UK) and fresh media replacement (to prevent the occurrence of strong PDT effect exerted by photosensitiser residing in the extracellular membrane). Incubation was repeated for a further 4 hours and then the cells treated with light irradiation using blue lamp (Lumisource, 7mW/cm^2, PCI Biotech, Norway) (shown in Figure 9) with peak emission at 423 nm for periods of 3 minutes, 5 minutes and 7 minutes. The cells were again incubated for either a further 48 or 96 hours at 37℃ before being subjected to termination of the experiment using the Alamar blue or MTT assay.

Figure 9: Blue lamp (Lumisource, 7mW/cm^2, PCI Biotech) used for the irradiation of the constructs. The constructs were illuminated for less than 10 minutes for each experiment.

2.9 *In vitro* PDT/PCI phototoxicity studies in 3D cancer constructs

The non-spheroid 3D constructs of SKOV3, HEY and MCF-7 cells were seeded at densities of 75,000 cells/well. Cell densities of 50,000 cells/well were used for spheroid constructs of SKOV3 and HEY cells as well as tumouroid constructs of HEY cells. The non-spheroid cultures were treated following the same protocol, which was used for 2D monolayer cell cultures for all three cell lines with the concentrations of the drugs used in the non-spheroid constructs also remaining the same as those used in the 2D monolayer cultures as the pilot studies indicated that the same concentrations of the drugs were appropriate. Saporin (40nM) was also used for treating SKOV3 and MCF-7 non- spheroid constructs. For the spheroid and tumouroid cancer models however the addition of drugs for either PDT or PCI was carried out on day 7 (ie 7 days post initial seeding) and the rest of the experiment continued until day 10 (termination point). Pilot studies showed that the concentrations of $TPPS_{2a}$ used for HEY and SKOV3 cells in the spheroid constructs and the HEY tumouroid constructs also varied from the ones used for both 2D and non-spheroid cultures. Such concentrations were 0.5μg/mL (HEY cells) and 0.7μg/mL (SKOV3 cells). Saporin concentrations ranging 20-40 nM were used for spheroid constructs and 20nM for tumouroid constructs. In the tumouroid constructs concentrations of $TPPS_{2a}$ used for the PDT experiments were 0.5μg/mL and 1μg/mL although for the PCI experiments the concentration 0.5μg/mL was determined to be appropriate based on previous experiments with spheroid cancer constructs, which indicated that such concentration caused sub-

lethal PDT effect. While the non-spheroid and spheroid constructs underwent light illuminations of 3, 5 and 7 minutes using blue lamp (Lumisource, 7mW/cm^2, PCI Biotech, Norway) the tumouroid constructs were illuminated for 3 minutes (PCI experiment) and 5 minutes (PDT experiment). The non-spheroid, spheroid and tumouroid constructs were incubated at 37℃ for a further 48 hours post illumination before the termination of the experiment. Upon termination of the experiments, the cell viabilities in the non-spheroid and spheroid constructs were measured using Alamar blue assay and fluorescence plate reader (Fluoroskan, Ascent FL, Thermo Fisher Scientific, UK) and images were obtained with Live-dead imaging assay (non-spheroid and spheroid) and Phalloidin/ Hoechst 33258 staining (spheroid) using EVOS fluorescence microscope (EVOS FL color, Life Technologies, Thermo Fisher Scientific, UK). The tumouroid constructs were stained with Cytokeratin 7 (Alexa Fluor 488) $\lambda_{Ex/Em:}$ 490/525 conjugated antibody (Abcam, UK) (for HEY cells), Anti- Vimentin (Alexa Fluor 405) $\lambda_{Ex/Em:}$ 401/421 conjugated antibody (Abcam, UK) (for HDFs) and Anti-CD31 (PerCP-eFluor 710) $\lambda_{Ex/Em:}$ 482/709 conjugated antibody (eBioscience, Thermo Fisher Scientific, UK) and imaged using Olympus fluorescence microscope (Olympus BX63).

For studying the effect of PDT/PCI on invasion of stroma by cancer cells in tumouroid constructs, 8 measurements were taken from the original cancer mass of each construct to the longest distance invaded (starting clockwise and covering all the angles around the original cancer mass).

2.10 *In vitro* PDT/PCI phototoxicity studies in 3D fibroblast constructs

The effect of PDT/PCI on the stroma environment of the tumouroid construct was studied separately. HDF and HUVEC cells were seeded in compressed collagen construct in 24 well plate and densities of 25,000 and 50,000 cells/construct respectively. The constructs were incubated at 37℃ for 7 days before being incubated with either $TPPS_{2a}$ (0.5μg/mL) for (PDT) or $TPPS_{2a}$ (0.5μg/mL) and saporin (20nM) for (PCI) for 20 hours. The constructs were then washed with PBS and incubated with fresh media at 37℃ for a further 4 hours before undergoing 3 minutes of irradiation with blue lamp (Lumisource, 475nm, 7mW/cm^2, PCI Biotech, Norway). 48 hours post illumination, the fibroblast cells were stained with Anti- Vimentin (Alexa Fluor 405) $\lambda_{Ex/Em:}$ 401/421 conjugated antibody (Abcam, UK) and imaged using Olympus fluorescence microscope (Olympus BX63) (shown in Figure 10).

Figure 10: EVOS Fluorescence microscope (EVOS FL color, Life Technologies).

2.11 Tumouroid re-growth studies

The tumouroid constructs were treated with PDT using $TPPS_{2a}$ (0.5μg/mL) and 3 minutes illumination period 7 days post-seeding. The constructs were then incubated at 37℃ for a further 7 days prior to termination of the experiment. Upon termination of the experiment the constructs were stained with Cytokeratin 7 (Alexa Fluor 488) conjugated antibody and imaged using Olympus fluorescence microscope.

2.12 *In vitro* PCI phototoxicity studies in monolayer and 3D cancer cultures in hypoxic conditions

Monolayer and non-spheroid cultures of SKOV3 cells were seeded at densities of 5,000 cells/well and 75,000 cells/construct respectively and incubated at 37℃ in normoxic conditions (20% oxygenation) for 24 hours. The constructs were then incubated in the same conditions with $TPPS_{2a}$ (0.3 μg/mL) only, saporin (40 nM) only or combination of saporin and $TPPS_{2a}$ for 20 hours before undergoing washing with PBS. Afterwards the constructs were incubated for a further 4 hours with fresh medium without drug or photosensitiser in a hypoxia incubator (Innova co-48, New Brunswick™ scientific, UK) (Figure 11) (1% oxygenation) prior to light exposure; the well plates were sealed just

before light irradiation to prevent reoxygenation. The constructs were then exposed to blue light for 7 minutes, which under normoxia elicits a large reduction in viability. The experiment was terminated by measuring cell viability using Alamar blue assay (Invitrogen, Thermo Fisher Scientific, UK) and live-dead staining (Molecular Probes, Thermo Fisher Scientific, UK) and imaging. For the spheroid constructs the same process was repeated after 7 days of incubation (cell seeding density: 50,000 cell/ construct) at 37℃ in normoxic conditions (to allow spheroids to form) using $TPPS_{2a}$ (0.7 μg/mL).

Figure 11: Hypoxia incubator (Innova co-48, New Brunswick™ Scientific).

2.13 *In vitro* PCI phototoxicity studies in 3D cancer cultures pre-incubated with drugs

The SKOV3 and MCF-7 cells were pre-incubated with either $TPPS_{2a}$ only (0.3 μg/mL), saporin (20nM) or both drugs 24 hours prior to seeding in 3D constructs. The constructs underwent light illumination using a blue lamp for 7 minutes (light source), 24 hours after seeding. Alamar blue assay (Invitrogen, Thermo Fisher Scientific, UK) ($\lambda_{Ex/Em}$ 530nm/620nm) and live-dead assays (Thermo Fisher scientific, UK) were carried

out 48 hours post light illumination. The alarm blue measurements were obtained using fluorescence plate reader (Fluoroskan Ascent FL, Thermo Fisher Scientific, UK) and live-dead images were obtained using fluorescence microscope (EVOS FL color, Life Technologies, Thermo Fisher Scientific, UK).

2.14 PCI experiment without chasing in 2D and 3D cancer cultures

The SKOV3 and MCF-7 monolayer and 3D cultures were seeded in a 96 well plate and incubated with $TPPS_{2a}$ only (0.3 μg/mL), saporin (20nM) or both drugs 24 hours after seeding. The drugs remained in the culture medium and the chasing step omitted, ie the drug removal and washing step. The cells underwent light illumination using the blue lamp for various periods, 24 hours after initial incubation with the drugs. The Alamar blue assay (Section 2.12) was carried out 48 hours post illumination with measurements being taken using a fluorescence plate reader (Fluoroskan Ascent FL, Thermo Fisher Scientific, UK).

2.15 Temperature based mode of dactinomycin uptake by ovarian cancer cells in monolayer cultures

This purpose of this experiment was to confirm the uptake of Dactinomycin via endocytosis. For this experiment SKOV3 cells were seeded in a 96 well plate and incubated with Dactinomycin (1nM) (Sigma Aldrich, UK) for 2 hours either at 4°C or 37°C, 24 hours after seeding. The drug was removed at the end of the 2-hour incubation period and the cells were washed with PBS prior to being treated with fresh drug-free media. The cells were incubated at either 4°C or 37°C for a further two hours before the fluorescence levels were measured using a fluorescence plate (TECAN, infinite M200 PRO, Switzerland) at ($\lambda_{Ex/Em}$ 420/580nm).

2.16 Live/dead staining for fluorescence imaging

At set time points following treatment, the 3D constructs were stained for viability imaging using the Live-dead viability kit (Molecular Probes, Thermo Fisher Scientific, UK). 3D constructs were incubated with the Live-dead solution containing 0.05% of 4 mM Calcein-AM ($\lambda_{Ex/Em}$ 495/515 nm) and 0.2% of 2 mM Ethidium homodimer-1 ($\lambda_{Ex/Em}$ 495/635 nm) at room temperature for 30 minutes before imaging with an inverted fluorescence microscope (EVOS FL color, Life Technologies, Thermo Fisher Scientific, UK).

2.17 Immunostaining for fluorescence imaging

Following the termination of the experiment, the tumouroids were stained using Anti-Cytokeratin 7 (Alexa Fluor 488) $\lambda_{Ex/Em:}$ 490/525 conjugated antibody (Abcam, UK) (for HEY

cells), Anti- Vimentin (Alexa Fluor 405) $\lambda_{Ex/Em:}$ 401/421 conjugated antibody (Abcam, UK) (for HDFs) and Anti-CD31 (PerCP-eFluor 710) $\lambda_{Ex/Em:}$ 482/709 conjugated antibody (eBioscience, Thermo Fisher Scientific, UK) to image the constructs. Prior to the staining process, the tumouroids were fixed using Formalin (10%) (CellPath) solution for 10 minutes before being washed with PBS. The cells in constructs were then permeabilised using 1% BSA and 0.3% triton X solution for 30 minutes before undergoing washing with PBS once again. The anti-cytokeratin 7 (Alexa Fluor 488) and anti-CD31 (PerCP-eFluor 710) antibody conjugated solution was prepared with the immunostains being mixed in 1% BSA and 0.3% triton X solution at ratios of 1/100 and 1/500 Respectively before being added to the tumouroid constructs and incubating at 4℃ overnight (20 hours). The stains were then removed, and the constructs were washed 3 times with PBS each time incubating at room temperature for 5 minutes. Finally, the anti-vimentin (Alexa Fluor 405) conjugated antibody stain was mixed in PBS at ratio of 1/200 before being added to the tumouroid constructs and incubating for 3 hours at room temperature. At the end of the 3 hours, the constructs were washed with PBS and placed between a glass slide and cover slip in preparation for imaging. Images were taken with Olympus fluorescence microscope (Olympus BX63) using the pre-selected filter channels, FITC (for HEY cells), DAPI (for HDFs) and Cy7 (for HUVECS), and either 4x and 10x objectives.

2.18 Imaging hypoxia levels in 3D constructs

The reductions in oxygen levels within the cellular aggregates in the spheroid constructs as well as treated non-spheroid constructs of both cell lines were imaged using Image-iT Hypoxia reagent kit (488 nm excitation/ 610 nm peak emission, Molecular Probes by Life Technologies, Thermo Fisher Scientific, UK) according to the protocol supplied by the manufacturer. Two μL of 1 mM hypoxia reagent were added and mixed with 100 μL of cell culture medium in each well. Imaging of the well plates was carried out with an inverted fluorescence microscope (EVOS FL color, Life Technologies, Thermo Fisher Scientific, UK).

The Image-iT Hypoxia Reagent is a fluorogenic compound which fluoresces in environments with low oxygen concentrations and therefore the emission intensity of this reagent correlates inversely to the oxygen partial pressure. Control constructs had cells incubated without the hypoxia reagent in normoxic conditions, and cells incubated with the hypoxia reagent in normoxic conditions.

2.19 $TPPS_{2a}$ uptake and localisation

To examine the uptake of $TPPS_{2a}$ within the SKOV3 and HEY cells in non-spheroid

constructs (75,000 cells/construct), the constructs were incubated with $TPPS_{2a}$ (1μg/mL), for 20 hours. Afterwards, the constructs were washed with PBS and incubated with fresh cell culture medium without photosensitiser for a further 4 hours before imaging. The constructs were imaged with a fluorescence microscope with quasi-confocal structured illumination capability (20x objective, Apotome.2, Carl Zeiss). The optical sectioning capability of this microscope enabled imaging within the 3D gels with retention of imaging resolution. Fluorescence from the photosensitiser was recorded within the range of 600-700 nm using Alexa Fluor 647 channel. To determine the intracellular localisation of $TPPS_{2a}$ within non-spheroid constructs, separate constructs of both cell lines were prepared (10,000 cells/model). The constructs were incubated with $TPPS_{2a}$ (3 μg/mL) for 20 hours before washing with PBS and incubating with fresh medium for 3.5 hours. The medium was then replaced with fresh medium containing LysoTracker Green (Molecular Probes, Thermo Fisher Scientific, UK) at 100 nM concentration for 30 minutes before microscope imaging. The constructs were washed 2 times with PBS and incubated with drug-free medium for imaging with Olympus fluorescence microscope (20x objective, Olympus BX63). The fluorescence from LysoTracker green and $TPPS_{2a}$ were recorded at 520 nm and 650nm respectively. A lower number of cells were used in these constructs as it allowed the co-localisation of Lysotracker Green and $TPPS_{2a}$ to be observed more clearly. Confocal imaging was also used to look at the uptake of $TPPS_{2a}$ in 3D, however the system was not sensitive enough to provide any suitable results.

2.20 Intracellular uptake of Dactinomycin in monolayer and 3D cultures

Both cell lines were seeded on Petri dishes with a central glass cover slip base (Fluorodishes, WPI, UK) at density of 5000 cells/dish (monolayer cultures) and SKOV3 cells were seeded at density of 10,000 cells/ construct (3D non-spheroid cultures) and incubated at 37℃ for 24 hours. The cells were then treated with Dactinomycin (Sigma-Aldrich, UK) at 50nM concentration for 4 hours at 37℃. At the end of that incubation period the excess drug was removed from the dishes and the cells were washed with PBS before being incubated with fresh medium containing Lysotracker red (Molecular Probes, Thermo Fisher Scientific, UK) at 100 nM concentration for 30 minutes before microscope imaging. The constructs were washed with PBS and incubated with drug-free medium for imaging with Olympus fluorescence microscope (60x objective (2D) and 20x objective (3D), Olympus BX63). The fluorescence from LysoTracker red and Dactinomycin were recorded at 590 nm and 520nm respectively.

2.21 Mode of cell death (apoptosis/necrosis studies)

Annexin V-FITC apoptosis detection kit (Abcam, UK) was used to confirm the initiation of necrosis and apoptosis in different treated 3D non-spheroid (SKOV3 and HEY cells) and spheroid (HEY cells) cancer constructs compared to non-treated control 3D cancer constructs. The cells were seeded at density of 75,000 cells (non-spheroid) and 50,000 (spheroid) per compressed collagen construct and incubated for either 24 hours (non-spheroid constructs) or 7 days (spheroid constructs) prior to treatment. The constructs were incubated with either $TPPS_{2a}$ only (0.3μg/mL for SKOV3 cells) (0.4μg/mL for HEY cells) (PDT) (for non-spheroid constructs) or (0.5μg/mL for HEY cells) (spheroid constructs), saporin only (20nM) or a combination of both drugs (PCI) and were illuminated 24 hours after initial incubation with the drugs (4 hours after drug removal, washing with PBS). Either 24 hours or 48 hours after being exposed to irradiation with blue lamp, 100μL of 1X Binding buffer was added to the models in each well before adding 1μL of Annexin V-FITC, ($\lambda_{Ex/Em}$ 488/525 nm) and 5μL of propidium iodide, ($\lambda_{Ex/Em}$ 535/617 nm) to the buffer solution in each of the wells. The models were then imaged using an EVOS fluorescence microscope (EVOS FL color, Life Technologies, Thermo Fisher Scientific, UK).

2.22 Evaluation of synergistic effects

To evaluate whether a synergistic interaction between the two separate therapies applied, we used the following equation to calculate the value of alpha (∝):

$$\propto = \frac{F_{PDT}\, x\, F_{cytotoxin}}{F_{combination}} \qquad \text{equation 1}$$

In the numerator of equation 1, the terms F_{PDT} and $F_{cytotoxin}$ designate the fractional viability for each separate therapy, PDT and the application of the cytotoxin, and the denominator is the fractional viability observed following the PCI combination treatment. If α > 1 then a synergistic effect is present whereas an antagonistic effect is denoted by α < 1. This analysis has been used previously by us and others to identify synergistic effects in PCI (130, 137, 213).

To assess the efficacy of PCI (PCI efficacy) versus cytotoxin alone, we calculated the ratio of the viability without PCI (i.e. cytotoxin alone) divided by the viability measured after PCI. Likewise, to assess the PCI efficacy versus PDT alone, we calculated the ratio of the viability with PDT divided by the viability measured after PCI.

2.23 Data analysis

Experiments were carried out in triplicate. Results were analysed using 2-way ANOVA with post-hoc analysis and values of $P < 0.05$ were considered to be statistically significant. Error bars from the mean show +/- standard deviation (SD).

2.24 Image analysis

The images used for finding the distance of which the cancer cells had invaded the stroma in tumouroid constructs were analysed using open source Image J software (NIH, US). An average from 8 measurements were taken from each tumouroid.

Chapter 3

3. Photochemical internalisation in 3D constructs of breast and ovarian cancer using saporin as the chemotherapeutic drug

In this chapter PDT/PCI experiments are described on 2D and 3D non- spheroid compressed collagen constructs of breast (MCF-7 cells) and ovarian cancer (SKOV3 and HEY cells) using $TPPS_{2a}$ as a photosensitiser and saporin as the chemotherapeutic agent. The compressed collagen constructs are approximately 200μm thick. The experiments on the monolayer cultures were initially carried out as pilot studies and for comparative purposes to the non-spheroid 3D constructs. The treatments were also repeated on spheroid 3D compressed collagen constructs of ovarian cancer (SKOV3 and HEY cells). In addition, the uptake of the photosensitiser by the SKOV3 and HEY cells (2D and 3D non-spheroid cultures) and the modes of cell death stimulated by each treatment (3D non-spheroid and spheroid cultures) were investigated. Due to the important role oxygen availability plays in the effectiveness of both PDT and PCI, the dependence of the treatment efficacy on oxygen levels in non-spheroid and spheroid cultures was examined. The effects of pre-incubating the cells with the drugs prior to seeding (to study the effect of the collagen matrix on drug uptake and efficacy) as well as applying the treatments without chasing were also investigated.

3.1 *In vitro* PDT/PCI phototoxicity studies in 2D monolayer cancer cultures

PDT experiments were initially carried out using a range of $TPPS_{2a}$ concentrations to determine the concentration, which results in sub-lethal PDT effect and is therefore suitable for PCI experiments. In HEY cells, PDT using $TPPS_{2a}$ concentrations ranging from 0.2-0.6 μg/mL were first tested with the MTT assay (Figure 12): 0.4 μg/mL was found to cause a suitable sub-lethal PDT effect (66% cell viability) required for PCI to work after treatment with the lowest illumination period used in our studies (3 minutes). The sublethal PDT effect would also be important for reducing side effects caused by PDT clinically. Since Alamar blue was the assay used in the PDT/PCI studies on the 3D constructs, this assay was also tested on some of the monolayer cultures for comparative purposes. When testing with Alamar Blue the sub-lethal concentration (0.4 μg/mL) identified by MTT was used as the lowest concentration in the range studied. The Alamar blue results (Figure 13) also showed that 0.4 μg/mL was the suitable $TPPS_{2a}$ concentration to use as it resulted in 82% viability in the HEY cells after 3 minutes of light illumination. Although

in the two assays a difference of 16% can be seen in the percentage viabilities achieved post PDT with $TPPS_{2a}$ 0.4 μg/mL, both assays reveal this to be the most appropriate concentration to use for PCI compared to the other concentrations of $TPPS_{2a}$ tested.

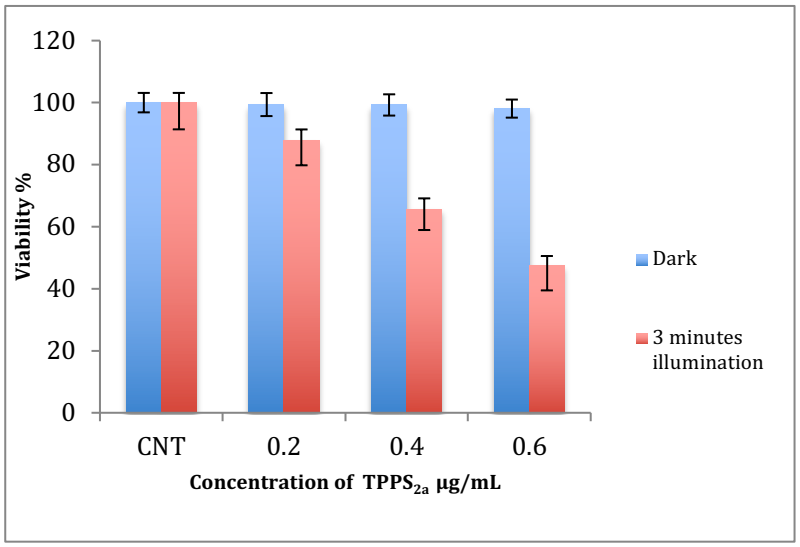

Figure 12: Viability of HEY cells post PDT treatment using different concentrations of $TPPS_{2a}$ (MTT assay). The samples were illuminated with blue lamp (420nm). MTT assay was used measurement of cell viability in this experiment.

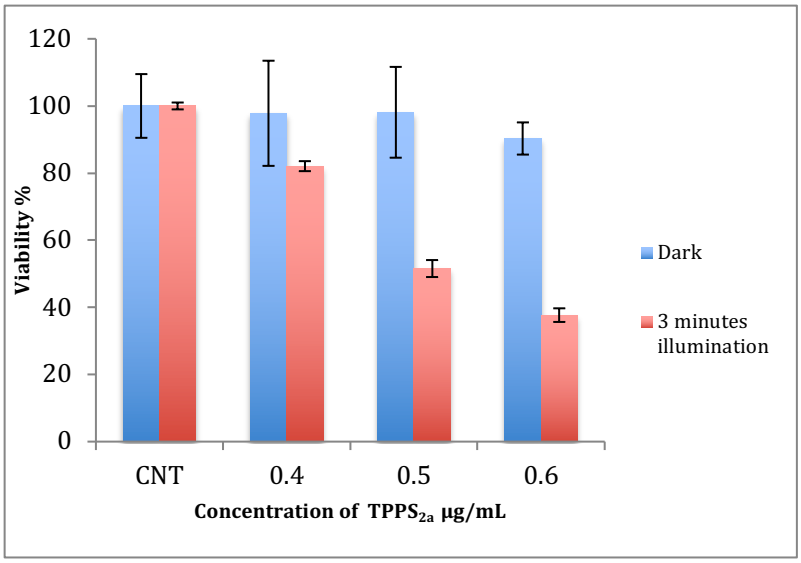

Figure 13: Viability of HEY cells post PDT treatment using different concentrations of $TPPS_{2a}$ (Alamar blue assay). The samples were illuminated with blue lamp (420nm). Alamar Blue assay was used measurement of cell viability in this experiment.

In SKOV3 monolayer cultures, from the MTT assay results (Figure 14) it was deduced by interpolation that 0.3 μg/mL should be the appropriate concentration of $TPPS_{2a}$ since

0.2 µg/mL caused an inadequate PDT effect (88% cell viability) and 0.4 µg/mL caused a higher level of toxicity than required for PCI (57% cell viability). The Alamar Blue assay results also confirmed that 0.3 µg/mL was the most suitable concentration to use (Figure 15). MTT assay was carried out initially with the maximum concentration of photosensitiser tested being 0.6 µg/mL. However, since 0.2 µg/mL caused a slightly lower cell kill then required and 0.4 µg/mL caused a slightly higher cell kill than required, 0.3 µg/mL was also tested using the Alamar blue assay. Since the MTT results showed that 0.6 µg/mL resulted in a significant reduction in percentage viability of SKOV3 cells, such concentration was not tested again with the Alamar blue assay.

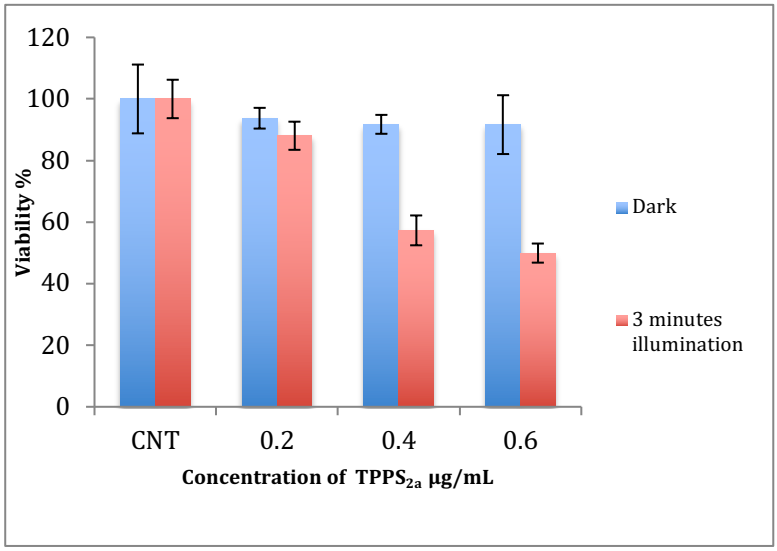

Figure 14: Viability of SKOV3 cells post PDT treatment using different concentrations of $TPPS_{2a}$ (MTT assay). The samples were illuminated with blue lamp (420nm). MTT assay was used measurement of cell viability in this experiment.

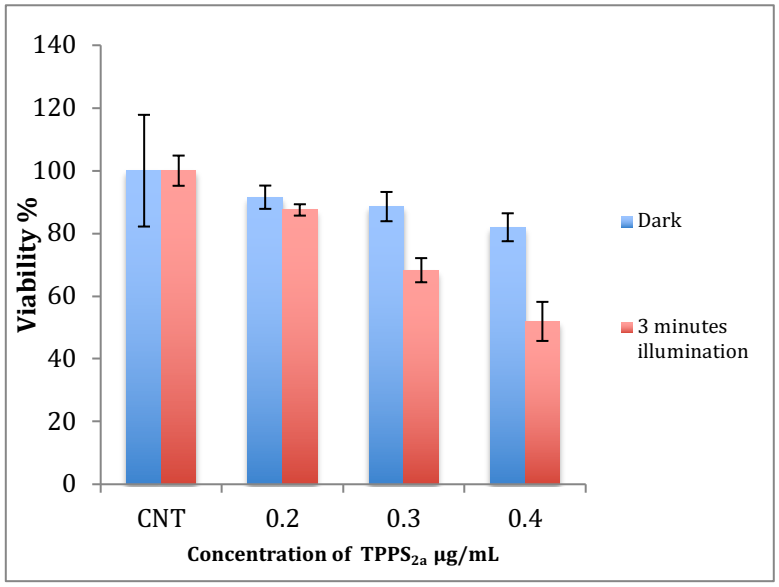

Figure 15: Viability of SKOV3 cells post PDT treatment using different concentrations of $TPPS_{2a}$ (Alamar blue assay). The samples were illuminated with blue lamp (420nm). Alamar Blue assay was used measurement of cell viability in this experiment.

As the $TPPS_{2a}$ concentrations indicated to be appropriate for PCI studies in the SKOV3 and HEY monolayer cultures by both MTT and Alamar blue the same, only the MTT assay was carried out on the MCF-7 cells. The MTT assay showed that $TPPS_{2a}$ at concentration of 0.3 µg/mL was suitable for PCI studies in MCF-7 cells (data not shown).

Saporin concentrations used in the PCI studies in the monolayer cultures ranged from 10nM- 20nM. MTT, Alamar blue or Total DNA studies were carried out either 48 hours or 96 hours post illumination (termination point). According to MTT assay results in comparison to saporin only, viability reductions from 93% to 44% (3 minutes), 97% to 20% (5 minutes) and 95% to 17% (7 minutes) were seen in HEY cells using 10nM saporin (Figure 16A) with the PCI efficacies being (1.6 and 2.1) (3 minutes), (2.2 and 4.9) (5 minutes) and (1.9 and 5.6) (7 minutes) compared to PDT and saporin only respectively. To evaluate the extent of synergistic interaction between PDT and saporin, calculation of the alpha values were found to be 1.5 (3 minutes), 2.2 (5 minutes) and 2 (7 minutes).
The alpha value is the fractional viability for each separate therapy, PDT and the application of the cytotoxin, divided by the fractional viability observed following the PCI combination treatment. If $\alpha > 1$ then a synergistic effect is present whereas an antagonistic effect is denoted by $\alpha < 1$.

With the same saporin concentration viability reductions from 91% to 42% (3 minutes), 97% to 32% (5 minutes) and 98% to 27% (7 minutes) were achieved in SKOV3 cells (Figure 16B) with the efficacies being (1.7 and 2.2), (1.6 and 3.1) and (1.4 and 3.6) for

each increasing illumination period compared to PDT and saporin only. In this experiment the alpha values were calculated to be 1.5 (3 minutes), 1.5 (5 minutes) and 1.4 (7 minutes). In MCF-7 cells saporin (10nM) the viabilities dropped from 95% to 32% (3 minutes), 95% to 17% (5 minutes) and 93% to 11 (7 minutes) compared to saporin only with the efficacies for each illumination period being (2.4 and 3), (1.7 and 5) and (2.4 and 8.5) compared to PDT or saporin only respectively (Figure 16C). The alpha values for this concentration of saporin were 2.3 (3 minutes), 1.7 (5 minutes) and 2.2 (7 minutes), which are all greater than unity and demonstrate a synergistic effect.

The increase of saporin concentration to 20nM showed that the viabilities dropped from 95% to 20% (3 minutes), 93% to 16% (5 minutes) and 96% to 12% compared to saporin alone in HEY cells (Figure 17A) with the efficacies being (3.8 and 4.7), (3.2 and 5.9) and (2.9 and 8) for each illumination period compared to PDT and saporin only. The alpha values calculated after this experiment were 3.7, 3.0 and 2.8 for the HEY cells. For the same concentration of saporin, their SKOV3 counterparts on the other hand showed decreases from 93% to 22% (3 minutes), 83% to 15% (5 minutes) and 92% to 10% (7 minutes) compared to saporin only (Figure 17B) with the efficacies being (2.9 and 4.2) (3 minutes), (3 and 5.5) (5 minutes) and (3.3 and 9.6) (7 minutes) compared to PDT and saporin only. The alpha values were calculated to be 2.7, 2.5 and 3.0. Similar to the ovarian cancer cells using 20nM saporin caused a more increased cell killing in MCF-7 cells with the viabilities being reduced from 93% to 25% (3 minutes), 89% to 10% (5 minutes) and 96% to 6% (7 minutes) compared to saporin only with the efficacies for each increasing illumination period being (2.8 and 3.7), (2.5 and 8.9) and (2.8 and 16) compared to PDT or saporin only respectively (Figure 17C). The alpha values for this experiment were calculated to be 2.6 (3 minutes), 2.2 (5 minutes) and 2.7 (7 minutes).

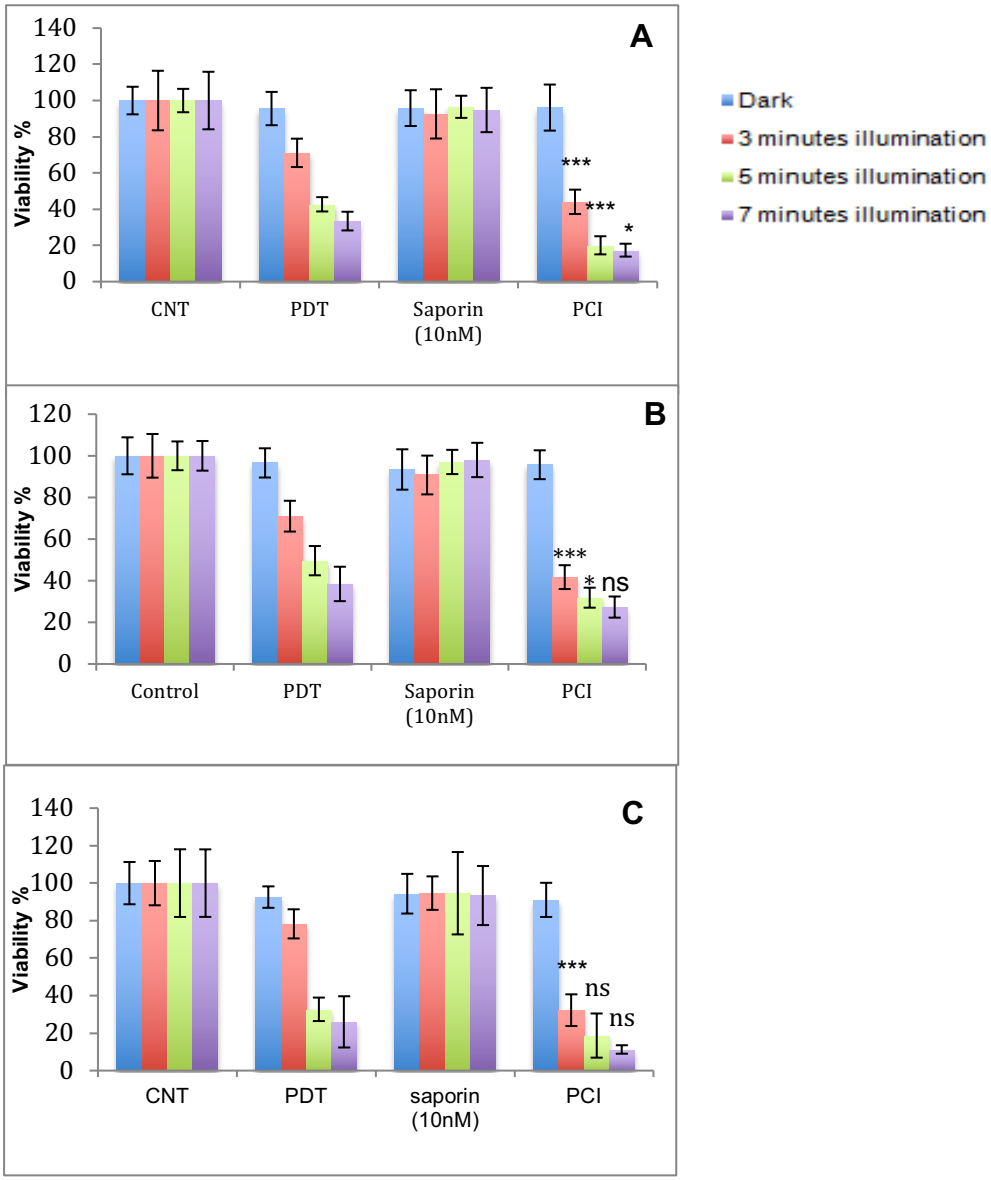

*Figure 16: Viability of HEY (A), SKOV3 (B) and MCF-7 (C) monolayer cultures post treatment with PDT, saporin only and PCI using saporin (10nM). The cells were treated with PDT ($TPPS_{2a}$ 0.4 µg/mL (HEY) or 0.3 µg/mL (SKOV3 and MCF-7)), Saporin only (10nM) and PCI. The samples were illuminated with blue lamp (420nm). MTT was carried out 48 hours after illumination. ***P<0.001, *P<0.05, ns: P>0.05.*

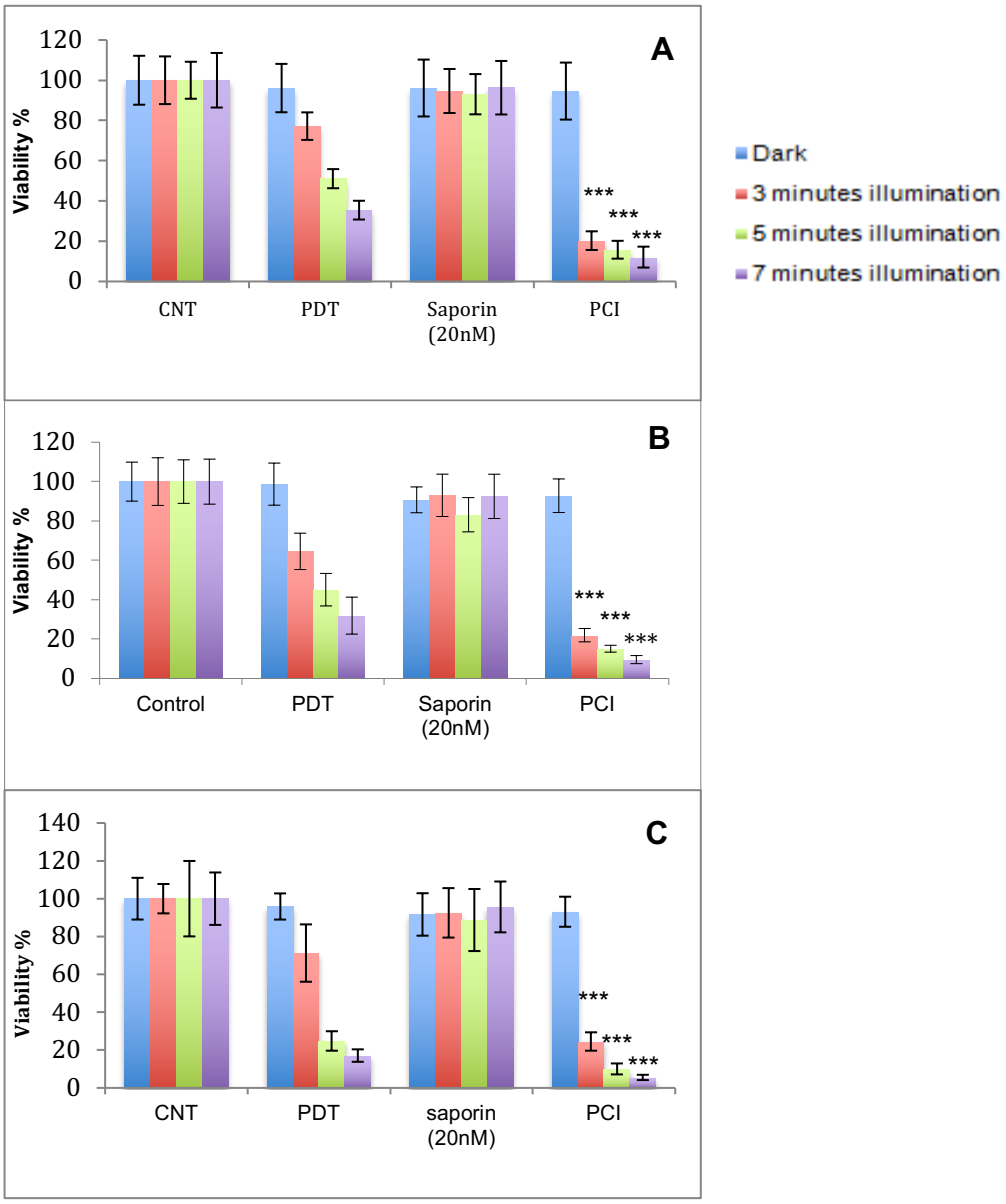

*Figure 17: Viability of HEY (A), SKOV3 (B) and MCF-7 (C) monolayer cultures post treatment with PDT, saporin only and PCI using saporin (20nM). The cells were treated with PDT ($TPPS_{2a}$ 0.4 µg/mL (HEY) or 0.3 µg/mL(SKOV3 and MCF-7)), Saporin only (20nM) and PCI. The samples were illuminated with blue lamp (420nm). MTT was carried out 48 hours after illumination. *** P<0.001.*

After elongating the incubation period post illumination to 96 hours and using saporin (20nM), a further reduction in viability was observed with the viabilities dropping from 86% to 16% (3 minutes), 90% to 9% (5 minutes) and 94% to 4% (7 minutes) in HEY cells and from 91% to 19% (3 minutes), 97% to 6% (5 minutes) and 95% to 3% (7 minutes) in SKOV3 cells.

The Alamar blue results however showed that 48 hours post illumination PCI using 10nM saporin and 3, 5 and 7 minutes light irradiation periods resulted in viability reductions of

from (92% to 38%), (98% to 18%) and (92% to 16%) in HEY 2D cultures respectively compared to using saporin alone. In comparison to using PDT and saporin (10nM) only, this meant a higher efficacy of almost (1.8 and 2.4), (2.2 and 5.3) and (1.7 and 5.9) fold for each illumination period respectively. For SKOV3 cells the same concentration of saporin and illumination periods led to roughly a decrease of viability from (94% to 44%), (94% to 24%) and (93% to 16%) compared to saporin only in the 2D cultures respectively. This again implied a (1.7 and 2.2), (1.5 and 4) and (1.5 and 5.8) fold higher efficacy in cell destruction compared to PDT or saporin alone respectively. Increasing the concentration of saporin to 20nM resulted in a more significant cell killing and PCI efficacies in both cell lines. In HEY cells, the cell viabilities reduced from 91% to 30% (3 minutes), 88% to 11% (5 minutes) and 92% to 6% (7 minutes) compared to saporin only. This meant that the PCI efficacies achieved in comparison to PDT and saporin alone for each ascending illumination period were (3.2 and 3.8), (3.5 and 7.7) and (5.5 and 16.9) respectively. In the SKOV3 cells, viabilities decreased from 91% to 27% (3 minutes), 92% to 18% (5 minutes) and 92% to 8 % (7 minutes) compared to saporin alone. For this cell line the PCI efficacies achieved for each increasing illumination period compared to PDT and saporin only were (2.9 and 3.4), (2.9 and 5.1) and (4.5 and 12.3) respectively. From the Alamar blue results obtained 48 hours post illumination, the alpha values calculated for each illumination period using 10nM saporin were 1.7, 2.1 and 1.5 (HEY cells) and 1.6, 1.4 and 1.4 (SKOV3 cells). Using 20M saporin such values were found to be 2.8, 3.2 and 4.6 (HEY cells) and 2.6, 2.7 and 3.9 (SKOV3 cells).

Experiments with 20nM saporin and 96 hours incubation post illumination period demonstrated further cell killing in the monolayer cultures of both cell lines compared to their counterparts which were incubated for 48 hours post illumination. In HEY cells the viabilities reduced from 90% to 14% (3 minutes), 94% to 8% (5 minutes) and 87% to 3% (7 minutes) compared to saporin alone with the PCI efficacies for each illumination period being (4.6 and 6.5), (4.1 and 12.0) and (7.1 and 31.6) fold higher compared to PDT and saporin alone respectively. A similar decrease was observed in the SKOV3 cells with the viabilities reducing from 94% to 21% (3 minutes), 95% to 13% (5 minutes) and 94% to 4% (7 minutes) compared to saporin only with the PCI efficacies for each corresponding illumination period being (3.2 and 4.5), (3.1 and 7.3) and (9.0 and 23.0) compared to PDT and saporin only respectively. The synergistic alpha values calculated for this experiment per increasing illumination period were 4.1, 3.7 and 5.8 (HEY cells) and 3, 2.9 and 8.5 (SKOV3 cells). Data obtained from PCI experiments on the monolayer SKOV3 and HEY cultures using Alamar blue assay are shown in Table 2.

	2D culture							
Cell line	Incubation period post light exposure (hour)	Light Exposure period (minute)	Saporin concentration (nM)	PDT only (% mean viability ± % SD)	Saporin only (% mean viability ± % SD)	PCI (% mean viability ± %SD)	PCI efficacy ratio vs. PDT	PCI efficacy ratio vs. saporin only
SKOV3	48	3	10	74.3 ±3.8	94.5 ±3.7	43.7±5.4	1.7	2.2
HEY	48	3	10	68.8±6.9	92.1 ±7.5	38.1 ±5.8	1.8	2.4
SKOV3	48	5	10	35.8 ±6.4	94.5 ±7.0	23.6±4.7	1.5	4.0
HEY	48	5	10	39.8±6.9	97.6±1.0	18.5 ±5.2	2.2	5.3
SKOV3	48	7	10	23.7±5.0	93.4±2.9	16.0 ±2.6	1.5	5.8
HEY	48	7	10	25.8±5.4	91.9±4.2	15.5±2.4	1.7	5.9
SKOV3	48	3	20	76.3 ±7.6	90.7±7.0	26.7±1.9	2.9	3.4
HEY	48	3	20	75.3 ±6.4	91.3 ±4.5	23.9±1.8	3.2	3.8
SKOV3	48	5	20	52.4 ±8.1	91.6±7.9	18.0 ±8.3	2.9	5.1
HEY	48	5	20	40.1 ±3.5	88.1 ±5.0	11.4 ±2.9	3.5	7.7
SKOV3	48	7	20	33.7±8.6	92.3 ±5.1	7.5±3.2	4.5	12.3
HEY	48	7	20	30.3 ±2.2	92.2 ±4.8	5.5 ±2.3	5.5	16.9
SKOV3	96	3	20	65.7±5.1	93.9±9.1	20.7±2.5	3.2	4.5
HEY	96	3	20	63.5 ±5.2	89.5±4.6	13.8±6.3	4.6	6.5
SKOV3	96	5	20	40.2 ±6.4	94.9±6.8	13.1±3.1	3.1	7.3
HEY	96	5	20	31.6±6.3	93.3 ±6.1	7.8±4.4	4.1	12.0
SKOV3	96	7	20	36.4±6.5	93.9±6.8	4.1 ±0.9	9.0	23.0
HEY	96	7	20	19.5 ±3.8	87.4 ±9.8	2.8±0.6	7.1	31.6

Table 2: Summary of percentage viabilities ± %SD and PCI efficacies in 2D monolayer cultures of SKOV3 and HEY cells. The values were calculated from data obtained via Alamar blue assay

The Total DNA assay was also carried out on SKOV3 cells after PCI treatment both 48 and 96 hours post illumination using saporin (20nM) as an alternative method of measuring viability of cells by quantifying the amount of undamaged DNA after each treatment condition. In terms of achieving a lower percentage viability and PCI effect after treatment with PCI compared to PDT or Saporin only, the results were consistent with the MTT and Alamar blue results (Figure 18). However, the viabilities measured after PCI using this assay were higher than those measured by MTT and Alamar blue. Measurements taken 48 hours post illumination showed the viabilities decreased from 95% to 40% (3 minutes), 93% to 28% (5 minutes) and 99% to 23% (7 minutes) after PCI compared to using saporin only. Results obtained 96 hours post illumination showed further reduction in percentage viability compared to the shorter incubation period (48 hours) with the viabilities being 32% (3 minutes), 21% (5 minutes) and 16% (7 minutes).

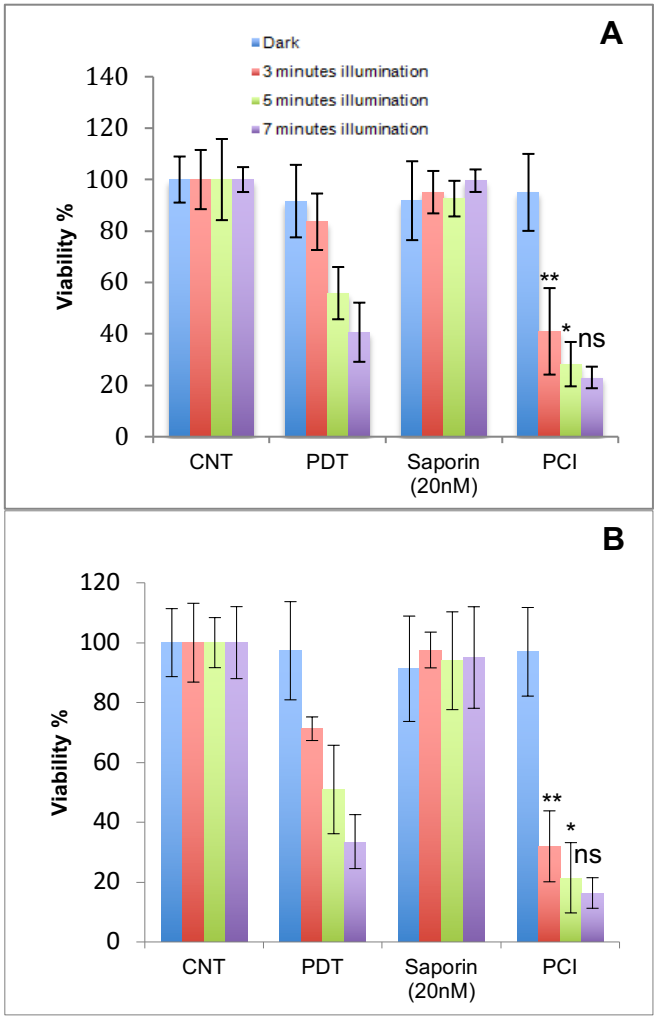

*Figure 18: Viability of SKOV3 monolayer cultures post treatment with PDT, saporin only and PCI (Total DNA assay). Cells were treated with PDT (0.3 μg/ml), Saporin only (20nM) and PCI. The samples were illuminated with blue lamp (420nm). Total DNA assay was carried out either 48 hours (A) or 96 hours (B) after illumination. **P<0.01, *P<0.05, ns: P>0.05.*

3.2 PCI experiment without chasing in monolayer cancer cultures

PCI experimental protocols generally employ a 'chasing' period so as to minimise the cell membrane content of the photosensitiser which can induce a strong PDT effect and mask the PCI effect. In this experiment the four-hour chasing period step was omitted and the efficacy was tested on one ovarian cancer cell line (SKOV3) and breast cancer cell line (MCF-7), ie the drugs were not removed, and the cells were not washed with PBS. The results showed a significant reduction in cell viability after both PDT and PCI post all illumination periods. In SKOV3 cells the viabilities after PDT and PCI were 18% vs. 9% (3 minutes), 7% vs. 6% (5 minutes) and 5% vs. 4% (7 minutes) respectively (Figure 19A). A similar effect was observed in MCF-7 cells with the viabilities being 22% vs. 10% (3 minutes), 6% vs. 5% (5 minutes) and 5% vs. 4% (7 minutes) when comparing PDT results to PCI (Figure 19B). As discussed later, these results confirm that chasing is required to reduce the PDT effect with respect to the PCI effect on cell viability. Such reduction in PDT effect can help to reduce side effects caused by PDT such as phototoxicity.

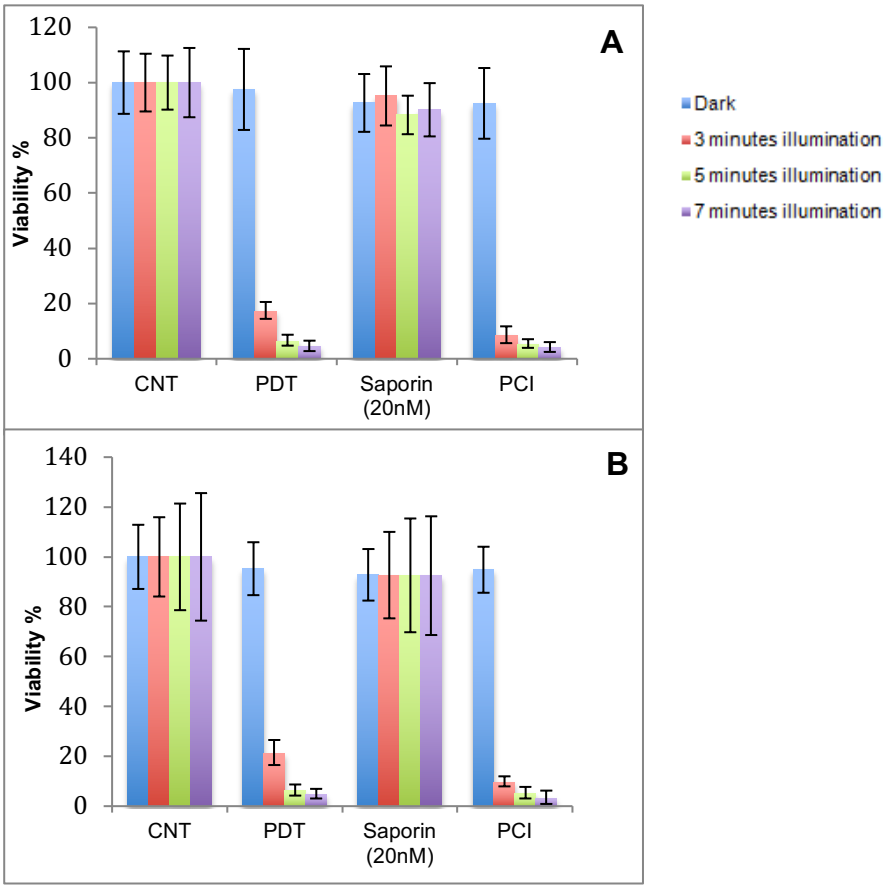

Figure 19: Viability of SKOV3 (A) and MCF-7 (B) cells post treatment with PDT, saporin only and PCI (without chasing). Cells were treated with PDT (0.3 μg/mL), Saporin only (20nM) and PCI without undergoing chasing. The samples were illuminated with blue lamp (420nm). MTT was carried out 48 hours after illumination.

3.3 *In vitro* PDT/PCI phototoxicity studies in early 3D cancer cultures

The Alamar blue assay was used for quantitative measurements of viability in the three cell lines. The preliminary PDT experiments on the 3D constructs indicated that $TPPS_{2a}$ concentrations 0.3 μg/mL (SKOV3 and MCF-7 cells) and 0.4 μg/mL (HEY cells) were suitable for carrying out PCI experiments.

The reductions in viability were lower in the 3D cultures compared to the monolayer cultures using similar drug and light doses. Using saporin 10nM, in HEY cells declines from (96% to 48%), (94% to 29%) and (97% to 22%) were achieved compared to saporin only for each irradiation period with the PCI efficacies being (1.5 and 2), (1.6 and 3.3) and (1.7 and 4.5) folds higher compared to PDT alone and saporin alone respectively for each time point, thus revealing a less major difference to the PDT. The 3D models of SKOV3 cells similarly showed reasonable drops in cell viability rates from (93% to 58%), (91% to 41%) and (92% to 29%) for each illumination period when $TPPS_{2a}$ and saporin were combined in comparison to using saporin alone. PCI also showed to be (1.3 and 1.6), (1.4 and 2.2) and (1.7 and 3.2) higher compared to using PDT and saporin alone respectively. Using this concentration of saporin the alpha values were calculated to be 1.2 (3 minutes), 1.3 (5 minutes) and 1.6 (7 minutes) in SKOV3 cells and 1.5, 1.5 and 1.6 in HEY cells following the same illumination period order. The results of this experiment in MCF-7 cells showed decreases from 96% to 60% (3 minutes), 96% to 60% (5 minutes) and 97% to 28% (7 minutes) in viability of cells compared to saporin only with the efficacies being (1.3 and 1.6), (1.3 and 2.1) and (1.7 and 3.5) compared to PDT and saporin only respectively. The alpha values calculated after the treatment of this cell line were 1.2, 1.3 and 1.6 after each illumination period.

Increasing the saporin concentration to 20nM produced a good PCI effect across all irradiation periods. The SKOV3 3D cultures the PCI treatments revealed cell viability decreases of from (96% to 40%) (3 minutes), (92% to 20%) (5 minutes) and (93% to 11%) (7 minutes) compared to saporin only. The PCI efficacies versus PDT alone and saporin alone after each irradiation period were respectively (2 and 2), (2.8 and 4.5) and (4.3 and 8.4) fold higher. The HEY 3D cultures similarly showed a good pattern of increasing cell destruction rate with PCI treatment and prolonging irradiation periods. Again, compared to saporin only, the cell viabilities in these cultures were lowered from (98% to 29%), (96% to 23%) and (97% to 12%) for each of the presented irradiation periods respectively. The PCI efficacies of these models versus PDT alone and saporin alone after each irradiation period were (2.8 and 3.4), (1.9 and 4.2) and (3.1 and 8) fold higher respectively. The alpha values for SKOV3 cells were 1.9, 2.5 and 4.1, and 2.7, 1.8 and 3.0 for the HEY cells. In MCF-7 cells the viabilities dropped from 98% to 34% (3 minutes), 94% to 13% (5 minutes)

and 91% to 11% (7 minutes) compared to saporin only with the efficacies being (2.2 and 2.9) (3 minutes), (5.2 and 7.2) (5 minutes) and (5.0 an 8.3) (7 minutes). The alpha values were calculated to be 2.2, 4.8 and 4.6. Figures 20, 21 and 22 show Live-dead images of HEY, SKOV3 and MCF-7 cell compressed collagen constructs obtained after PCI with saporin (20nM).

In a further experiment, the 3D cultures for all three cell lines treated with saporin 20nM were subjected to an extended incubation period of 96 hours post illumination prior to termination. The treatment not only elicited a good PCI effect in both cultures of both cell lines but also resulted in a further increased cytotoxic activity compared to cultures, which had been exposed to the same concentration of saporin but a shorter incubation post illumination period. In comparison to treatment with saporin only, the percentage cell viability rates were reduced to 18% (from 99%), 12% (from 98%) and 7% (from 90%) per ascending illumination period in 3D models of HEY cells and to 27% (from 98%), 17% (from 99%) and 6% (from 99%) in their SKOV3 cell counter parts. The alpha values calculated for each increasing illumination period were 3.7, 3.0 and 3.2 in HEY cells and 2.4, 3 and 7.4 in SKOV3 cells. The MCF-7 similarly showed significant drops in viability compared to using saporin only (99% to 32%), (95% to 10%) and (94% to 7%) after each increasing illumination period. The alpha values calculated for the MCF-7 cells after this experiment were 2.1, 5.1 and 6.3. The percentage viabilities of all three cell lines following the experiments discussed in this section and the PCI efficacies are summarised in Table 3. Table 4 shows a summary of synergistic alpha values calculated for each cell line in the non-spheroid cultures. Figure 23 also displays the results of the experiments using graphs.

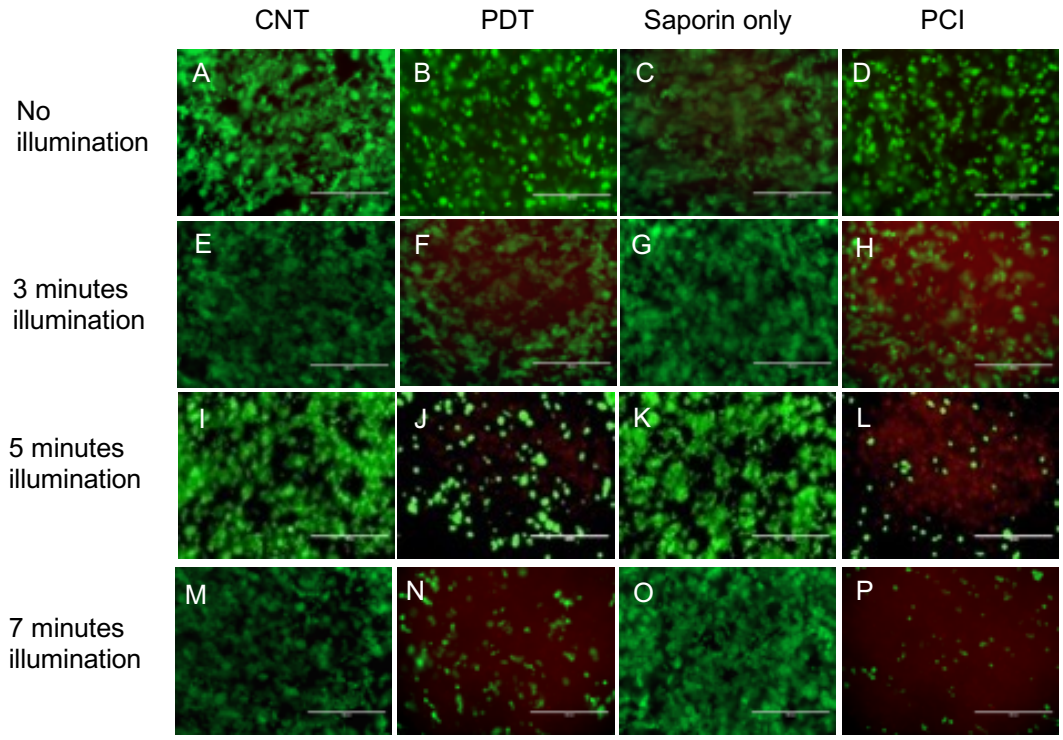

Figure 20: Live-Dead images of HEY 3D non-spheroid cultures. The cultures were treated with PDT (B, F, J and N), Saporin only (20nM) (C, G, K and O) and PCI (D, H, L and P) treatment using different light conditions. The samples were illuminated with blue lamp (420nm). The assay was carried out 48 hours post illumination. 3D constructs were incubated with the Live/dead solution containing Calcein-AM to stain live cells (green) and Ethidium homodimer-1 to stain dead cells (red). The scale bar presented in each image is 400μm.

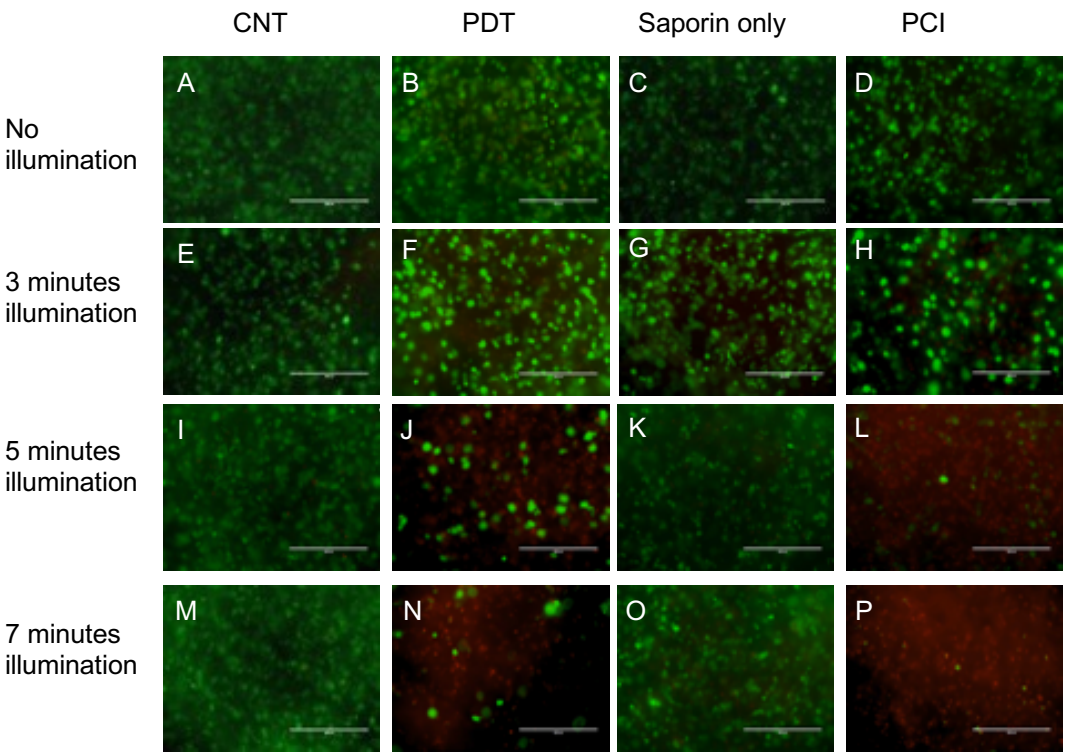

Figure 21: Live- Dead images of SKOV3 3D non-spheroid cultures. The cultures were treated with PDT (B, F, J and N), Saporin only (20nM) (C, G, K and O) and PCI (D, H, L and P) treatment using different light conditions. The samples were illuminated with blue lamp (420nm). The assay was carried out 48 hours post illumination. 3D constructs were incubated with the Live/dead solution containing Calcein-AM to stain live cells (green) and Ethidium homodimer-1 to stain dead cells (red). The scale bar presented in each image is 400μm.

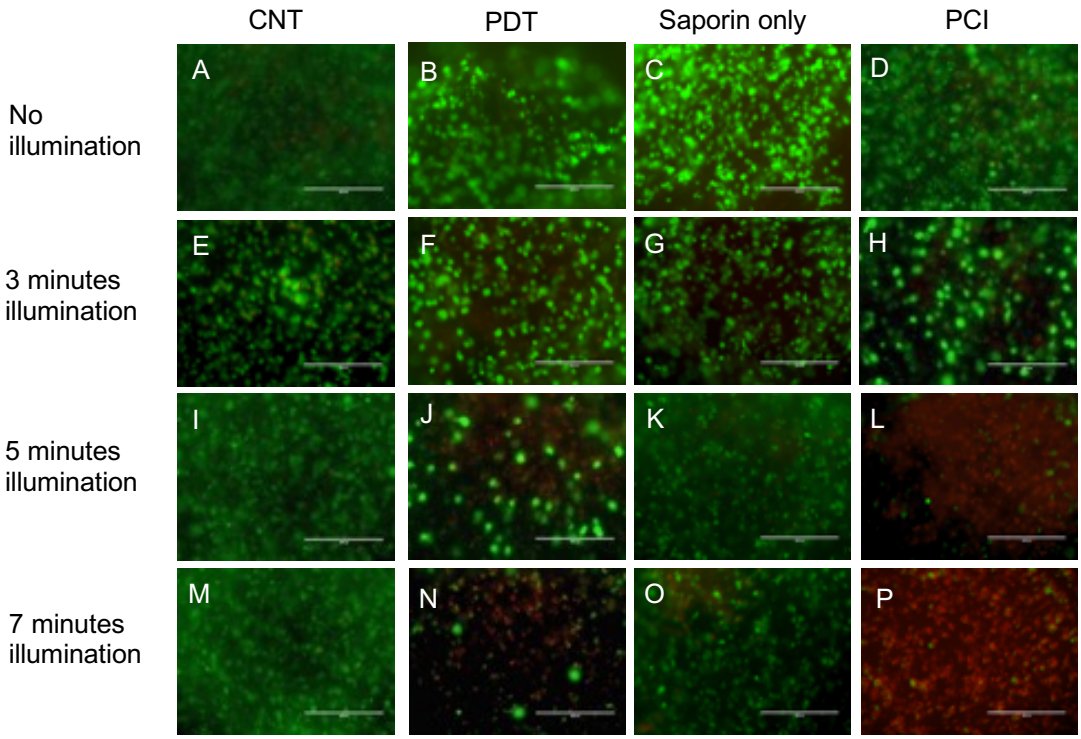

Figure 22: Live- Dead images of MCF-7 3D non- spheroid cultures. The cultures were treated with PDT (B, F, J and N), Saporin only (20nM) (C, G, K and O) and PCI (D, H, L and P) treatment using different light conditions. The samples were illuminated with blue lamp (420nm). The assay was carried out 48 hours post illumination. 3D constructs were incubated with the Live/dead solution containing Calcein-AM to stain live cells (green) and Ethidium homodimer-1 to stain dead cells (red). The scale bar presented in each image is 400μm.

				3D	culture			
Cell line	Incubation period post light exposure (hour)	Light exposure period (minute)	Saporin concentration (nM)	PDT only (% mean viability ± %SD)	Saporin only (% mean viability ± %SD)	PCI (% mean viability ± %SD)	PCI efficacy vs. PDT	PCI efficacy vs. saporin only
SKOV3	48	3	10	76.9±7.8	92.9±6.3	58.0 ±7.9	1.3	1.6
HEY	48	3	10	73.9±7.4	95.8±4.6	47.8±1.7	1.5	2.0
MCF-7	48	3	10	77.9±4.8	95.7±4.3	60.0±5.8	1.3	1.6
SKOV3	48	5	10	57.9±6.6	91.4 ±5.8	40.7±7.0	1.4	2.2
HEY	48	5	10	46.3 ±4.6	94.3 ±4.5	28.9±4.5	1.6	3.3
MCF-7	48	5	10	60.4±5.3	96.4±4.7	45.3±5.5	1.3	2.1
SKOV3	48	7	10	49.0 ±3.8	92.4 ±7.8	28.8±5.8	1.7	3.2
HEY	48	7	10	36.6±5.5	97.2 ±5.1	21.6±4.0	1.7	4.5
MCF-7	48	7	10	47.2±4.4	96.5±6.0	27.5±1.4	1.7	3.5
SKOV3	48	3	20	80.7±5.0	96.4 ±2.9	39.6±5.7	2.0	2.4
HEY	48	3	20	80.7±5.9	98.4 ±6.9	29.1 ±3.6	2.8	3.4
MCF-7	48	3	20	75.9±7.1	98.3±7.5	34.4±6.8	2.2	2.9
SKOV3	48	5	20	57.5±4.9	92.1 ±4.2	20.5 ±6.8	2.8	4.5
HEY	48	5	20	43.5±5.7	96.2 ±5.4	23.0 ±3.4	1.9	4.2
MCF-7	48	5	20	67.0±1.1	93.7±6.5	13.4±1.3	5.2	7.2
SKOV3	48	7	20	47.5 ±5.8	93.0 ±5.1	11.1 ±2.3	4.3	8.4
HEY	48	7	20	37.3 ±3.3	96.7±5.3	12.1 ±0.9	3.1	8.0
MCF-7	48	7	20	55.4±3.6	91.2±1.5	10.5±1.8	5.0	8.3
SKOV3	96	3	20	69.3 ±2.5	97.6±1.7	27.5 ±1.4	2.5	3.5
HEY	96	3	20	67.4 ±2.0	99.4 ±3.7	18.4 ±1.6	3.7	5.4
MCF-7	96	3	20	67.5±2.0	99.1±1.8	32.1±1.0	2.1	3.1
SKOV3	96	5	20	51.6±2.8	98.6±1.5	17.1 ±1.8	3.0	5.8
HEY	96	5	20	37.4 ±1.8	98.2 ±6.5	11.7±3.0	3.2	8.4
MCF-7	96	5	20	53.8±2.3	95.0±2.9	9.8±4.2	5.5	9.7
SKOV3	96	7	20	45.0 ±1.2	99.3 ±2.6	6.3 ±1.8	7.2	15.9
HEY	96	7	20	25.1 ±3.6	89.6±7.7	7.1 ±0.4	3.6	12.7
MCF-7	96	7	20	47.4±4.2	93.9±1.4	6.8±1.3	7.0	13.8

Table 3: Summary of percentage viabilities ± %SD and PCI efficacies in 3D non-spheroid cultures of SKOV3, HEY and MCF-7 cells

			3D Cultures	
Cell line	Incubation period post light exposure (hour)	Light exposure period (minute)	Saporin concentration (nM)	Alpha values
SKOV3	48	3	10	1.2
HEY	48	3	10	1.5
MCF-7	48	3	10	1.2
SKOV3	48	5	10	1.3
HEY	48	5	10	1.5
MCF-7	48	5	10	1.3
SKOV3	48	7	10	1.6
HEY	48	7	10	1.6
MCF-7	48	7	10	1.6
SKOV3	48	3	20	1.9
HEY	48	3	20	2.7
MCF-7	48	3	20	2.2
SKOV3	48	5	20	2.5
HEY	48	5	20	1.8
MCF-7	48	5	20	4.8
SKOV3	48	7	20	4.1
HEY	48	7	20	3.0
MCF-7	48	7	20	4.6
SKOV3	96	3	20	2.4
HEY	96	3	20	3.7
MCF-7	96	3	20	2.1
SKOV3	96	5	20	3.0
HEY	96	5	20	3.0
MCF-7	96	5	20	5.1
SKOV3	96	7	20	7.4
HEY	96	7	20	3.2
MCF-7	96	7	20	6.3

Table 4: Summary of synergistic alpha values for non- spheroid cultures of SKOV3, HEY and MCF-7 cells

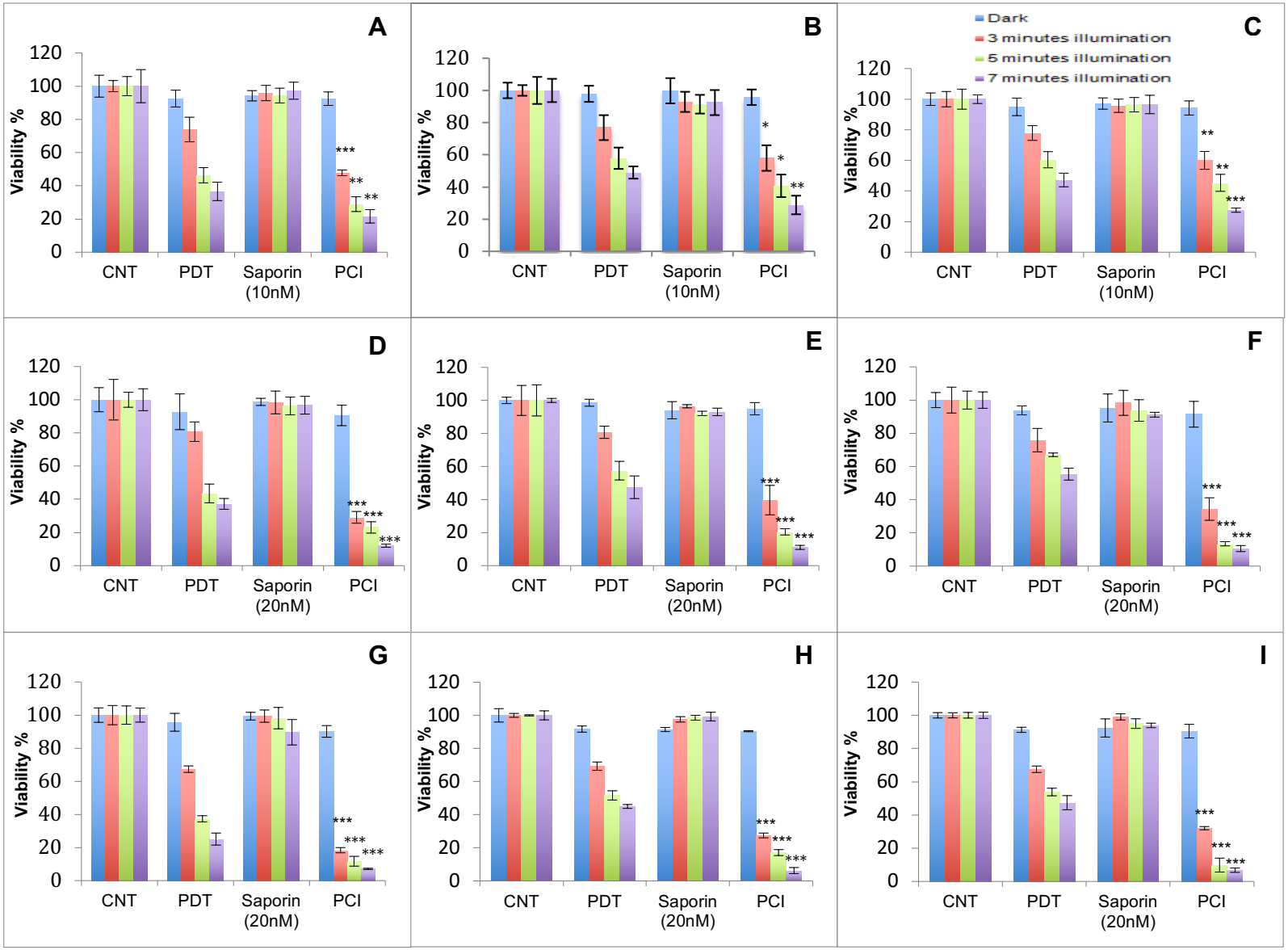

*Figure 23: Percentage viability of HEY (A, D, G), SKOV3 (B, E, H) and MCF-7 (C, F, I) cells in non-spheroid 3D compressed collagen constructs after treatment with PDT, saporin only and PCI. Constructs for graphs (A, B and C) were treated with 10 nM saporin, (D, E and F) with 20 nM saporin and assay at 48 hours incubation post illumination; (G, H and I) with 20 nM saporin and assay at 96 hours incubation post illumination. The samples were illuminated with blue lamp (420nm). *p<0.05, **p<0.01 and ***p<0.001. The p values show the significance difference between PDT and PCI.*

In a different experiment 3D non-spheroid constructs of SKOV3 and MCF-7 cells were subjected to PCI treatment using 40nM saporin (Table 5). This led to a further reduction in percentage viability of cells. The cell kill obtained post treatment with 40nM saporin and 7 minutes light illumination (48 hours incubation post illumination) was similar to that observed using the same illumination period and 20nM saporin in both cell lines (96 hours incubation post illumination) (Table 6). The Live-Dead images from this experiment have been presented in Figure 24.

Cell line	Incubation period post light exposure (hour)	Light exposure period (minute)	Saporin concentration (nM)	PDT only (% mean viability ± %SD)	Saporin only (% mean viability ± %SD)	PCI (% mean viability ± %SD)	PCI efficacy vs. PDT	PCI efficacy vs. saporin only
SKOV3	48	3	40	78.2 ± 1.9	84.3 ± 3.4	37.7 ± 2.4	2.1	2.2
MCF-7	48	3	40	73.1 ± 1.1	83.2 ± 3.6	32.8 ± 4.4	2.2	2.5
SKOV3	48	5	40	57.8 ± 4.2	84.6 ± 2.2	15.8 ± 2.3	3.6	5.3
MCF-7	48	5	40	58.0 ± 1.6	81.0 ± 1.6	11.3 ± 2.6	5.1	7.1
SKOV3	48	7	40	51.8 ± 2.7	84.5 ± 2.6	7.3 ± 2.8	7.1	11.5
MCF-7	48	7	40	54.2 ± 2.2	85.8 ± 1.0	8.3 ± 1.3	7.3	11.7

Table 5: Summary of percentage viabilities ± %SD and PCI efficacies in 3D non-spheroid cultures of SKOV3 and MCF-7 cells after treatment with saporin (40nM)

Cell line	Incubation period post light exposure (hour)	Light exposure period (minute)	Saporin concentration (nM)	PCI (% mean viability ± %SD)
SKOV3	48	7	40	7.3 ± 2.8
MCF-7	48	7	40	8.3 ± 1.3
SKOV3	96	7	20	6.9 ± 2.1
MCF-7	96	7	20	8.0 ± 0.9

Table 6: Comparison of percentage viabilities of SKOV3 and MCF-7 cells in 3D non- spheroid cultures after PCI treatment using 20nM saporin (96 hours incubation post illumination) vs. 40nM saporin (48 hours incubation post illumination). The constructs were illuminated for 7 minutes

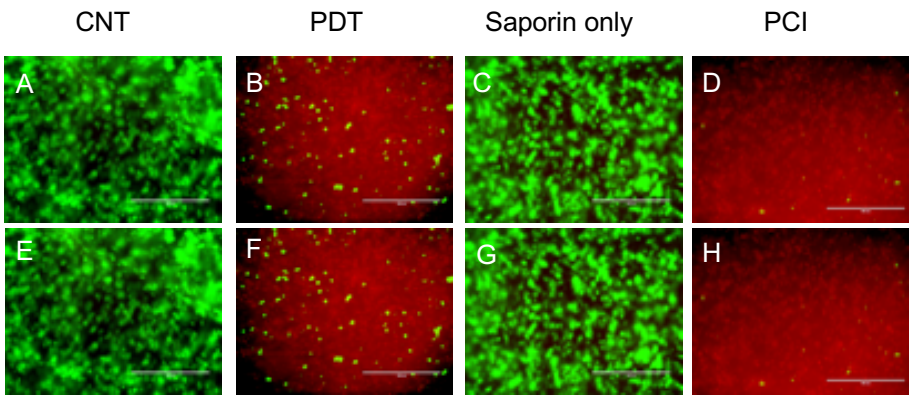

Figure 24: Live dead images of HEY 3D cultures post PDT, saporin only and PCI treatment using saporin (40nM). Constructs (B and F) underwent PDT treatment, (C and G) underwent saporin only (40nM) treatment and (D and H) underwent PCI treatment using 5 minutes light illumination period. The samples were illuminated with blue lamp (420nm). The scale bar presented in each image is 400μm.

3.4 Localisation of $TPPS_{2a}$ in 2D and 3D cultures of SKOV3 and HEY cells

In 2D cultures, 24 hours after seeding, the cells were treated with $TPPS_{2a}$ (1μg/mL) for 20 hours. The same incubation protocol was used as for the therapeutic PCI studies so after 20 hours the cells were washed with PBS and incubated with fresh drug free media for a further 4 hours before fluorescence microscopic imaging with Olympus fluorescence microscope (Olympus BX63) (60x magnification) using CY5 channel. Figure 25 shows the uptake of $TPPS_{2a}$ in SKOV3 (A and B) and HEY (C and D) monolayer cultures. As shown in the images higher fluorescence can be detected in cultures treated with $TPPS_{2a}$ (B and D) compared to the control cultures (A and C).

In the 3D cultures the cells were treated with $TPPS_{2a}$ (1μg/mL) for 20 hours to investigate cellular uptake of $TPPS_{2a}$ by SKOV3 and HEY cells in the constructs. The medium containing $TPPS_{2a}$ was then removed and the constructs were washed with PBS before being incubated with fresh photosensitiser-free medium for an additional 4 hours and imaged using a fluorescence microscope with quasi-confocal capability (20x objective, Apotome.2, Carl Zeiss). As shown in Figure 25, in comparison to the control 3D construct (A and C), bright fluorescence signals of the $TPPS_{2a}$ were observed in both SKOV3 and HEY constructs incubated with $TPPS_{2a}$, which indicated the intracellular uptake of the photosensitiser in the 3D constructs (Figure 26 B and D). Such results indicate that in the treated 3D constructs the $TPPS_{2a}$ was taken up by the cells instead of becoming bound in the collagen matrix. The both control collagen constructs for SKOV3 (A) and HEY (C) cells without photosensitiser showed negligible autofluorescence levels. The images at the side of the central show the cross-sectional pattern of fluorescence as a function of depth.

In a further experiment undertaken to confirm cellular uptake of $TPPS_{2a}$ in the 3D cultures, constructs containing a lower cell density of cells (10,000 cells/construct) were treated with $TPPS_{2a}$ (3 μg/mL) and additionally stained with LysoTracker Green (100nM) prior to imaging (Figure 27). Co-staining the cells with Lysotracker Green provided further evidence for intracellular uptake of $TPPS_{2a}$ in the 3D constructs. Confocal imaging was also attempted to obtain higher resolution, but the intensities were too weak. This is partly because the detectors used for confocal microscopy (photomultipliers) are less sensitive than the CCD cameras used to acquire the images shown here. Another compounding factor is that porphyrins are not efficient fluorophores compared to fluorescein for example.

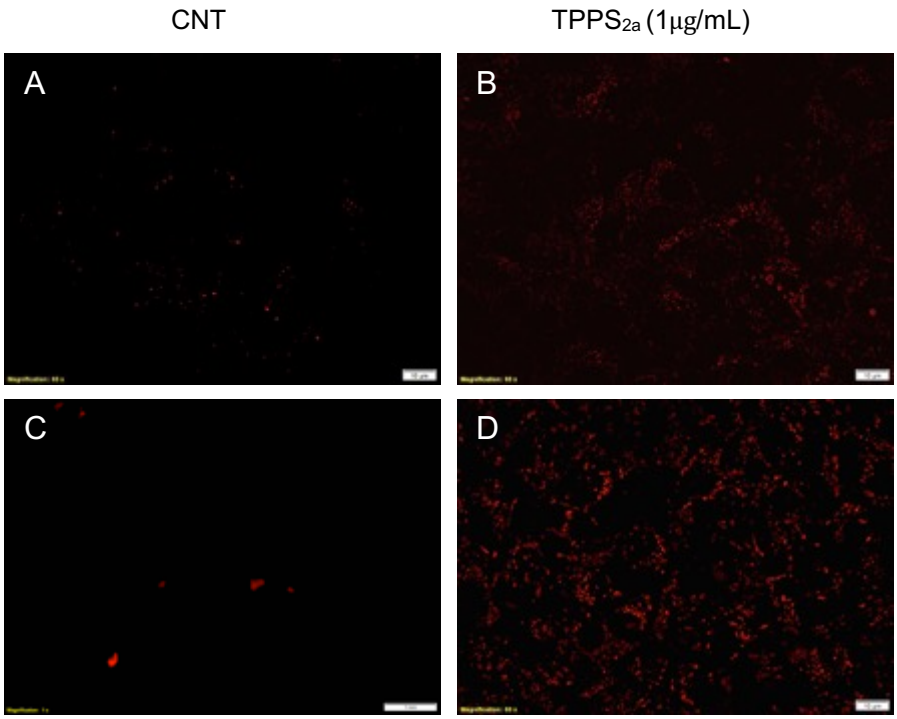

Figure 25: Uptake of $TPPS_{2a}$ by monolayer cultures of SKOV3 (A-B) and HEY (C-D) cells. A and C: control cultures treated with drug free media, B and D: cultures treated with $TPPS_{2a}$ (1μg/mL). Images were taken with Olympus BX63 (60x magnification). Scale bar presented is 10μm.

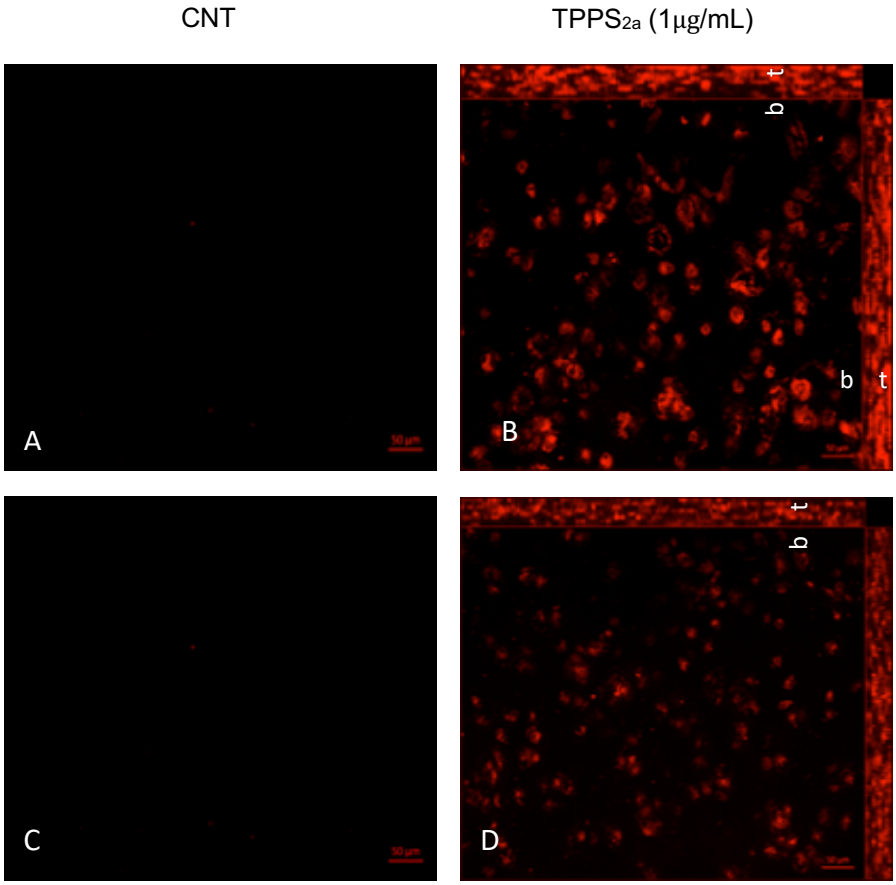

Figure 26: Intracellular uptake of $TPPS_{2a}$ in SKOV3 and HEY non-spheroid 3D compressed collagen cultures. (A): control SKOV3 cell constructs, (B): intracellular uptake of $TPPS_{2a}$ in SKOV3 non-spheroid 3D compressed collage constructs, (C): control HEY cell constructs, D: intracellular uptake of $TPPS_{2a}$ in HEY non-spheroid 3D compressed collagen construct. Images (B and D) were obtained through stacking with fluorescence microscope (20x objective, Apotome.2, Carl Zeiss). The photosensitiser fluorescence was measured between 600-700 nm using Alexa Fluor 647 channel. The scale bar presented in each image is 50 µm. t: top; b: bottom.

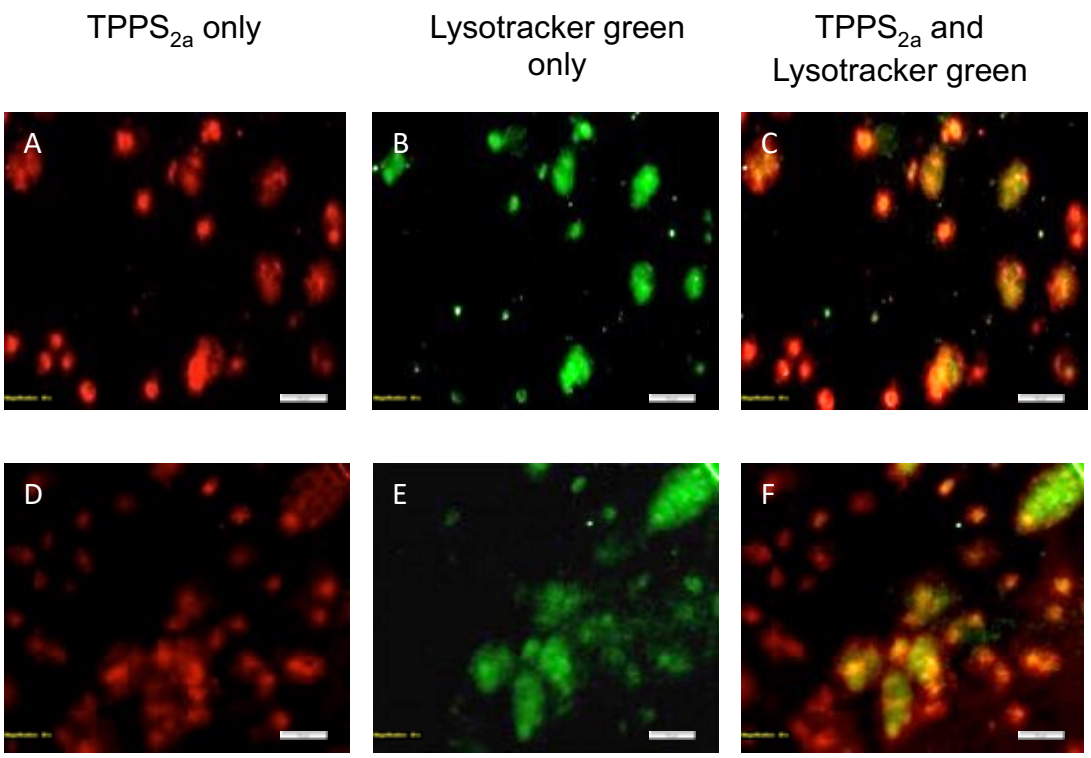

Figure 27: Intracellular localisation of $TPPS_{2a}$ in 3D compressed collagen non-spheroid constructs of SKOV3 (A-C) and HEY (D-F) cells. The constructs contained cell density of 10,000 cells/construct. The constructs were treated with $TPPS_{2a}$ (3μg/mL) and Lysotracker green (100nM) and imaged using a fluorescence microscope (20x objective, Olympus BX63). A and D show the localisation of $TPPS_{2a}$ and B and E show the localisation of Lysotracker green stain within the small cellular aggregates. The co-localisation of both $TPPS_{2a}$ and Lysotracker green is shown in C and F. The scale bar presented in each image is 50μm.

3.5 *In vitro* PCI phototoxicity studies in 3D cancer cultures pre-incubated with drugs

Pre-incubation of SKOV3 and MCF-7 cells with $TPPS_{2a}$ and saporin (20nM) 24 hours prior to seeding in 3D demonstrated a very low reduction in percentage viability of PCI treated cells even after 7 minutes of light illumination compared to the control constructs (81% and 70% viability in SKOV3 and MCF-7 cells respectively). Figure 28 shows live dead images of constructs pre-incubated with drugs of interest prior to seeding and PCI treatment.

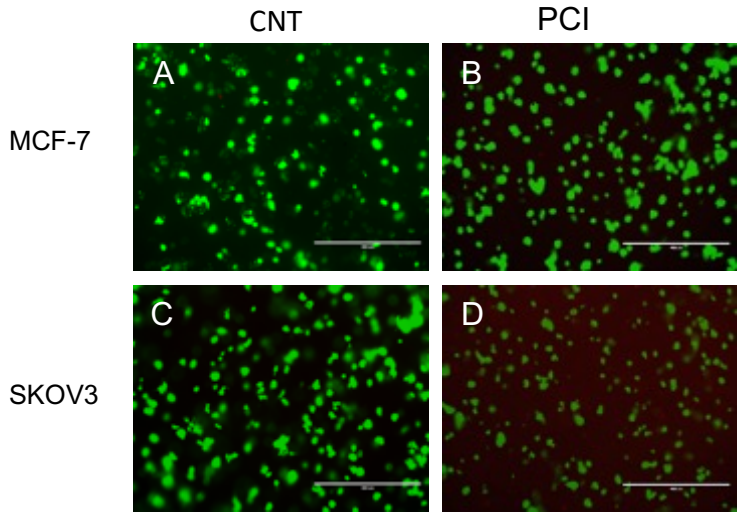

Figure 28: Live- Dead images of MCF-7 and SKOV3 cell 3D non- spheroid constructs pre-incubated with drugs prior to seeding. MCF-7 (A-B) and SKOV3 (C-D) cell 3D constructs were pre-incubated with $TPPS_{2a}$ and Saporin prior to seeding and PCI treatment (B and D) compared to control constructs (A and C). The samples were illuminated with blue lamp (420nm). The scale bar presented in each image is 400 μm.

3.6 PCI experiment without chasing in 3D cancer cultures

PDT and PCI experiments without removal of drugs and washing with PBS (ie 'chasing') resulted in 7% vs. 8% viability (PDT) and 1.8% vs. 2.2% viability (PCI) in SKOV3 (Figure 29A) and MCF-7 (Figure 29B) cells respectively after 7 minutes light illumination. A higher cell kill was therefore achieved after both PDT and combined treatment without chasing compared to with chasing, however no PCI effect was observed.

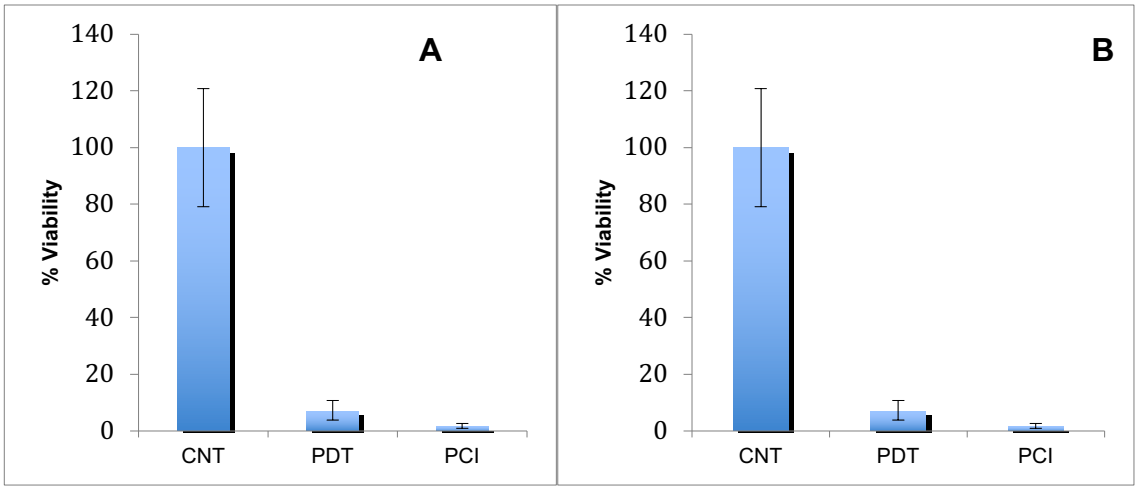

Figure 29: PDT and PCI without chasing in SKOV3 (A) and MCF-7 (B) cell 3D non- spheroid cancer constructs. The samples were illuminated with blue lamp (420nm). Alamar blue was carried out 48 hours post illumination.

3.7 *In vitro* PDT/PCI phototoxicity studies in mature 3D spheroid cancer cultures

The PCI experiments were repeated on spheroid 3D compressed constructs of SKOV3 and HEY cell lines since they are better representatives of a tumour model in terms of physiological properties. The compact structures formed by the cancer cells can affect drug uptake and their hypoxic cores can influence PDT/PCI efficacy. Furthermore, cancer cells can develop resistance towards treatments when they form aggregates.

The 'mature' constructs of this study developed after several days incubation enabling the cells to proliferate and develop into spheroids prior to undergoing treatment. The SKOV3 and HEY cells developed into sizable and measurable near spheroidal cellular aggregates by day 7. The aggregate sizes of 100 spheroids per cell line were measured and categorised into small, medium and large as shown in Figure 30 and Table 7. The HEY cells generally formed larger aggregates compared to SKOV3 cells. While the SKOV3 cells mainly formed small and medium aggregates, the HEY cells mostly formed medium and large aggregates. Phalloidin/ Hoechst staining was used to visualise the structure of the spheroids formed as well as their destruction after treatment. The green fluorescent Alexa fluor 488 dye of Phalloidin binds to filamentous actin in cells with high affinity thus allowing the cytoskeletal structure of the cells and spheroids to be explored. The Hoechst dye concurrently stains the nuclei which together with Phalloidin provides a clear image of the spheroids to be recognised.

	Aggregate type					
	Small		**Medium**		**Large**	
	Area (μm^2) (1000>5000)	Diameter (μm) (40>100)	Area (μm^2) (5000>12,000)	Diameter (μm) (100>160)	Area (μm^2) (12000 and above)	Diameter (μm) (160 and above)
SKOV3	1871- 4931	45-99	5000- 11723	100-159	12166 - 13714	166-171
HEY	3457- 4737	64-77	5309-11985	100-159	12666 - 82931	162-412

Table 7: The sizes of SKOV3 and HEY cell spheroids based on the area (μm^2) and diameter (μm). The diameter sizes presented have been calculated as mean diameters based on measurements taken from the two longest cross sections in every spheroid. The measurements were taken using Image J software.

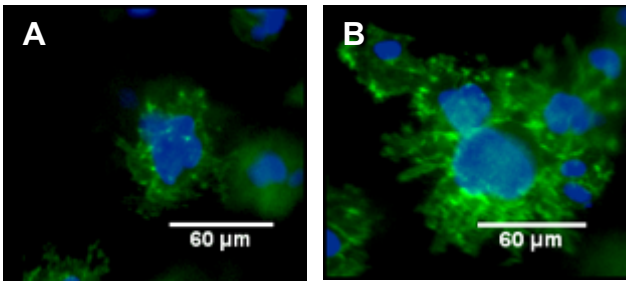

Figure 30: Examples of small (A) and large (B) spheroids of SKOV3 cells formed 7 days after seeding. The cytoskeletal structure of the cells in the aggregates was stained with Alexa Fluor 488 Phalloidin (Green) and the nucleus of cells was stained with Hoechst dye (Blue). The scale bar presented in each image is 60μm.

Earlier PDT experiments indicated that the concentrations of $TPPS_{2a}$, which were able to induce sub-lethal PDT effects, were 0.5 µg/mL in HEY cells and 0.7 µg/mL in SKOV3 cells (data not shown). The spheroid constructs of the SKOV3 cells demonstrated no PCI effect using saporin 20nM, however upon increasing the concentration of saporin to 40nM, the

viabilities showed significant reductions from (97% to 41%), (91% to 39%) and (92% to 31%) compared to saporin only therapy for each irradiation period as well as a slight PCI effect after 3 minutes of light irradiation with the PCI efficacy being (1.7 and 2.4) fold higher than PDT or saporin alone respectively.

The spheroid constructs of the HEY cells on the other hand displayed reasonable PCI effects using 20nM saporin with the % percentage viabilities dropping from (98% to 30%), (97% to 24%) and (97% to 19%) compared to saporin only treatment and the PCI efficacies being (2.5 and 3.3), (1.9 and 4.1) and (2 and 5.2) fold higher than using PDT or saporin alone for each irradiation period respectively (Figure 31).

Phalloidin/Hoechst (Figures 32 and 33) and live-dead (Figure 34) staining provide visual results that support the data obtained from Alamar blue assay.

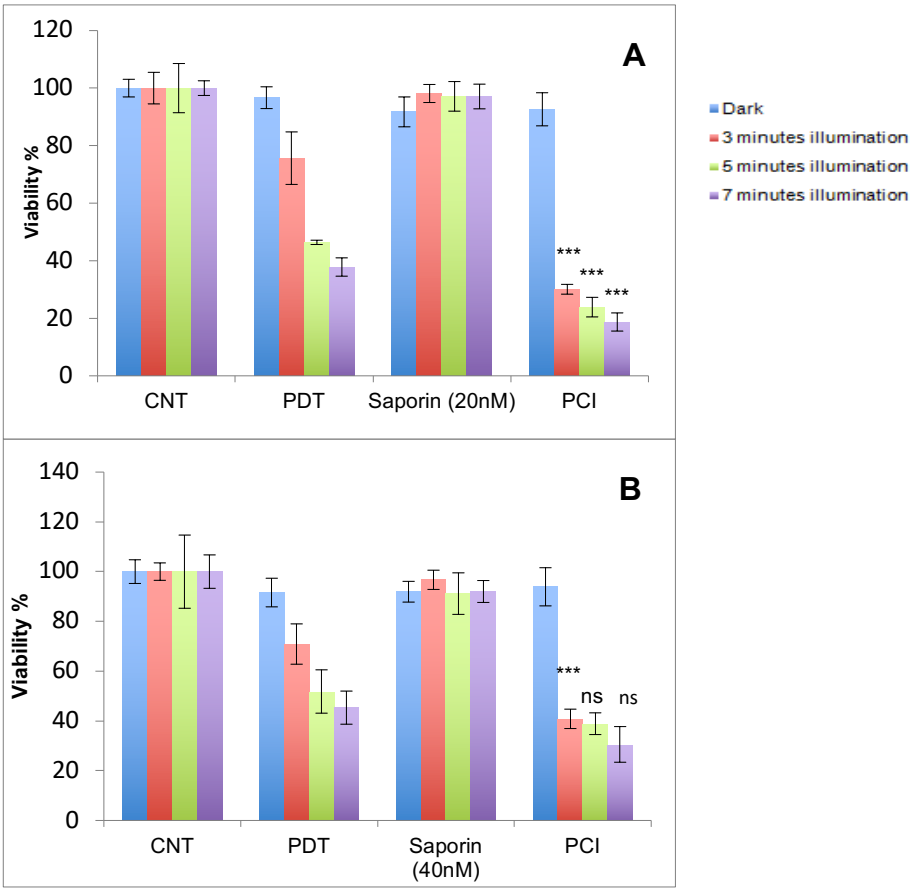

*Figure 31: Percentage viability of HEY (A) and SKOV3 (B) cells spheroid 3D compressed collagen constructs after treatment with PDT, saporin only and PCI. Constructs for the SKOV3 cells were treated with $TPPS_{2a}$ (0.7 µg/ml) and 40nM saporin, and for the HEY cells with TPPS2a (0.5 µg/ml) and 20nM saporin. The samples were illuminated with blue lamp (420nm). The constructs were incubated for 48 hours post illumination before terminating the experiment using Alamar Blue assay. *** p<0.001. These p values show the significance difference between PDT and PCI treatments.*

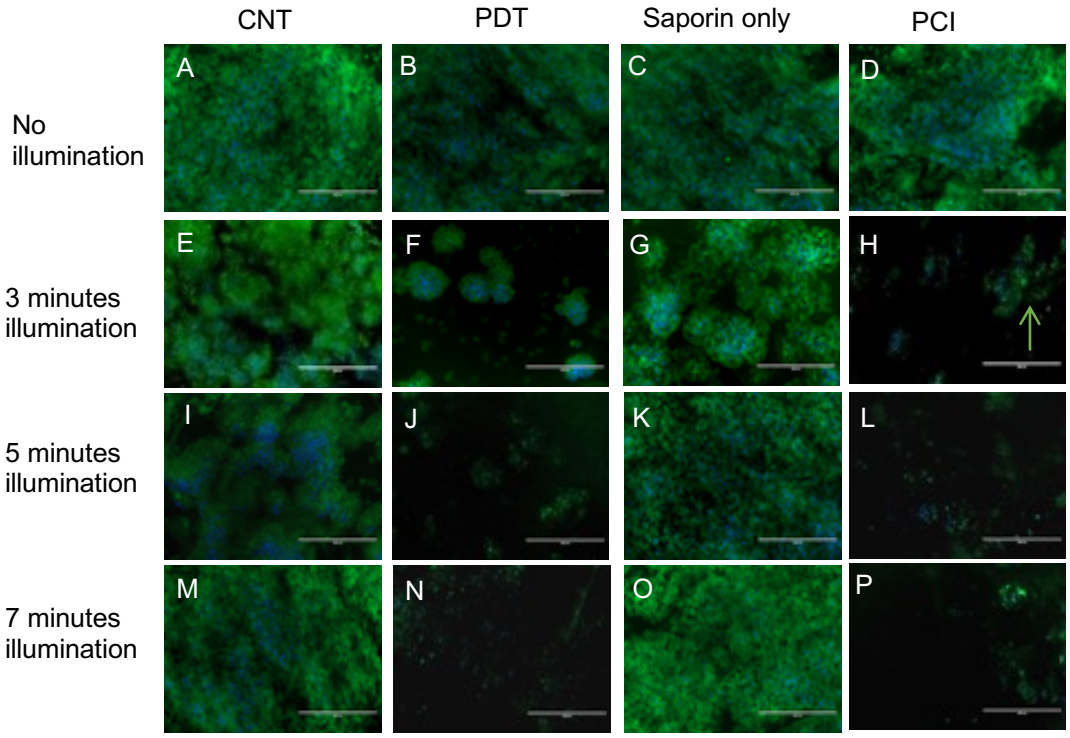

Figure 32: Phalloidin/ Hoechst stained images of HEY cell spheroid constructs upon treatment with PDT, saporin only and PCI. The constructs were treated using $TPPS_{2a}$ only at concentration 0.5 μg/ml (B, F, J and N), saporin only at concentration 20nM (C, G, K and O) and PCI (D, H, L and P) after different periods of illumination. A reduced number of spheroids is evident when $TPPS_{2a}$ and saporin are combined compared to using each drug alone. The samples were illuminated with blue lamp (420nm). HEY the arrow highlights a fragmented pattern of cell aggregates (IV). Alexa Fluor 488 phalloidin (green) was used to stain the cytoskeletal structure of the cells and Hoechst 33258 (blue) was used to stain the nuclei. The scale bar presented in each image is 400μm.

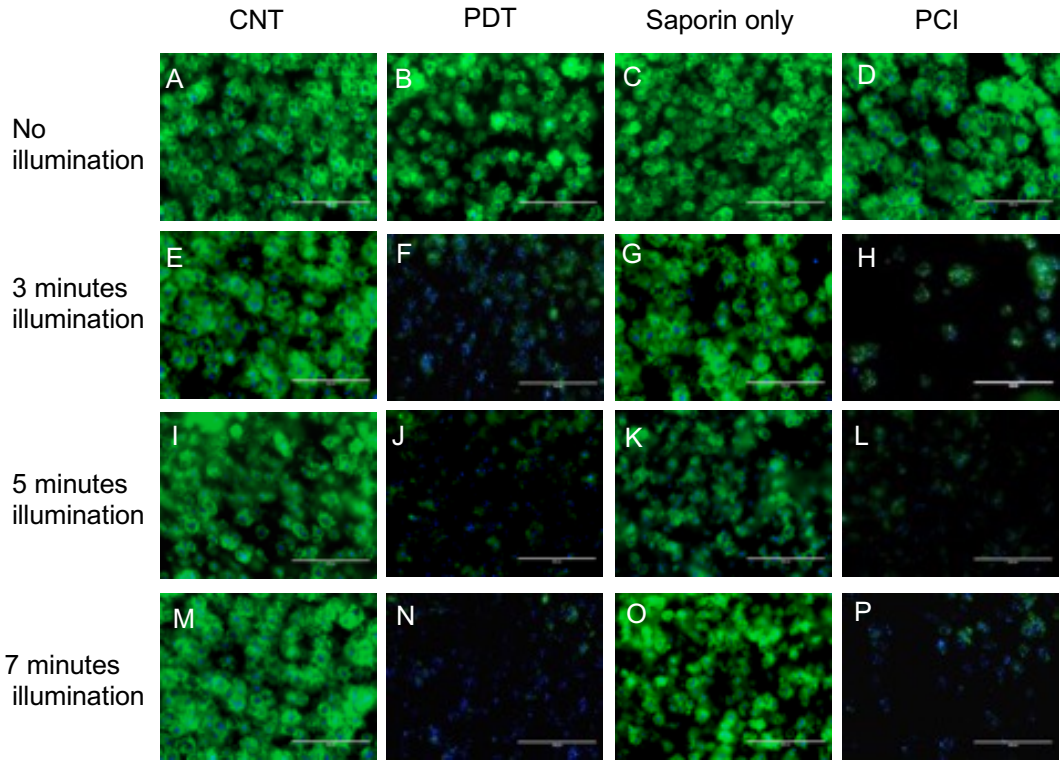

Figure 33: Phalloidin/ Hoechst stained images of SKOV3 cell spheroid constructs upon treatment with PDT, saporin only and PCI. The constructs were treated using $TPPS_{2a}$ only at concentration 0.7 μg/ml (B, F,J and N), saporin alone at concentration 40nM (C, G, K and O) and PCI (D, H, L and P) after different periods of illumination. A reduced number of spheroids is evident when $TPPS_{2a}$ and saporin are combined compared to using each drug alone. The samples were illuminated with blue lamp (420nm). Alexa Fluor 488 phalloidin (green) was used to stain the cytoskeletal structure of the cells and Hoechst 33258 (blue) was used to stain the nuclei. The scale bar presented in each image is 400μm.

Live dead images (Figure 34) acquired after treatment of spheroids using PCI also supported the data presented in Figures 32 and 33.

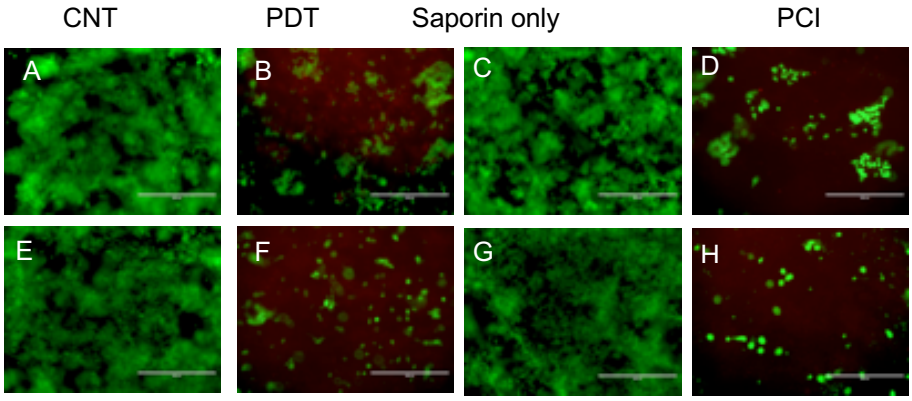

Figure 34: Live-dead images of spheroid 3D compressed collagen constructs of HEY (A-D) and SKOV3 (E-H) cells after undergoing PDT, saporin only and PCI treatment. The cells were treated with $TPPS_{2a}$ only (0.5μg/ml for HEY cells) (B) and (0.7μg/ml for SKOV3 cells) (F), saporin only (20nM for HEY cells) (C) and (40nM for SKOV3 cells) (G) and a combination of both drugs (D and H) following 3 minutes of exposure to light and a 48 hour post-illumination assay time point. The samples were illuminated with blue lamp (420nm). 3D constructs were incubated with the Live/dead solution containing Calcein-AM to stain live cells (green) and Ethidium homodimer-1 to stain dead cells (red). The scale bar presented in each image is 400μm.

3.8 Role of oxygen in PCI

A good supply of oxygen is required for the photosensitiser $TPPS_{2a}$ to generate ROS efficiently upon activation by light. These ROS are the means by which the sub-lethal PDT effect is produced that aids the occurrence of the PCI effect. Initial experiments were conducted to see if the higher cell density and therefore oxygen consumption had affected the oxygen levels within the construct. 3D spheroid constructs of both cell lines were imaged on day 7 and compared to the O_2 levels in the 3D non-spheroidal constructs one day after seeding using the Image-iT hypoxia reagent. The reagent consists of a fluorogenic compound which is weakly fluorescent in environments with normal O_2 level as well as live cells and becomes strongly fluorescent as the O_2 concentrations decrease. As figure 35 shows the O_2 concentrations are far lower on day 7 (B and D) when the SKOV3 and HEY spheroids have been formed since the O_2 consumption levels are higher than in non-spheroidal constructs (day 1) (A and C) and this may therefore reduce the PCI effect due to the lack of sufficient O_2 in the models.

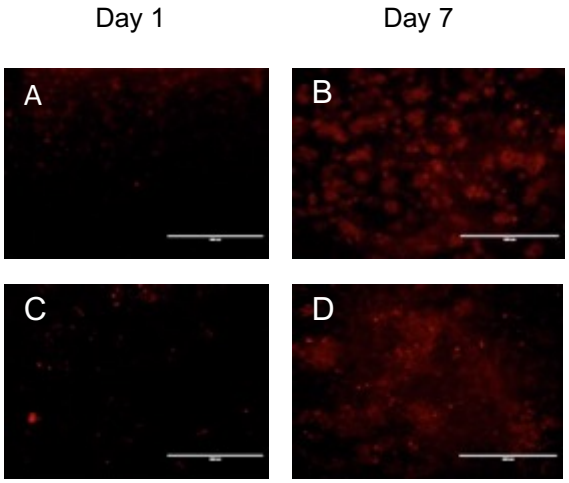

Figure 35: Reduction of oxygenation with spheroid formation. Images of oxygen reduction in SKOV3 cells (A-B) and HEY cells (C-D) non-spheroid and spheroid constructs were obtained as spheroids formed on day 7 (B and D), compared to one day post seeding before the formation of spheroids (A and C), The hypoxia levels within the spheroids were measured using the Image-iT™ Red Hypoxia reagent. The scale bar presented in each image is 400μm.

In another experiment, the effect of different oxygenation levels ie normoxia (20% oxygenation) and hypoxia (1% oxygenation) on PDT and PCI in monolayer cultures and 3D non-spheroid SKOV3 cell constructs were studied since as both treatments rely on the generation of reactive oxygen species. As shown in Figure 36A although the PDT/PCI treatments were carried out in hypoxic conditions in monolayer cultures of SKOV3 cells, a significant reduction in percentage viability was still achieved compared to PDT and

saporin only treatments. For the 3D non-spheroid constructs (Figure 36B) under normoxic conditions significant cell killing was achieved in PDT/PCI treated constructs. Using 40 nM saporin and 7 minutes exposure, the viability using PDT was reduced to 33.5% and 7.3 % for PCI. However, under hypoxia, no significant decrease in cell viability was seen. Although a PCI elicited a small reduction in mean viability to 82% was observed with PCI, this was not found to be statistically significant compared to normoxia. Using saporin alone, comparable small reductions in viability were observed for both normoxia and hypoxia. The Live-dead assay images shown in Figure 37 obtained after PDT/PCI using hypoxic constructs are consistent with the viability data. These data show that both PDT and PCI were strongly inhibited at low oxygenation levels. Figures 38 and 39 compare PDT/PCI in hypoxic vs. normoxic conditions in spheroid constructs of SKOV3 cells. As the Live-dead images (Figure 39) show no PDT/PCI effect occurs in spheroid constructs in hypoxic conditions compared to normoxic conditions.

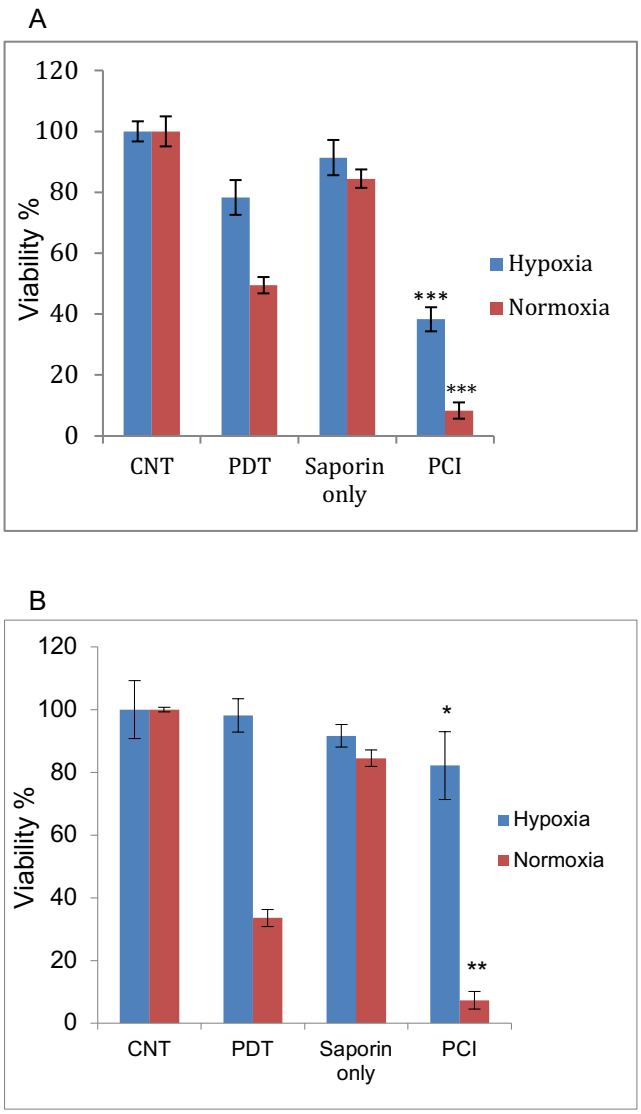

*Figure 36: Effect of hypoxia on PCI and PDT. A. Percentage viability of SKOV3 cell in 2D monolayer experiments after PCI treatment in normoxic condition compared to hypoxic condition using $TPPS_{2a}$ only (0.3μg/ml) only for PDT, saporin 40 nM only and a combination of both drugs for PCI as well as a light irradiation period of 7 minutes. ***p<0.001, the p values show the significance difference between PDT and PCI. B. Percentage viability of SKOV3 cell 3D non-spheroid constructs after PCI treatment in normoxic condition compared to hypoxic condition using $TPPS_{2a}$ only (0.3μg/ml) only for PDT, saporin 40 nM only and a combination of both drugs for PCI as well as a light irradiation period of 7 minutes. The samples were illuminated with blue lamp (420nm). Alamar Blue assay was carried out 48 hours after exposure to light.*

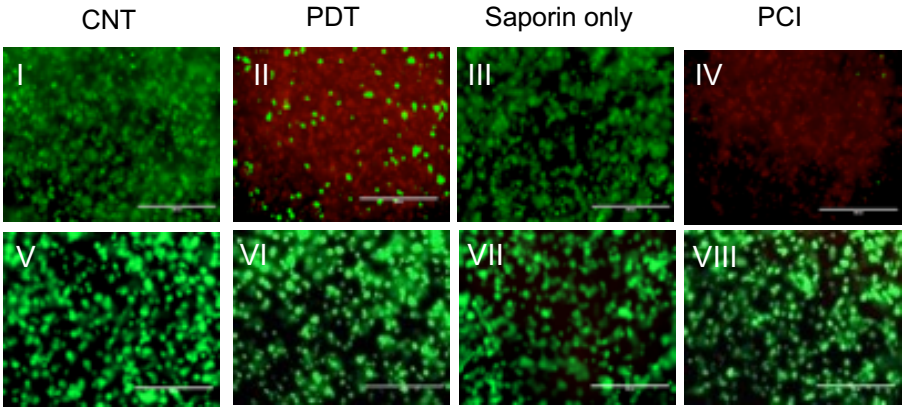

Figure 37: Live- dead images showing effect of hypoxia on PCI and PDT in SKOV3 cell non-spheroid constructs. PCI treatment in normoxic condition (I-IV) was compared to PCI treatment in hypoxic condition (V-VIII). The therapies used were $TPPS_{2a}$ (0.3µg/ml) only for PDT, saporin 40 nM only and a combination of both drugs for PCI as well as a light irradiation period of 7 minutes. The samples were illuminated with blue lamp (420nm). The scale bar presented in each image is 400µm.

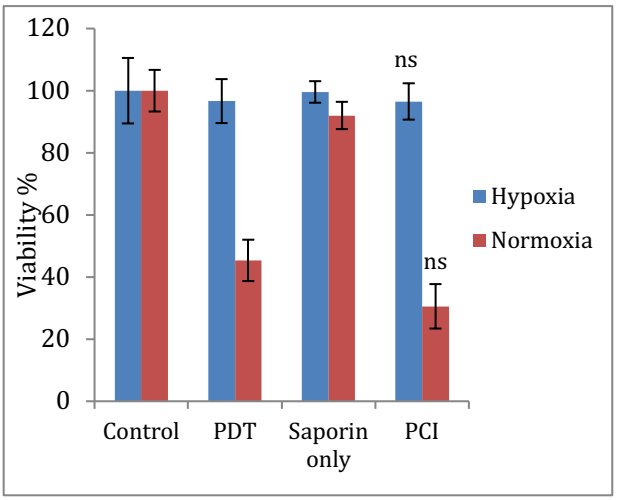

Figure 38: Percentage viability of SKOV3 cell 3D spheroid constructs after PDT, saporin only and PCI treatment in normoxic condition compared to hypoxic condition. The constructs were treated using $TPPS_{2a}$ only (0.7µg/ml) only for PDT, saporin 40nM only and a combination of both drugs for PCI as well as a light irradiation period of 7 minutes. The samples were illuminated with blue lamp (420nm). Alamar Blue assay was carried out 48 hours after exposure to light. No significance difference (ns) between PDT and PCI can be observed.

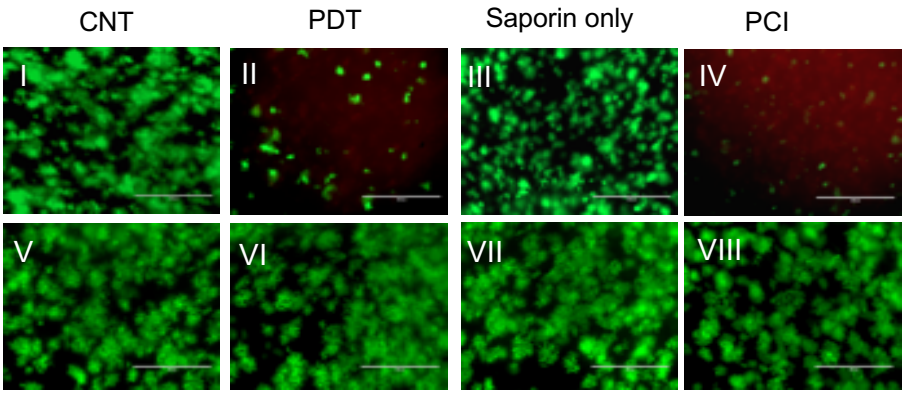

Figure 39: Live-dead images of SKOV3 cell spheroid constructs after PDT, saporin only and PCI treatment in normoxic condition (I-IV) compared to hypoxic condition (V-VIII). The constructs were treated using $TPPS_{2a}$ (0.7µg/ml) only for PDT, saporin 40nM only and a combination of both drugs for PCI as well as a light irradiation period of 7 minutes. The samples were illuminated with blue lamp (420nm). The scale bar presented in each image is 400µm.

3.9 Stimulation of apoptotic cell death in PCI treated 3D constructs

To determine the mode of cell death (necrosis or apoptosis) induced after treatment with PCI and other conditions, the non-spheroid 3D constructs were stained with Annexin V (for detection of apoptosis- shown in green) and Propidium iodide (for detection of necrosis – shown in red) either 24 hours or 48 hours after illumination. Without light illumination (Figure 40) a much lower level necrosis and apoptosis can be observed compared to samples exposed to irradiation with a slightly higher level of both type of cell death being detected in constructs treated with both $TPPS_{2a}$ and saporin (D and H) compared to monotherapies and control (A, B, C, E, F and G). As shown in Figure 41, for both cell lines a stronger apoptotic effect can be seen in constructs treated with PCI (D, H, L and P) than those treated with $TPPS_{2a}$ (PDT) (B, F, J and N) or saporin (C, G, K and O) only. In contrast, the necrotic effect observed in constructs treated with PDT only is noticeably higher than those treated with PCI or saporin only. Furthermore, a greater apoptotic effect is observed at 48 hours (H and P) compared to 24 hours (D and L).

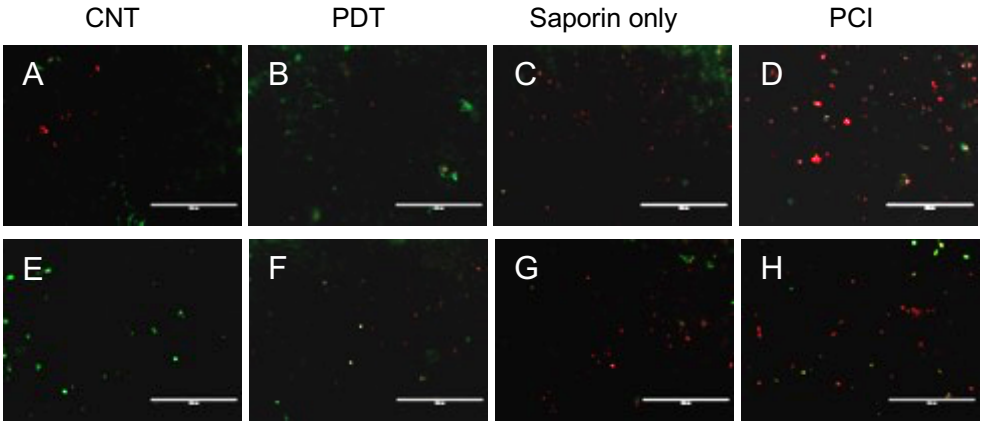

Figure 40: Apoptotic and necrotic induced cell death in 3D compressed constructs of SKOV3 and HEY cells. Comparison of cell death pathways induced after PCI compared to PDT or saporin alone in non-spheroid constructs of SKOV3 (A-D) and HEY (E-H) cells without light illumination. In PDT only treated constructs $TPPS_{2a}$ was used at concentrations of 0.3 μg/ml in SKOV3 cells (B) and 0.4 μg/ml in HEY cells (F). The saporin concentration used in this experiment was 20nM. The assay was carried out 24 hours post removal of drugs and chasing. Annexin V- was used to indicate apoptosis (green) and propidium iodide was used to indicate necrosis (red). The scale bar represents 400μm.

In an additional experiment, spheroid constructs of HEY cells were also stained with Annexin V FITC and Propidium iodide after treatment with PDT and PCI. As shown in Figure 42, higher level of necrosis can be detected in PDT treated samples (B and F) than PCI treated samples (D and H) whereas apoptotic cell death is more visible in PCI treated constructs. Furthermore, in the PDT treated constructs a greater degree of necrosis can be observed 48 hours after illumination (F) compared to 24 hours post illumination (B). In the PCI treated constructs on the other hand, the degree of both necrosis and apoptosis is greater in constructs incubated for 48 hours post illumination (H) than those incubated for 24 hours post illumination (D).

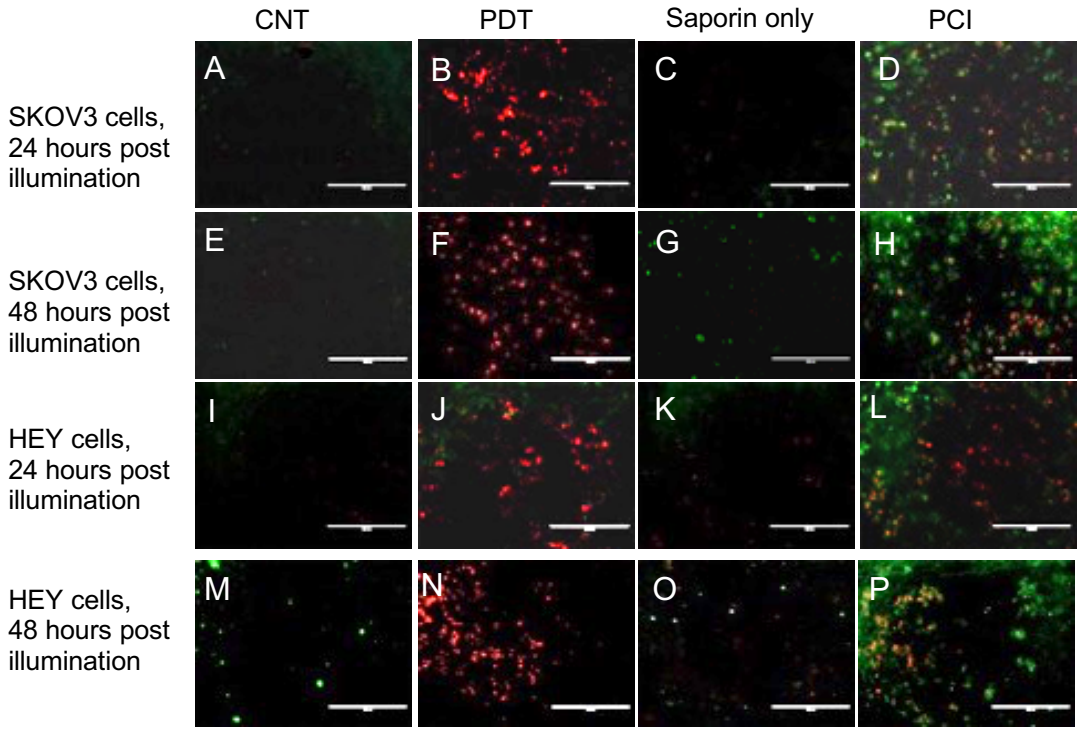

Figure 41: Apoptotic and necrotic induced cell death in 3D compressed constructs of SKOV3 and HEY cells. Comparison of cell death pathways induced after PCI compared to PDT or saporin alone in non-spheroid constructs of SKOV3 (A-H) and HEY (I-P) cells at 24 hours (A-D) and (I-L) and 48 hours post illumination (E-H) and (M-P) have been shown. In PDT only treated constructs $TPPS_{2a}$ was used at concentrations of 0.3 μg/ml in SKOV3 cells (B and F) and 0.4 μg/ml in HEY cells (J and N). The saporin concentration used in this experiment was 20nM. The constructs were illuminated for 7 minutes using blue lamp (420nm). Annexin V- was used to indicate apoptosis (green) and propidium iodide was used to indicate necrosis (red). The scale bar represents 400μm.

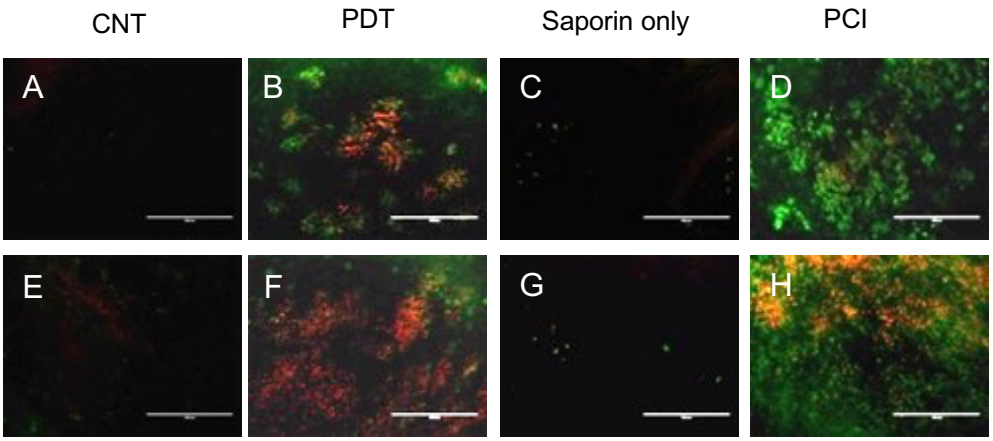

Figure 42: Apoptotic and necrotic induced cell death in 3D spheroid constructs of HEY cells. Constructs were treated with PDT (B and F) and PCI (D and H) 24 hours (A- D) and 48 hours (E- H) post illumination. In PDT only treated constructs $TPPS_{2a}$ was used at concentrations of 0.5 μg/ml (B and F). The saporin concentration used in this experiment was 20nM. The samples were illuminated with blue lamp (420nm) for 7 minutes. Annexin V- was used to indicate apoptosis (green) and propidium iodide was used to indicate necrosis (red). The scale bar presented in each image is 400μm.

Chapter 4

4. PCI in 3D non-spheroid constructs of ovarian cancer using Dactinomycin as chemotherapeutic drug

In this chapter another anti-cancer drug called dactinomycin or actinomycin D, with a high molecular weight (approximately 1255 Da) has been used for PCI studies as it is likely to be uptaken via endocytosis which makes it suitable candidate for such study. Dactinomycin is a clinically approved agent which acts as an anti-tumour antibiotic and functions through DNA intercalation as well as inhibition of RNA and protein synthesis. This agent has not been tested for PCI before and based on its molecular weight, it should be taken up partly via endocytosis like bleomycin which has a molecular weight of approximately 1400 Da. Furthermore, Dactinomycin is fluorescent unlike bleomycin, therefore fluorescence imaging can be carried out to show endolysosomal localisation of this drug.

The experiments carried out for this chapter include investigating lysosomal uptake of the drug since PCI is designed to deliver drugs that are prone to endolysosomal entrapment and degradation, PCI treatment of 2D and 3D cultures of SKOV3 and HEY cells and investigation of dactinomycin uptake at different temperatures to confirm occurrence of endocytosis. Preliminary studies were carried out to determine the correct parameters for the PCI treatment and treatments on monolayer cultures were carried for comparison purposes to the 3D cultures. The molecular structure of dactinomycin is shown in figure 43.

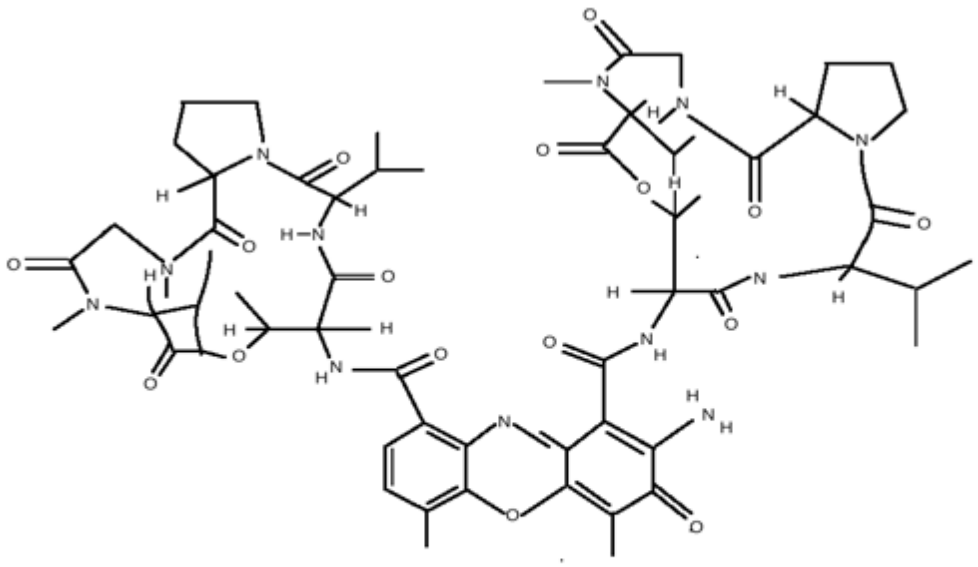

Figure 43: Structure of Dactinomycin (Actinomycin D).

4.1 Intracellular uptake and localisation of Dactinomycin in HEY and SKOV3 cells

Dactinomycin uptake studies were carried out monolayer cultures of HEY and SKOV3 cells as well as 3D non-spheroid cultures of SKOV3 cells by incubating the cells with the drug at 50nM concentration for 4 hours before washing and additionally staining them with lysotracker red to determine co-localisation.

As shown in Figure 44, bright fluorescence can be detected from both Dactinomycin (A, D, G, J) (green) and Lysotracker red (B, E, H, K) (red) in monolayer cultures of both cell lines. Such can also be observed in the 3D cultures (Figure 45) where the cells have also begun forming very small aggregates. The exact overlap of the green and fluorescence (C, F, I, L) indicated that both the Dactinomycin drug and Lysotracker red are co-localised within the lysosomes of the cells.

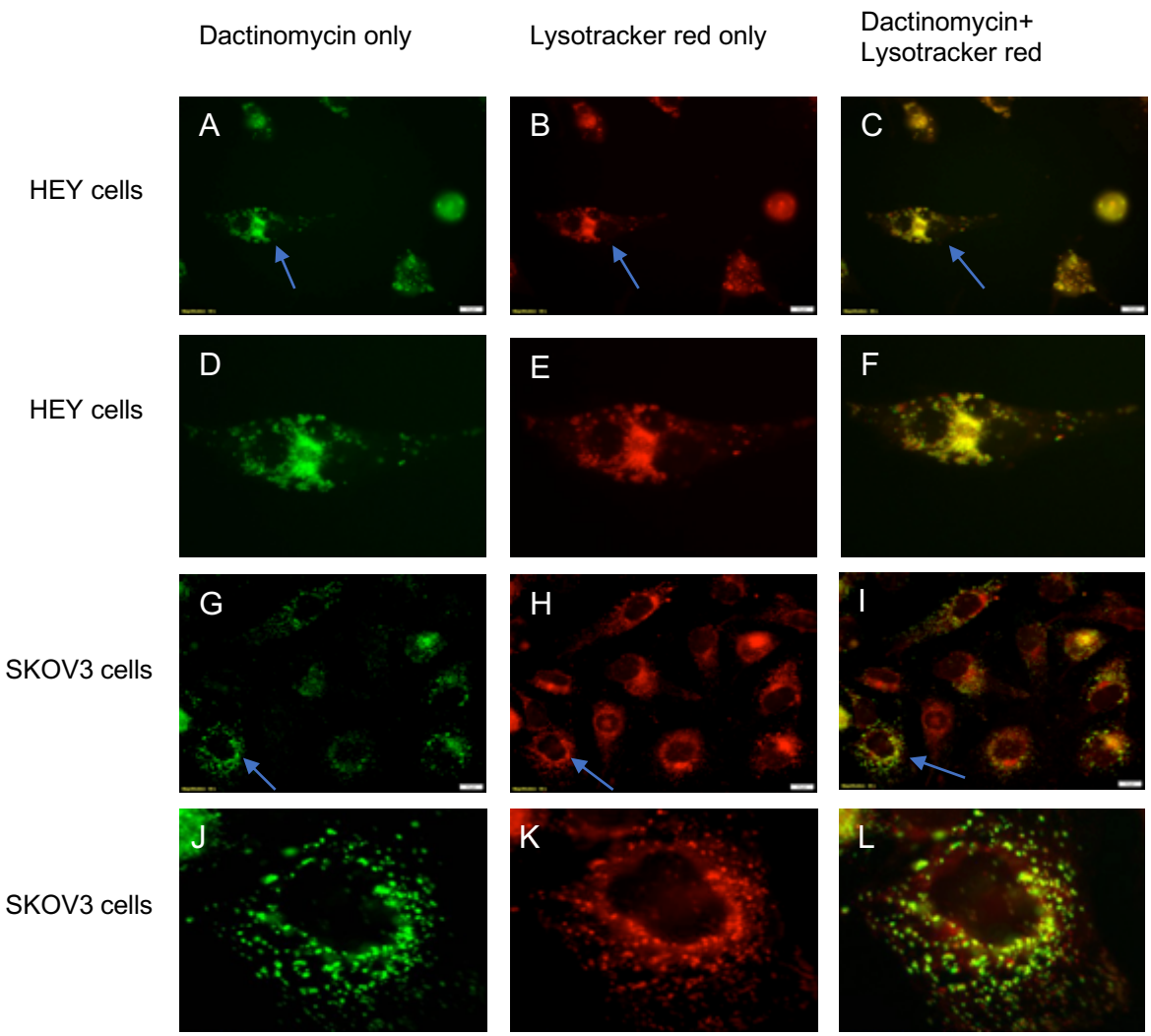

Figure 44: Intracellular uptake of dactinomycin in HEY (A-F) and SKOV3 (G-L) monolayer cultures. (A and G): intracellular uptake of dactinomycin in HEY and SKOV3 monolayer cultures, (B and H): intracellular uptake of lysotracker red in HEY and SKOV3 monolayer cultures, (C and I): co-localisation of dactinomycin and lysotracker red in HEY and SKOV3 monolayer cultures. The blue arrows show a single cell from each cell line magnified and shown in figures D-F (HEY cells) and J-L (SKOV3 cells). Images were obtained with fluorescence microscope (60x objective, Olympus BX63). The fluorescence of dactinomycin was measured at 520nm using FITC channel. The scale bar presented in images A-C and G- I is 10µm.

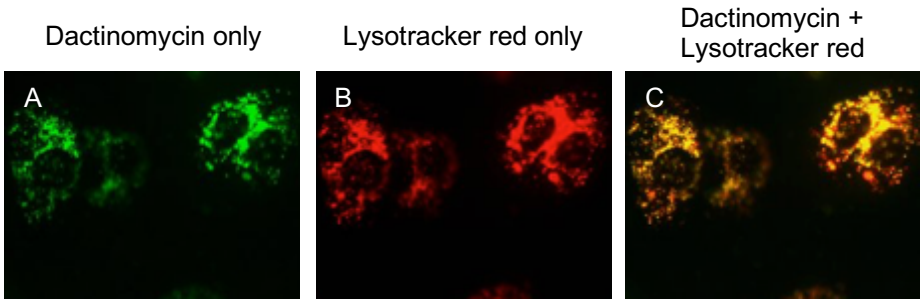

Figure 45: Intracellular uptake of dactinomycin in 3D constructs of SKOV3 cells. A: intracellular uptake of dactinomycin in SKOV3 3D constructs, B: intracellular uptake of lysotracker red in SKOV3 3D constructs, C: co-localisation of dactinomycin and lysotracker red in SKOV3 3D constructs. Images were obtained with fluorescence microscope (20x objective, Olympus BX63). The dimensions of the images are 72μm x42μm.

4.2 *In vitro* PDT/PCI phototoxicity studies in monolayer and 3D non-spheroid cancer cultures using dactinomycin as anti-cancer drug

Using the fluorometric Alamar blue cell viability assay, the cell viabilities in both monolayer and 3D cultures post treatment with different conditions were measured. For comparative purposes 2D monolayer cultures were initially used in the study. The same $TPPS_{2a}$ concentrations used in earlier PDT/PCI studies for monolayer and non-spheroid constructs (0.3μg/mL for SKOV3 cells and 0.4μg/mL for HEY cells) were used in this study.

Toxicity studies using dactinomycin only indicated that 1nM concentration resulted in low cell death (≤10%) in the monolayer cultures and was therefore declared as suitable for use in this experiment. Figure 46 shows reductions in cell viability using various concentrations of dactinomycin.

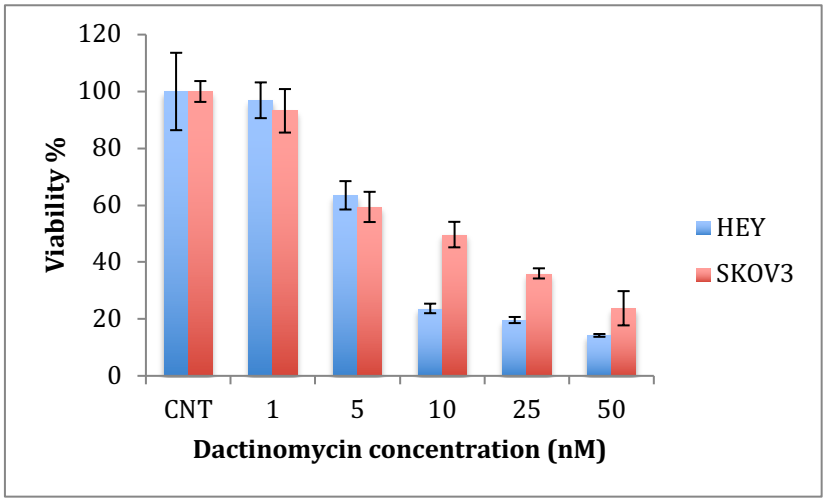

Figure 46: Percentage viability of cells post treatment with various concentrations of dactinomycin. MTT assay was carried out 48 hours after removal of drug and washing the cells with PBS.

The MTT results showed that viabilities after PCI dropped to 48% vs. 55% (3 minutes), 13% vs. 17% (5 minutes) and 4% vs. 5% (7 minutes) in HEY and SKOV3 monolayer cultures respectively. The alpha values for each illumination period were calculated as 1.4, 2.8 and 6.4 in HEY cells and 1.4, 2.8 and 4.9 in SKOV3 cells. Figure 47 shows the percentage viabilities of both cell lines after PCI compared to monotherapies and control.

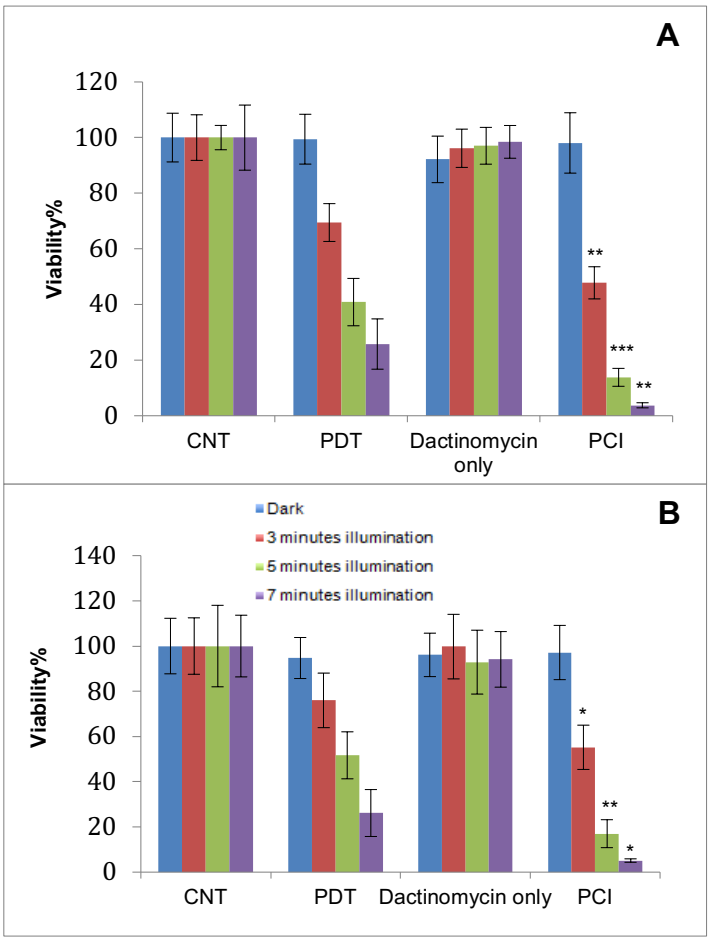

*Figure 47: Percentage viability of HEY (A) and SKOV3 (B) cells in monolayer cultures after treatment with PDT, Dactinomycin and PCI (MTT assay). The cells were treated with $TPPS_{2a}$ (0.4µg/ml for HEY cells, 0.3µg/ml for SKOV3 cells), Dactinomycin only (1nM) and PCI. The samples were illuminated with blue lamp (420nm). The cultures were incubated for 48 hours post illumination before terminating the experiment using MTT assay. *p<0.05, **p<0.01, *** p<0.001. These p values show the significance difference between PDT and PCI treatments.*

The Alamar blue study results also showed that in 2D monolayer cultures a significant PCI effect and reduction in percentage viability was achieved particularly compared to treatment with Dactinomycin alone. In SKOV3 cells the viabilities were reduced from 94% to 38% (3 minutes), 88% to 14% (5 minutes) and 89% to 6% (7 minutes) compared to dactinomycin only with the PCI efficacies being 1.9 and 2.5 (3 minutes), 2.1 and 6.3 (5 minutes) and 2.7 and 14.8 (7 minutes) compared to using PDT and dactinomycin alone respectively (Figure 48). The corresponding alpha values for each of the mentioned irradiation periods were 1.8, 1.9 and 2.4.

PCI continued to show a significant effect in the HEY cell monolayer cultures as well with the viabilities being reduced from 96% to 28% (3 minutes), 97% to 14% (5 minutes) and 98% to 4% (7 minutes) compared to dactinomycin alone. The PCI efficacies achieved for each illumination period were 2.5 and 3.2 (3 minutes), 3.8 and 8.9 (5 minutes) and 9.0

and 46 (7 minutes) versus PDT and dactinomycin alone respectively with the highest PCI efficacy observed after 7 minutes (P<0.001) (Figure 48). Good synergistic alpha values of 2.2, 3.3 and 8.3 were calculated after each irradiation period. The percentage viabilities, PCI efficacies and synergistic values are also tabulated in table 8.

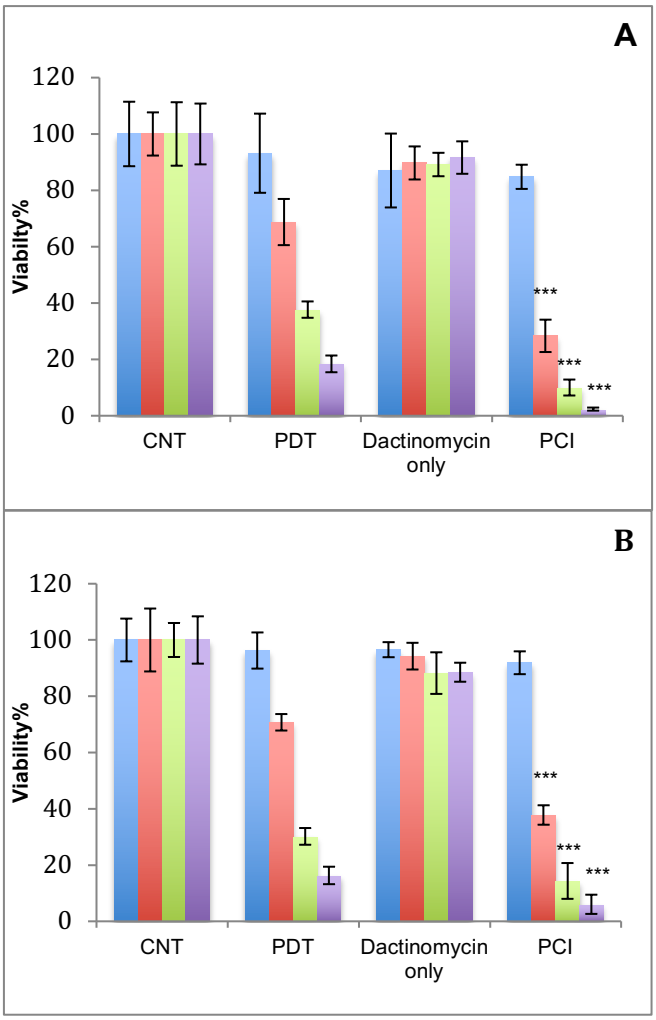

*Figure 48: Percentage viability of HEY (A) and SKOV3 (B) cells in monolayer cultures after treatment with PDT, Dactinomycin and PCI (Alamar blue). The cells were treated with $TPPS_{2a}$ (0.4µg/ml for HEY cells, 0.3µg/ml for SKOV3 cells), Dactinomycin only (1nM) and PCI. The samples were illuminated with blue lamp (420nm). The cultures were incubated for 48 hours post illumination before terminating the experiment using Alamar blue assay. *** p<0.001. These p values show the significance difference between PDT and PCI treatments.*

	2D Culture							
Cell line	Incubation period post light exposure (hour)	Light Exposure period (minute)	PDT only (% mean viability ± % SD)	Dactinomycin only (% mean viability ± % SD)	PCI (% mean viability ± %SD)	PCI efficacy ratio vs. PDT	PCI efficacy ratio vs. Dactinomycin only	Alpha values
SKOV3	48	3	70.7 ±2.9	94.3 ±4.7	37.8±3.5	1.9	2.5	1.8
HEY	48	3	68.7±8.2	89.7 ±5.9	28.4±5.7	2.5	3.2	2.2
SKOV3	48	5	30.2 ±3.0	88.2 ±7.4	14.4±6.4	2.1	6.3	1.9
HEY	48	5	37.7±2.9	89.2±4.2	10.0±2.8	3.8	8.9	3.4
SKOV3	48	7	16.3±3.1	88.5±3.4	6.0±3.4	2.7	14.8	2.4
HEY	48	7	18.4±3.0	91.6±5.8	2.4±0.54	9.0	46	8.3

Table 8: Summary of percentage viabilities ± %SD, PCI efficacies and alpha values in 2D monolayer cultures of SKOV3 and HEY cells

Although there was a lower reduction in percentage viability of both cell lines in the 3D constructs, PCI still caused a significant effect in the cells as shown in Figure 49. For example, in SKOV3 the viabilities reduced from 96% to 42% (3 minutes), 93% to 22% (5 minutes) and 91% to 9% (7 minutes) compared to dactinomycin alone with the PCI efficacies being 1.9 and 2.3 (3 minutes), 1.7 and 4.7 (5 minutes) and 2.2 and 10.1 (7minutes) compared to PDT alone and dactinomycin alone respectively. Similarly, the HEY cells showed reduction in viability from 91% to 33% (3 minutes), 88% to 15% (5 minutes) and 89% to 4% (7 minutes) compared to dactinomycin alone. The PCI efficacies for this cell line compared to PDT alone and dactinomycin alone were 2.2 and 2.8 (3 minutes), 2.9 and 5.9 (5 minutes) and 5.5 and 22.3 (7 minutes). In this experiment the alpha values after each illumination period were calculated as 1.8, 1.6 and 2.0 for SKOV3 cell constructs as well as 2.0, 2.5 and 4.9 for HEY cells. Overall the HEY cells showed more sensitivity to PCI treatment using dactinomycin than SKOV3 cells. Table 9 also shows a summary of the results discussed.

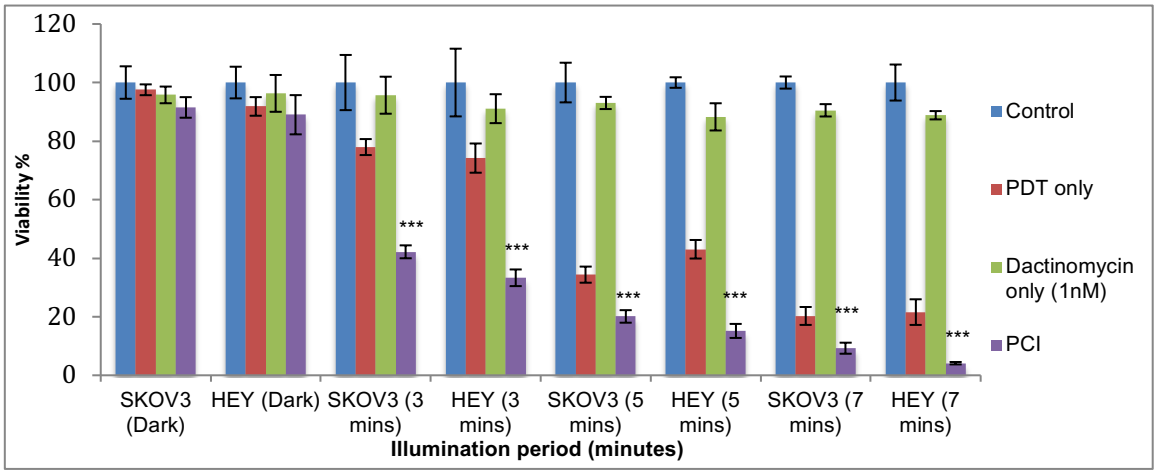

*Figure 49: Percentage viability of SKOV3 and HEY cells in non-spheroid 3D compressed collagen constructs after treatment with PDT, dactinomycin only and PCI. Constructs were treated with $TPPS_{2a}$ $(0.3\mu g/mL)$(SKOV3 cells) and $(0.4\mu g/mL)$(HEY cells), 1 nM dactinomycin, as well as 48 hours incubation post illumination. The samples were illuminated with blue lamp (420nm). ***p<0.001. The p values show the significance difference between PDT and PCI treatments.*

	3D culture							
Cell line	Incubation period post light exposure (hour)	Light Exposure period (minute)	PDT only (% mean viability ± % SD)	Dactinomycin only (% mean viability ± % SD)	PCI (% mean viability ± %SD)	PCI efficacy ratio vs. PDT	PCI efficacy ratio vs. Dactinomyin only	Alpha values
SKOV3	48	3	78.0±2.7	95.7±6.3	42.2±2.2	1.9	2.3	1.8
HEY	48	3	74.2±5.0	91.1 ±4.9	33.3 ±2.8	2.2	2.8	2.0
SKOV3	48	5	34.4±2.8	93.0±2.1	20.1±2.1	1.7	4.7	1.6
HEY	48	5	43.1±3.2	88.3±4.6	15.2±2.4	2.9	5.9	2.5
SKOV3	48	7	20.3±5.0	90.5±2.9	9.2±2.6	2.2	10.1	2.0
HEY	48	7	21.6±4.4	88.8±1.4	4.1±0.4	5.5	22.3	4.9

Table 9: Summary of percentage viabilities ± %SD, PCI efficacies and alpha values in 3D cultures of SKOV3 and HEY cells

Live-dead images at the end of each experiment also confirmed the results displayed in Figure 49. As shown in figures 50 and 51, with the increase in illumination periods some consistent increase in the level of cell kill can be seen in both cell lines using PDT only.

However, such cytotoxic effect is much more significant in PCI treated samples than the montherapies.

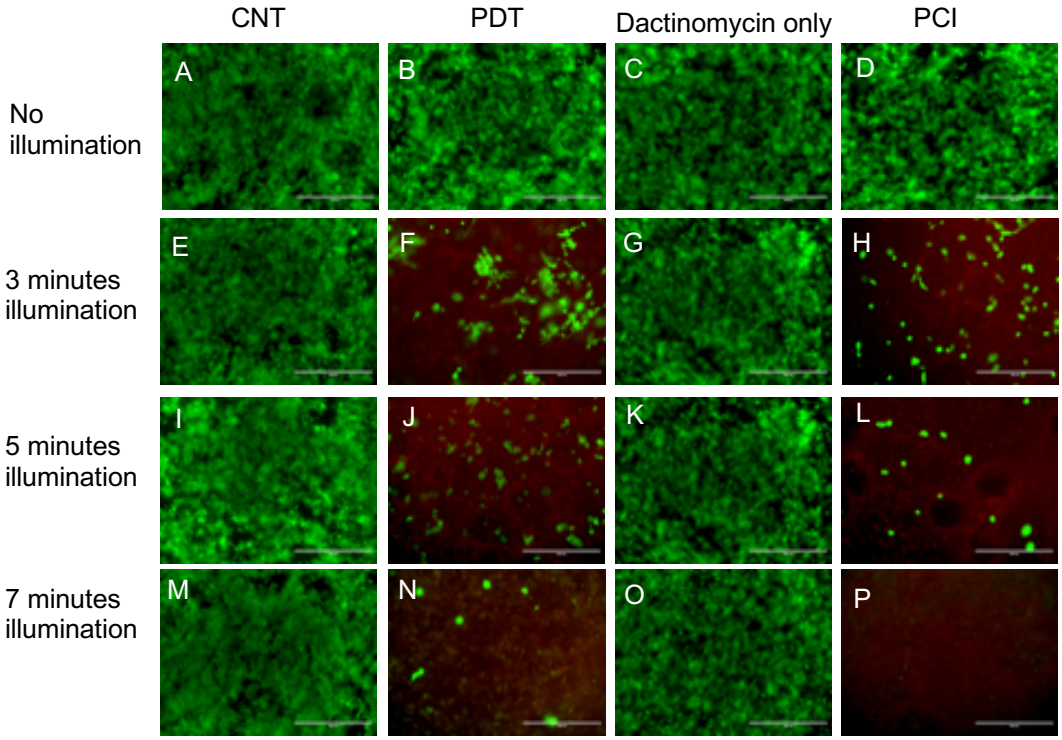

Figure 50: Live dead images of HEY 3D cultures post PDT (B, F, J and N), Dactinomycin only (1nM) (C, G, K and O) and PCI (D, H, L and P) treatment using different light conditions. The samples were illuminated with blue lamp (420nm). The assay was carried out 48 hours post illumination. 3D constructs were incubated with the Live/dead solution containing Calcein-AM to stain live cells (green) and Ethidium homodimer-1 to stain dead cells. The scale bar presented in each image is 400μm.

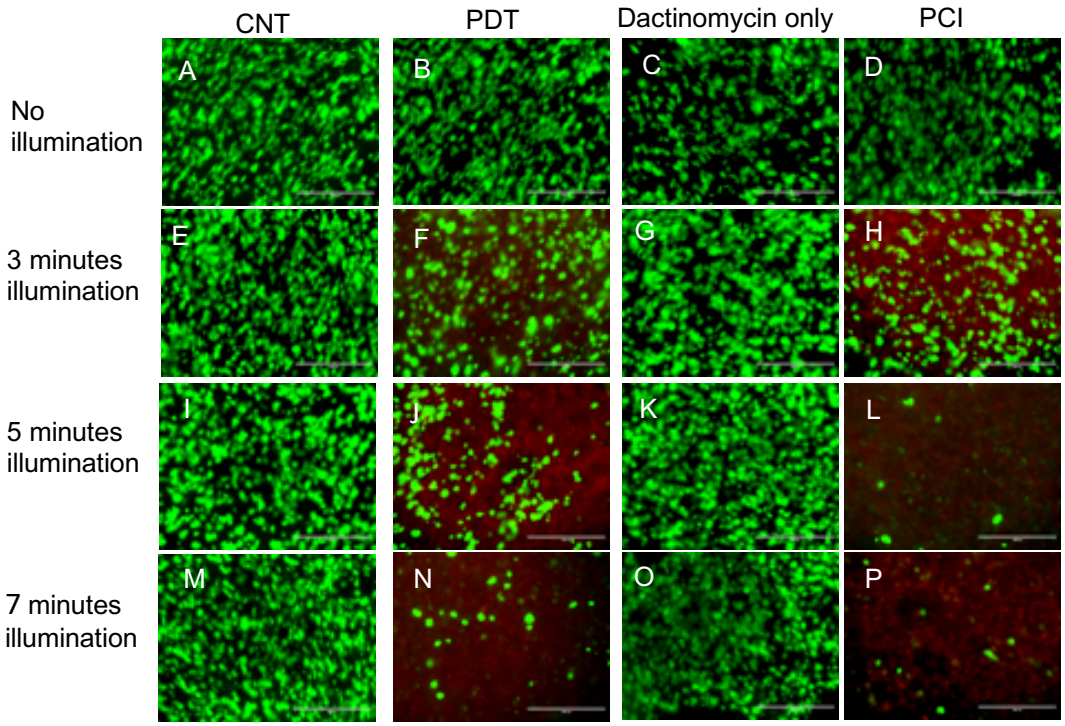

Figure 51: Live dead images of SKOV3 3D cultures post PDT (B, F, J and N), Dactinomycin only (1nM) (C, G, K and O) and PCI (D, H, L and P) treatment using different light conditions. The samples were illuminated with blue lamp (420nm). The assay was carried out 48 hours post illumination. 3D constructs were incubated with the Live/dead solution containing Calcein-AM to stain live cells (green) and Ethidium homodimer-1 to stain dead cells. The scale bar presented in each image is 400μm.

4.3 Temperature dependence of dactinomycin uptake by ovarian cancer cells in monolayer cultures

In this experiment SKOV3 monolayer cultures were incubated with dactinomycin (1nM) for 2 hours either at 4℃ or 37 ℃ to confirm if the drug is taken up via endocytosis. At the end of the 2 hours incubation with dactinomycin the cells were washed with PBS and treated with fresh drug-free media and were incubated for a further 2 hours at either 4℃ or 37 ℃ before terminating the experiment.

The results showed that the fluorescence detected from cells incubated at 37 ℃ was 5.8 times higher than that detected from cells incubated at 4℃ indicating that uptake was higher at 37 ℃ and confirming that it occurred through endocytosis. The results are presented in Figure 52.

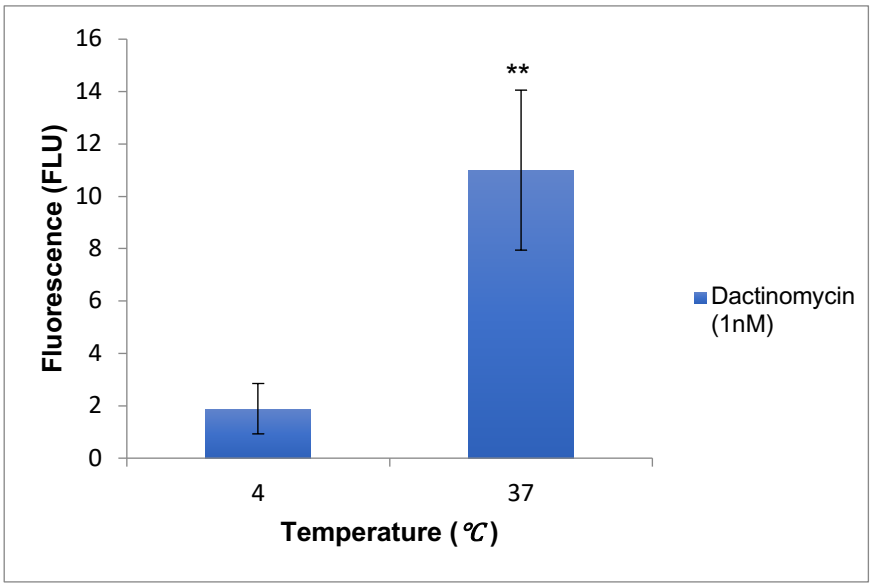

*Figure 52: Fluorescence detected from dactinomycin after incubation of SKOV3 cells with the drug at different temperatures (4℃ or 37 ℃). **P<0.01 shows the significance difference in the dactinomycin fluorescence in the two temperatures.*

Chapter 5

5. PCI using saporin in tumouroid constructs of ovarian cancer

Since tumours *in vivo* are more complex than the simple models created *in vitro*, tumouroid constructs of ovarian cancer which consist of stromal cells as well as cancer cells have been used for PDT/PCI studies in this chapter. These constructs were also incubated for 7 days prior to undergoing treatment. However, embedding the original cancer mass in a bigger compressed collagen construct consisting of stromal cells allows the growing cancer cells to invade the stromal environment unlike the spheroid constructs where the cells could only grow within the simple cancer mass model. The regrowth of cancer cells post PDT treatment has also been studied. Figure 5 and 53 demonstrate the steps involved in the creation of the 3D compressed collagen cancer constructs. Figure 5A also shows the original method used for fabricating both 3D simple and tumouroid compressed collagen constructs through partial plastic compression (174). A schematic diagram of the ovarian tumouroid used in the experiments presented in this chapter has been shown in Figure 54.

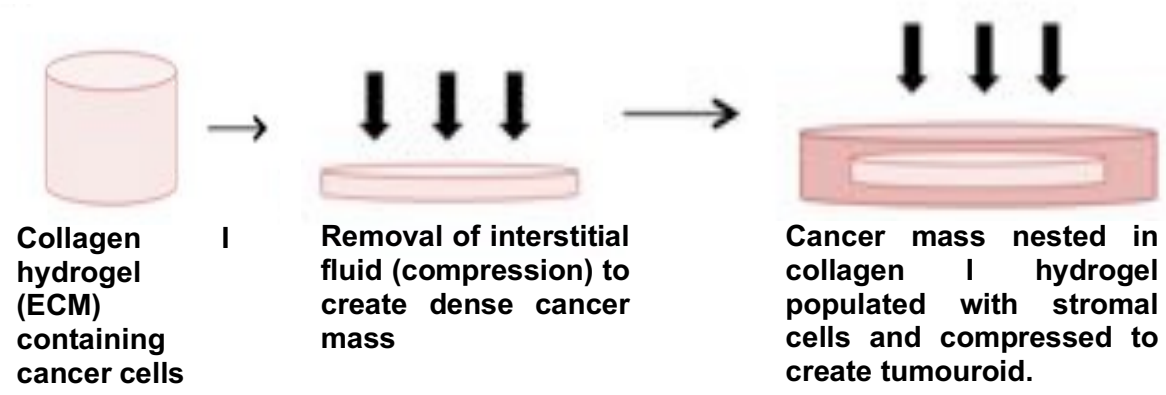

Figure 53: Steps involved in creating tumouroid construct (212). The diameter of the tumouroid construct created is approximately 15mm.

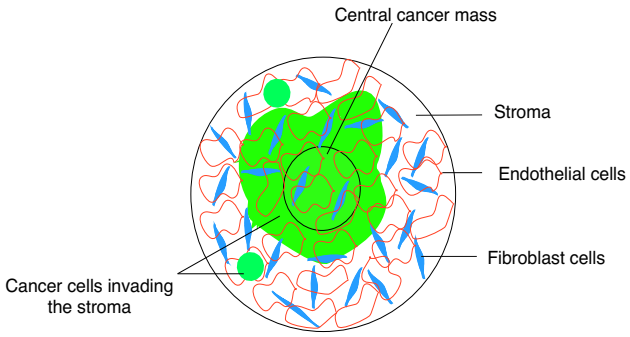

Figure 54: Schematic of ovarian tumouroid. The central cancer mass is manufactured by mixing HEY cancer cells and collagen type 1, allowing to set as hydrogel and applying absorbers (RAFT™) to remove liquid and create a more stiff, compressed 3D tissue. The cancer mass is placed in a large "stromal" hydrogel populated by fibroblasts (HDF) and endothelial cells (HUVECs), with further addition of stroma hydrogel. The whole construct is compressed (RAFT™) to produce tumouroids. Tumouroids are allowed to mature for 7 days, with cancer invading from the cancer mass into the stroma, prior to drug assault.

5.1 Tumouroid growth and stroma invasion

In this experiment constructs consisting of cancer cells (HEY cells) and stromal cells (fibroblasts: HDFs and endothelial cells: HUVECS) were incubated for 7 days prior to undergoing treatment. By day 10 (termination point of experiment) the cancer cells had managed to proliferate and invade the stroma both in the area surrounding the central cancer mass and further into the stroma. The staining for each cell line was carried out as described in the methods and materials section. The experiments were repeated 3-5 times. As shown in Figure 55, the HEY cancer cells are able to invade the stroma with stromal cells present (fibroblast and endothelial cells) (B and C) as effectively as they could invade the a-cellular stroma (A). Although (bi and bii) show a tumouroid consisting of all three cell lines, only the stained HEY and HDF cells have been presented.

A

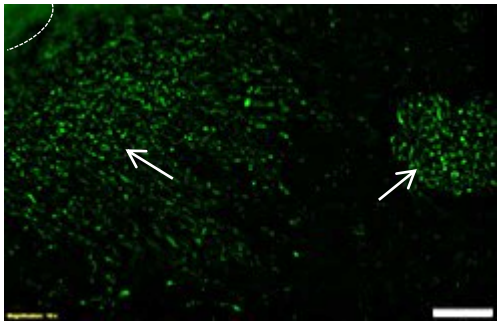

B

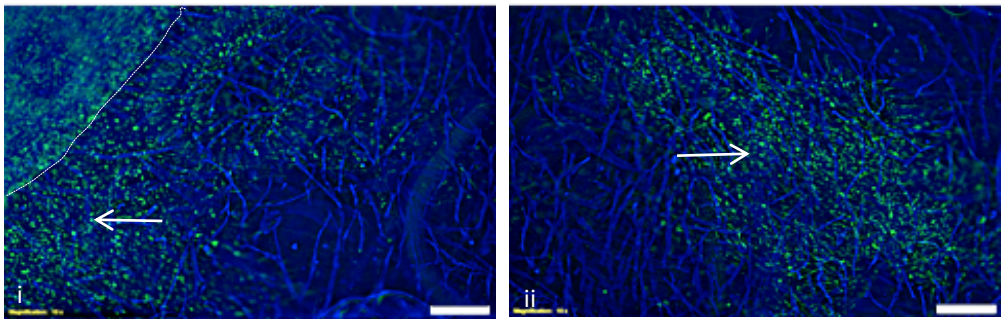

C

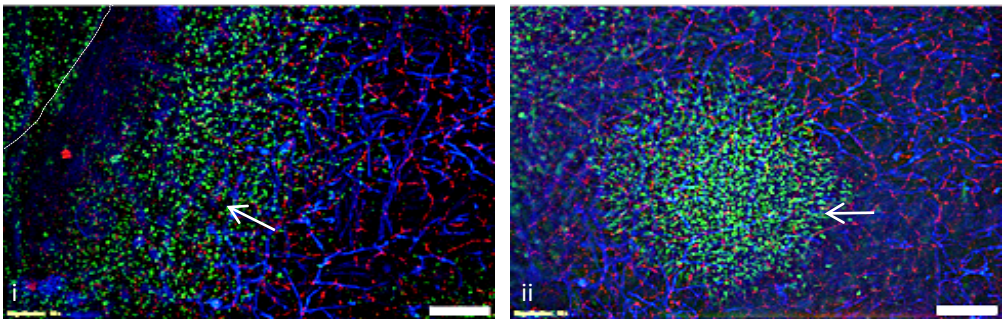

Figure 55: Cancer cell invasion into the stroma in ovarian tumouroids 10 days post manufacture. Invasion of cancer cells (HEY, arrows) from original cancer mass (denoted with dotted line) into acellular stroma (A), and stroma with fibroblast (HDF) and endothelial cells (HUVEC) (B and C; I = stroma adjacent to cancer mass; ii = deeper stroma). HEY, HDF and HUVECS were stained with Anti-cytokeratin 7 (Alexa Fluor 488) $\lambda_{Ex/Em:}$ 490/525 (green), Anti-Vimentin (Alexa Fluor 405) $\lambda_{Ex/Em:}$ 401/421 (blue) and Anti-CD31 (PerCP-eFluor 710) $\lambda_{Ex/Em:}$ 482/709 (red) conjugated antibodies respectively. Scale bar = 100μm.

5.2 PDT and PCI in tumouroid constructs

In one experiment the tumouroid constructs were exposed to PDT treatment using $TPPS_{2a}$ (1μg/mL) and 5 minutes illumination period to study the effect of a stronger PDT treatment on the cancer mass and the stroma (Figure 56). Compared to the control construct (Figure 56A) which shows invasion of cancer cells from the central cancer mass into the stroma with normal shaped HDF and HUVECS, the PDT treated constructs (Figure 56B) show destruction in the invading cancer mass as well as the HUVEC cells and a reduction in the number of cancer cells in the central cancer mass and the HDFs.

PCI treatment using $TPPS_{2a}$ (0.5 μg/mL) and Saporin (20nM) and 3 minutes illumination period was carried out on the tumouroid constructs (Figure 57D) basing the concentrations and the illumination period on previous PCI experiments on simple spheroid constructs (chapter 3.6). Treatment using PDT only (Figure 57B) caused a reduction in cancer cells invading the stroma and HDFs in comparison to the control and saporin only treated constructs (Figure 57A and 57C). In the PCI treated constructs a further destruction of the cancer cells in the central cancer mass and those invading the stroma was observed as well as destruction of HUVEC and HDF cells in the stroma (Figure 57D). One interesting point noticed in the studies was that the HEY cells showed a tendency to migrate and some of the cells populated in the border of the central cancer mass which possibly resulted in a higher destruction of cells in the center of the cancer mass than those in the edges of the cancer mass (Figure 60).

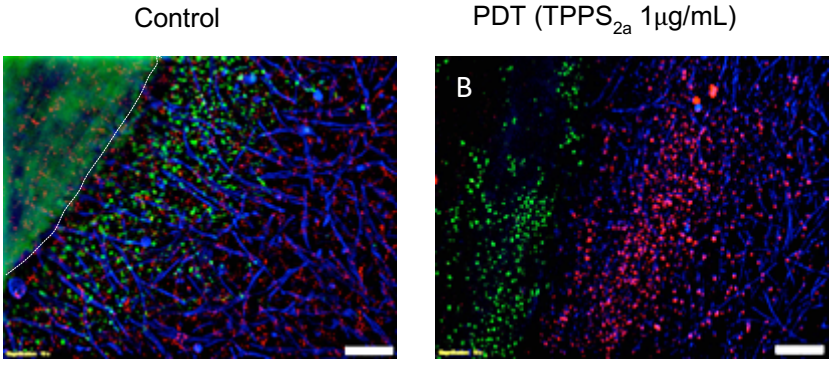

Figure 56: PDT treatment in ovarian tumouroids. (A) control tumouroid showing invasion of stroma by cancer cells (HEY, green) from original cancer mass (denoted by white dotted line). (B) PDT of tumouroids using $TPPS_{2a}$ (1 μg/mL) and 5 minutes of illumination, showing tissue-wide disruption. The samples were illuminated with blue lamp (420nm). The images were obtained 48 hours post illumination. HEY, HDF and HUVECS were stained with Anti-cytokeratin 7 (Alexa Fluor 488) $\lambda_{Ex/Em:}$ 490/525 (green), Anti-Vimentin (Alexa Fluor 405) $\lambda_{Ex/Em:}$ 401/421 (blue) and Anti-CD31 (PerCP-eFluor 710) $\lambda_{Ex/Em:}$ 482/709 (red) conjugated antibodies respectively. Scale bar =100μm.

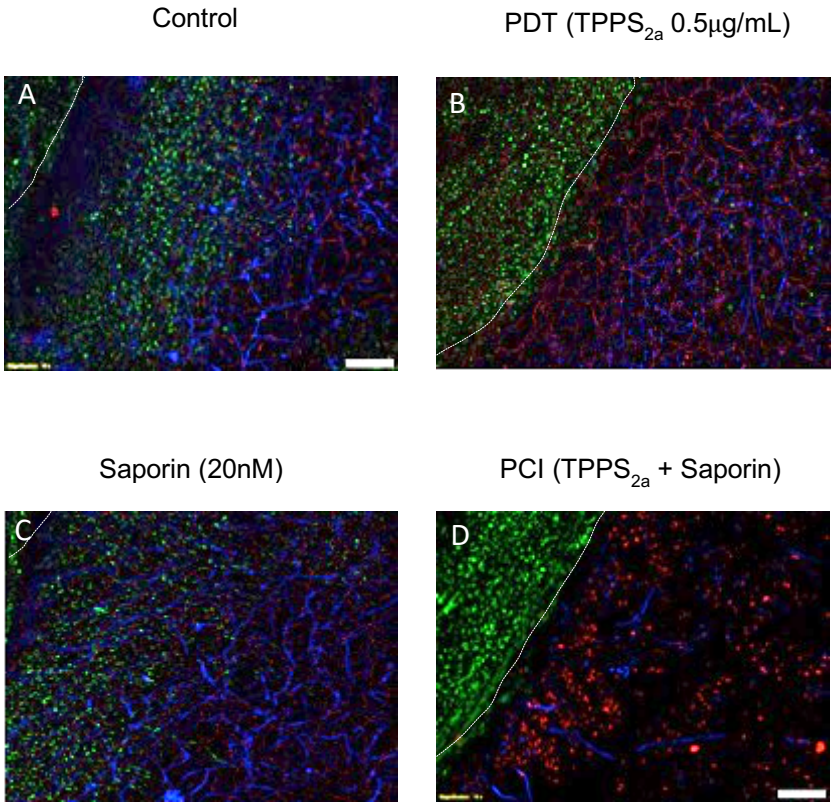

Figure 57: PDT and PCI treatment with 3 minutes of light illumination in ovarian tumouroids. Original cancer mass denoted by white dotted line in all images (A): Control tumouroid construct; cancer cells (HEY, green) have invaded into the stroma. (B) PDT of tumouroid using $TPPS_{2a}$ (0.5 μg/mL). (C) Tumouroid treated with Saporin (20nM) only. (D) PCI of tumouroid using a combination of both drugs. The samples were illuminated with blue lamp (420nm). The images were obtained 48 hours post light illumination. HEY, HDF and HUVECS were stained with Anti-cytokeratin 7 (Alexa Fluor 488) $\lambda_{Ex/Em:}$ 490/525 (green), Anti-Vimentin (Alexa Fluor 405) $\lambda_{Ex/Em:}$ 401/421 (blue) and Anti-CD31 (PerCP-eFluor 710) $\lambda_{Ex/Em:}$ 482/709 (red) conjugated antibodies respectively. Scale bar presented = 100μm.

The treatment of constructs with $TPPS_{2a}$ (1μg/mL) and PCI ($TPPS_{2a}$ (0.5μg/mL) + Saporin (20nM) in the dark showed no evidence of significant toxicity due to lack of reduction in the cancer and stromal cells which again proves importance of an appropriate light source being available for the treatment to elicit good results (Figure 58).

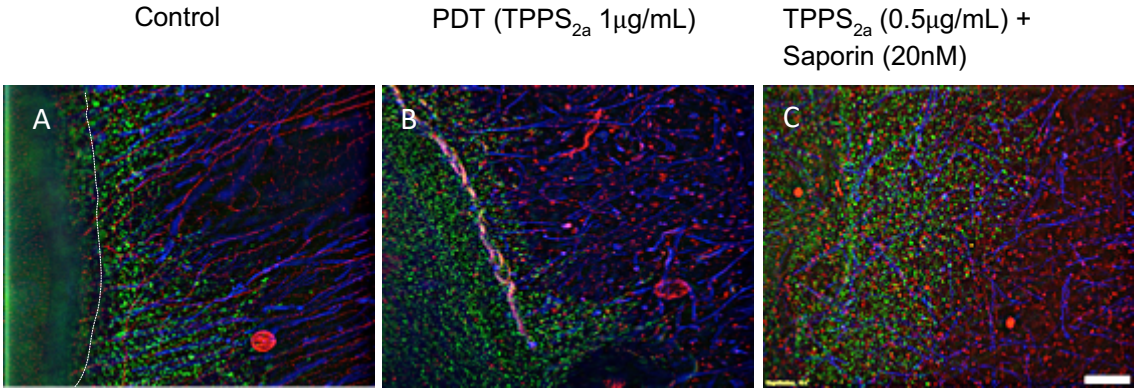

Figure 58: (A): Control untreated tumouroids, (B): tumouroids treated with PDT using $TPPS_{2a}$ (1 μg/mL), (C): PCI using combination of $TPPS_{2a}$ (0.5 μg/mL) and Saporin (20nM) without light illumination. The images were obtained 48 hours after treatment. The HEY, HDF and HUVECS were stained with Anti-cytokeratin 7 (Alexa Fluor 488) $\lambda_{Ex/Em:}$ 490/525 (green), Anti-Vimentin (Alexa Fluor 405) $\lambda_{Ex/Em:}$ 401/421 (blue) and Anti-CD31 (PerCP-eFluor 710) $\lambda_{Ex/Em:}$ 482/709 (red) conjugated antibodies respectively. Scale bar = 100μm.

In another experiment the effect of PDT/PCI on the stroma (HDFs in particular for this experiment) was investigated as cancer associated fibroblasts can play an important role in cancer progression (214). Although the fibroblasts used in this experiment are not a cancer associated phenotype, they still provide a representation of how PDT/PCI can affect such stromal cells. As figure 59 shows both PDT (59B) and PCI (59C) cause destruction of fibroblast cells, with PDT showing slightly more effect than PCI.

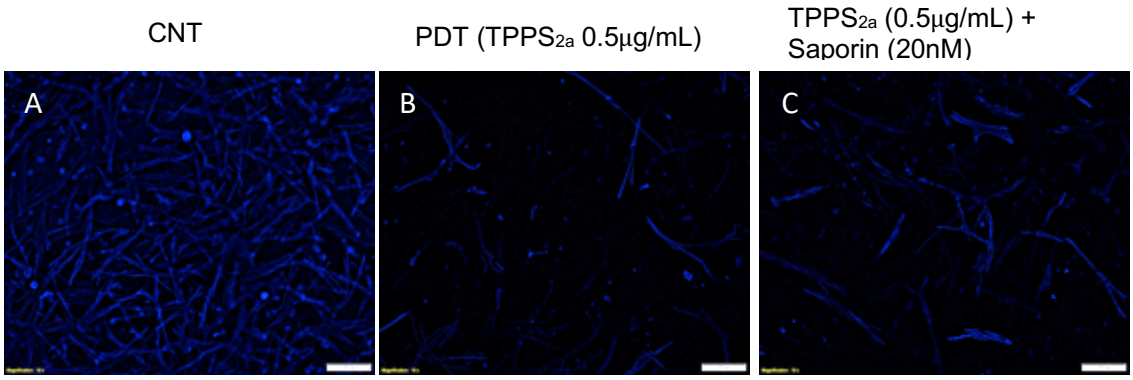

Figure 59: PDT and PCI treatment of fibroblast cells (HDFs) using 3 minutes light illumination. (A) control 3D constructs populated with fibroblasts and undergoing (B) PDT treatment using $TPPS_{2a}$ (0.5 μg/mL). (C) PCI treatment using combination of $TPPS_{2a}$ (0.5 μg/mL) and Saporin (20nM). The samples were illuminated with blue lamp (420nm). The images were obtained 48 hours post light illumination. The HDFs were stained with Anti-Vimentin (Alexa Fluor 405) $\lambda_{Ex/Em:}$ 401/421 (blue). Scale bar = 100μm.

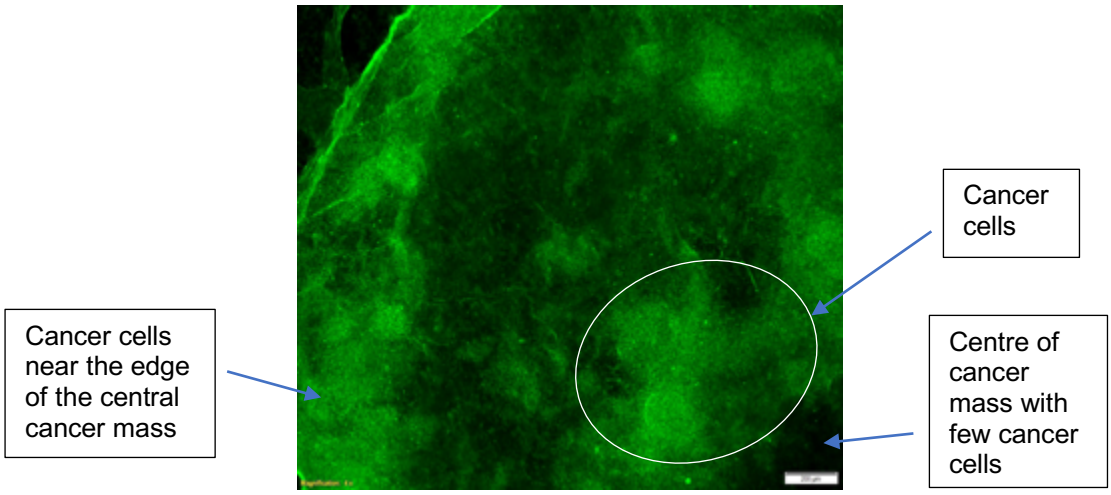

Figure 60: Distribution of HEY cells in the central cancer mass. The cells were stained with Anti-cytokeratin 7 (Alexa Fluor 488) $\lambda_{Ex/Em:}$ 490/525 (green) conjugated antibody. The scale bar presented is $200\mu m$.

Measurements of distance within the stroma invaded by cancer cells were taken from constructs treated with PDT (conditions presented in Figure 56) and PCI (Conditions presented in Figure 57) to generate graphs in figure 61. An average was taken from 24 areas (3 repeats, 8 areas each) for each condition. As histogram 61(A) shows the cancer cells have invaded far into the stroma in the control samples but such invasion is almost non-existent in the PDT treated samples. Histogram 61(B) also shows a similar pattern to that observed in Figure 57 with invasion of stroma by cancer cells being major in the control and saporin only constructs but lower in the PDT and PCI treated samples with a stronger effect being observed in the PCI treated samples.

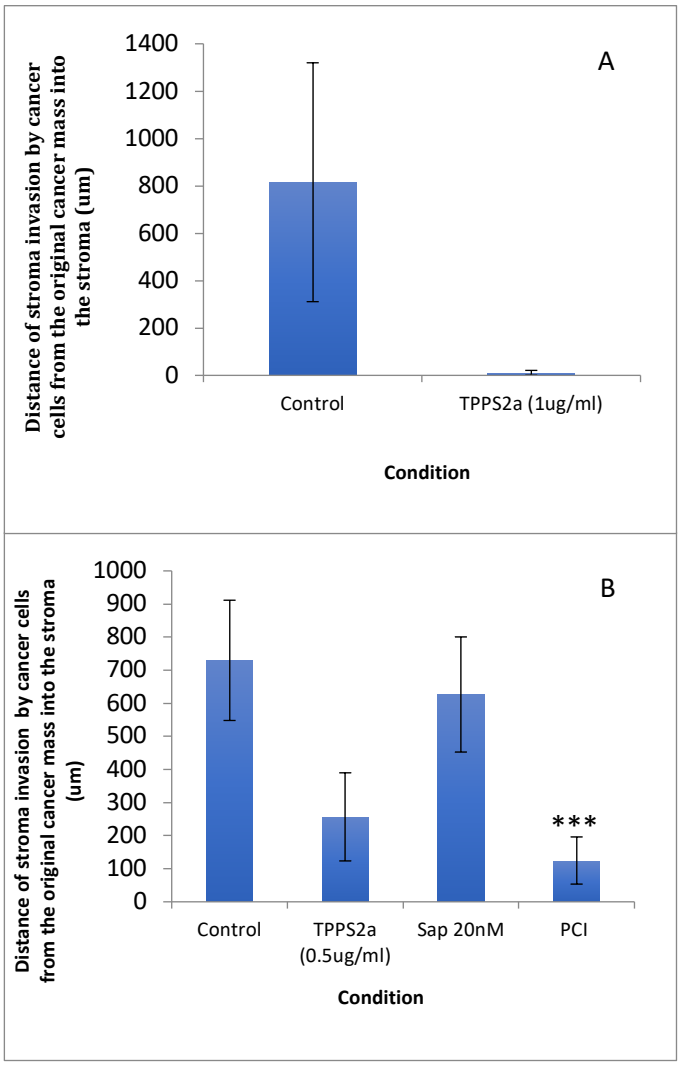

*Figure 61: Histograms showing distance (μm) of invasion into the stroma of the tumouroid by HEY ovarian cancer cells post PDT and PCI treatments, measured from experiments depicted in figures 57 and 58. A: Distance (μm) of invasion into the stroma after PDT treatment using $TPPS_{2a}$ ($1\mu g/mL$). B: Distance (μm) of invasion into the stroma after PCI treatment using $TPPS_{2a}$ ($0.5\mu g/mL$) and saporin (20nM). The samples were illuminated with blue lamp (420nm). (n=8 measurements / tumouroid). Each measurement was taken from the border of the original cancer mass to the furthest point of invasion in the stroma, taken vertically to the cancer mass. ***P<0.001 shows the significance difference versus control.*

5.3 Tumour regrowth after PDT

In a further experiment rate of cancer cell regrowth post PDT was examined where the constructs were incubated for a further 7 days after PDT treatment before the experiment was terminated. Figure 62 shows an example of construct that had undergone PDT using $TPPS_{2a}$ $(0.5\mu g/mL)$ in addition to 3 minutes of light illumination and was incubated for 7 days prior to staining. In comparison to figure 62A where the construct was given the same PDT treatment but was stained 2 days after the treatment (5 days earlier than the construct in figure 62B), a higher population of cancer cells can be seen in the central cancer mass as well as a massive invasion of the stroma by the cancer cells.

PDT ($TPPS_{2a}$ 0.5μg/mL)- 48 hours post illumination

PDT ($TPPS_{2a}$ 0.5μg/mL)- 7 days post illumination

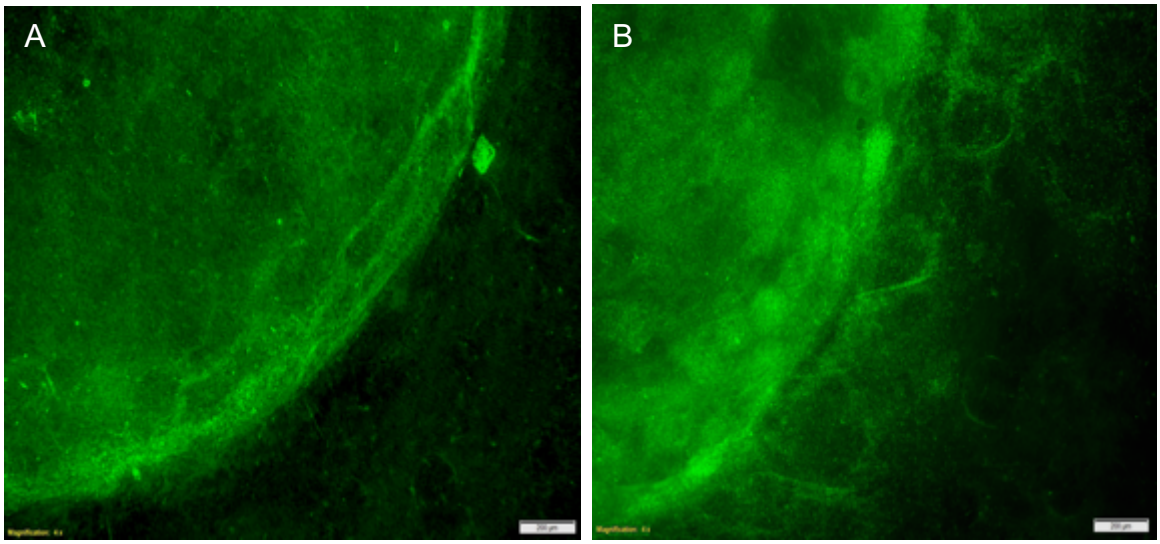

Figure 62: Regrowth of HEY cancer cells in PDT treated ovarian tumouroid, 7 days post treatment. The tumouroid was previously treated with $TPPS_{2a}$ $(0.5\mu g/mL)$, 3 minutes of light illumination. A: Tumouroid image obtained 48 hours post light illumination to demonstrate effect on treatment. B: Tumouroid image obtained 7 days post illumination to demonstrated ability to recover. The samples were illuminated with blue lamp (420nm). The cells were stained with Anti-cytokeratin 7 (Alexa Fluor 488) $\lambda_{Ex/Em:}$ 490/525 (green) conjugated antibody. Scale bar = $200\mu m$.

Chapter 6

Discussion

The studies presented in the previous chapters have examined the efficacy of Photochemical Internalisation in 3D cancer models for enhancing the cytoxicity of agents that are susceptible to entrapment within endolysosomes. The key aim of this work was to show that administration of sub-lethal PDT and the cytotoxic agent could act synergistically to enhance the cytotoxicity over the sum of the two individual therapies. This is based on the concept that PCI-induced intracellular release of the agents from the endolysosomes into the cytosol can enhance the efficacy of the agents by enabling them to reach their optimum intracellular target such as the nucleus where they exert their toxic effect.

PDT and PCI share several common features: both are minimally invasive light-activated modalities primarily for the treatment of solid tumours. In PDT the treatment is used as the sole method for eradicating cancer cells whereas in PCI low dose PDT is used to aid the delivery of chemotherapeutic drugs to their intracellular target sites. For clinical treatment both rely on light delivery to the target lesion using similar wavelengths and light sources.

Despite these similarities, PCI has several potential advantages over using PDT such as reduced skin photosensitivity since relatively low photosensitiser doses are required for PCI. There is also a decreased likelihood of vascular shut-down in normal healthy tissue using PCI as a result of less damage caused to endothelial cells which should reduce damage to normal tissue adjacent to the treated tumour. PCI may also be effective at counteracting multi-drug resistance in cancer cells (127, 202-208). Whereas PDT photosensitisers are often subject to multi-drug resistance mechanisms (e.g ABCG2 efflux transporters) the disulfonated photosensitisers used for PCI are not substrates for these efflux transporters (127, 205-207). A Study by Lou *et al* .(2006) showed that PCI treatment using doxorubicin of cells resistant to doxorubicin restored the cytotoxicity to levels comparable to the doxorubicin-sensitive clones (209).

Most *in vitro* PCI studies to date have been carried out on 2D (monolayer) cultures. However, such simple cultures have several deficiencies that prevent them from mimicking the conditions *in vivo.* Some of these limitations include the lack of hypoxic conditions found *in vivo* and ease of drug penetration (155). The use of 3D models on the

other hand has helped to overcome some of the limitations seen in 2D cultures as they can encapsulate several physiological properties observed *in vivo*, such as hypoxia. Therefore, more PCI studies in 3D models are required to allow better optimisation of treatments prior to moving onto *in vivo* studies.

Since PCI involves the combination of PDT with a bioactive agent, in this case cytotoxins, in order to verify that PCI can induce significantly higher cytotoxicity, control experiments with PDT alone and cytotoxin alone had to be performed. Therefore, as part of this work, information about PDT efficacy in 3D models was also obtained.

For testing PCI, three subtypes of 3D compressed collagen construct were used in order of complexity: non-spheroid, spheroid and tumouroid constructs. For the simple non-spheroid constructs, for which experiments began 24 hours after preparation of the constructs, the cells still largely exhibited a "single isolated cell" distribution within the construct. In the next stage, for comparing how the efficacy and optimum treatment parameters change in in multicellular deposits of cells, spheroid constructs were employed where the cells had formed spheroidal aggregates after 7 days incubation in the constructs. Finally, the treatments were applied to tumouroid constructs to study the effectiveness of the treatments in a more complex system which also included other cell types that can normally be found in the stroma of a tumour.

The photosensitiser used throughout was meso-tetraphenyl porphine disulfonate ($TPPS_{2a}$) which has been used in several previous studies including those in our laboratory (138, 215). Two cytotoxic chemotherapeutic agents, saporin and dactinomycin, were investigated for the treatment of various breast and ovarian cancer 3D compressed collagen constructs were evaluated. Dactinomycin functions through DNA intercalation as well as inhibition of RNA and protein synthesis whilst saporin acts as a Type 1 ribosome-inactivating protein (RIP). The PCI photosensitiser, $TPPS_{2a}$, is suitable for PCI since it has two sulfonate groups substituted on adjacent phenyl rings of the porphyrin macrocycle which can localise at the aqueous-lipid interface of endolysosomes with the hydrophobic portion of the porphyrin macrocycle inserted into the lipid bilayer.

Moreover, the $TPPS_{2a}$ porphyrin photosensitser has an analogous structure to the clinical disulfonated chlorin photosensitiser ($TPCS_{2a}$, Fimaporfin) and is therefore a good choice as the photosensitiser to test using PCI, particularly since blood absorption is not a factor affecting the photosensitiser efficacy in the studies presented here.

6.1 Intracellular uptake of $TPPS_{2a}$

In both 2D and 3D constructs of SKOV3 and HEY cells, intracellular uptake of $TPPS_{2a}$ was observed when treated with concentration (1μg/mL). Further experiment involving co-localisation with Lysotracker green in 3D also confirmed that the photosensitiser is in fact taken up and localised in both SKOV3 and HEY cells rather than becoming engulfed in collagen (Figures 25, 26 and 27). High resolution imaging was not possible in these models but numerous other studies have demonstrated lysosomal uptake of this photosensitiser. In one of the first studies by Berg *et al.*(1991) before PCI was developed, $TPPS_{2a}$ was found to localise in endocytic vesicle and relocate to other intracellular compartments upon exposure to visible light (216). This relocalisation is consistent with the light-induced rupture of the endolysosomal membranes by oxidative damage which releases the bound photosensitiser.

6.2 PDT/PCI studies in 2D and non-spheroid 3D constructs

Measurements obtained through different viability assays presented a significant reduction in percentage viabilities of SKOV3, HEY and MCF-7 monolayer cultures after treatment with PCI (photosensitiser combined with anticancer drug) compared to control as well as monotherapies with PDT ($TPPS_{2a}$ only) or anti-cancer drug (saporin/dactinomycin) only.

Using both viability assays it was found that the cell viabilities of all 3 cell lines reduced steadily with increasing illumination periods after PDT treatment in monolayer cultures. However, such reductions were not as significant as the those resulting from PCI treatment. The MTT vs. Alamar blue results showed that the viabilities after PDT treatment in HEY cells were 71% vs. 77% (3 minutes), 43% vs. 51% (5 minutes) and 33% vs. 35% (7 minutes). In SKOV3 cells such results were 71% vs. 65% (3 minutes), 50% vs. 45% (5 minutes), 38% vs. 32% (7 minutes). Finally, the results for MCF-7 cells showed viabilities of 78% vs. 71% (3 minutes), 33% vs. 25% (5 minutes) and 26% vs. 17% (7 minutes) after PDT treatment (Figures 16 and 17).

The measurements however varied slightly between the assays at times. For example, PCI using saporin (10nM) and 3 minutes illumination in HEY cells showed viability reductions from 93% to 44% (MTT assay) (Figure 16) vs. 92% to 38% (Alamar blue assay) (Table 2) compared to saporin only. However, PCI with the same concentration of saporin but 7 minutes light illumination in SKOV3 cells resulted in viability reductions from 98% to 27% (MTT assay) and 93% to 16% (Alamar blue assay) compared to using saporin only. From measurements with Alamar blue assay the alpha values were calculated to be 1.6

(3 minutes), 1.4 (5 minutes) and 1.4 (7 minutes) in SKOV3 cells and 1.7 (3 minutes), 2.1 (5 minutes) and 1.5 (7 minutes).

The cytotoxin and photosensitiser were both co-incubated with the cells for 20 hours, followed by a 4-hour chasing period where the cells were resuspended in drug-free medium prior to light exposure. This is the standard PCI protocol, as originally established by Berg et al and renders the cells less sensitive to PDT-induced damage of the extracellular membrane that can mask the PCI effect.

The pre-incubation of SKOV3 and MCF-7 cells with $TPPS_{2a}$ and saporin, 24 hours prior to seeding in 3D (for PDT/PCI studies in non-spheroid constructs) resulted in a low reduction in percentage viability even after the longest irradiation period (7 minutes) compared to the non-spheroid constructs that were treated after seeding (Figure 28). This could suggest that the drugs may begin to leach out of the cells 24 hours after they have been incubated with the drugs.

However, a test without the chasing period was also carried out to confirm that this was indeed necessary by pre-incubation of the cells with drugs prior to seeding and then PCI without chasing. In this experiment PDT and PCI without chasing led to a much higher reduction in percentage viability compared to cultures which underwent chasing in both 2D and 3D non-spheroid cultures of SKOV3 and MCF-7 cells (Figures 19 and 29). This is attributable to the much stronger PDT photocytotoxic effect exerted by photosensitiser residing in the extracellular membrane, whereas the chasing will dilute the membrane levels of the photosensitiser and lessen this direct PDT effect.

Another important result was that increasing the incubation period post illumination with saporin in SKOV3 and HEY monolayer cultures from 48 hours to 96 hours resulted in significant further reductions in percentage viability and an increase in PCI efficacies in some cases. Although the difference in the viability of PCI treated cultures was higher compared to control or anticancer drug monotherapies than compared to PDT monotherapies, the PCI efficacies (Table 2) calculated indicated that, the reduction in viability obtained after combining the photosensitiser with each anti-cancer drug was significant enough to claim that a PCI reaction had taken place. While it was determined that the appropriate concentration of saporin for the PCI studies were 10 and 20nM, for dactinomycin 1nM concentration was found to be suitable making it the more effective and potent drug, as discussed in further detail below.

For treatments using dactinomycin (1nM) the monolayer cultures of SKOV3 cells showed

viability reductions from 94% to 38% after 3 minutes irradiation compared to dactinomycin only (Figure 48) with the alpha values being 1.8 (3 minutes), 1.9 (5 minutes) and 2.4 (7 minutes). PCI continued to show a significant effect in the HEY cell monolayer cultures as well with the viabilities being reduced from 96% to 28% after 3 minutes irradiation compared to dactinomycin alone. The corresponding alpha values for this treated cell line were 2.2 (3 minutes), 3.3 (5 minutes) and 8.3 (7 minutes).

A previous study by Fretz *et al*. (2009) (217) also showed that PCI treatment using saporin, in the human ovarian cancer cell line OVCAR-3 in 2D culture was effective. In their study, reduction in cell viability over a range of saporin doses at a fixed light dose were investigated, in contrast to this study where we have also varied the light dose. Interestingly, Fretz *et al* found that targeted liposomal delivery of saporin was more effective for PCI than free saporin. Successful PCI treatment of SKOV3 cells in 2D using a targeted recombinant fusion toxin incorporating another Type 1 ribosome-inactivating protein toxin, gelonin has also been demonstrated (3).

As shown in Figures 20 and 49, a similar pattern of results was observed in the 3D non-spheroid cultures of all 3 cell lines which were respectively found to require the same $TPPS_{2a}$ concentrations as their monolayer counterparts for the PCI studies with saporin and dactinomycin. However, the viability reductions measured and calculated post treatment in the 3D cultures were lower than the monolayer cultures. For example, in PCI treated SKOV3 monolayer cultures the viabilities were reduced from 91% to 27% compared to saporin only when using 20nM saporin and 3 minutes light illumination. In their 3D non-spheroid counterparts however, the viabilities were reduced from 96% to 40% compared to saporin only.

In 3D cultures treated with PCI-dactinomycin a significant PCI effect was also observed with the viability reductions again being mostly lower than those observed in their monolayer counterparts. In SKOV3 3D cultures viability reduction from 96% to 42% were observed after 3 minutes irradiation compared to dactinomycin only. For the same treatment conditions, HEY cultures showed viability reduction from 91% to 33% compared to dactinomycin alone (Figure 49). The lower reduction in viability in the 3D cultures could be due to the dense collagen matrix acting as a barrier which can limit drug delivery in a manner similar witnessed *in vivo*. Despite the lower viability reductions achieved in 3D, the good PCI efficacies and synergistic alpha values indicate (Tables 3, 4 and 9) the treatment is also effective in a more restricted environment than the 2D monolayer cultures.

A key result from this work is the observation of different responses between the cell lines when comparing 2D vs. 3D non-spheroid experiments. Even though the HEY cells required a higher concentration of $TPPS_{2a}$ (0.4 µg/ml) than SKOV3 and MCF-7 cells (0.3 µg/ml) in the non-spheroid cultures, they exhibited more sensitivity towards the PCI treatment (ie were killed more efficiently) than the other two cell lines.

As with the monolayer cultures, elongating the incubation period post illumination from 48 hours to 96 hours resulted in further reductions in percentage viability in all 3 cell lines as confirmed by Alamar blue and live-dead assays. Apoptosis is a slower process than necrosis (218, 219) therefore elongating the incubation time after illumination to 96 hours demonstrates a more increased reduction of cell viability compared to models, which were incubated for 48 hours prior to termination of the experiment. Selbo *et al*. (2009) found that increasing incubation period post light exposure from 24 hours to 48 hours resulted in an increased cytotoxic activity in PCI (137, 220). Therefore, as shown in Table 6 a longer incubation period post illumination (96 hours) with saporin (20nM) results in similar cell kill to using Saporin (40nM) but shorter incubation period (48 hours) so a lower concentration of the drug may be required for treatment thus reducing side effects from saporin.

PDT or PCI in Type 1 collagen constructs developed without the plastic compression step has been examined by A few other studies. The sensitivity of neurons and glia to PCI using either a chlorin ($TPCS_{2a}$) or the same porphyrin, $TPPS_{2a}$, and bleomycin (chemotherapeutic drug) compared to PCI30 cells (head and neck squamous cell carcinoma) was examined by O'Rouke *et al*. (186) in order to find means of minimising nerve toxicity following PCI treatment. In their study, 3D non-spheroid uncompressed hydrogel co-cultures were used. The results showed that neural and mixed glial cell death was lower than PCI30 cell death following PCI using $TPCS_{2a}$ or $TPPS_{2a}$ suggesting that neurons have a higher resistance towards PCI treatment than PCI30 cells and can survive conditions that are adequate for destroying tumour cells such as those induced by PCI. A similar study by Wright *et al.* (187) used the same 3D culture system to investigate the sensitivity of neurons and glia cells to PDT using meta-tetrahydroxyphenyl chlorin (mTHPC) (photosensitiser) compared MCF-7 cells (breast adenocarcinoma). Reduction in cell viability of 48% in MCF-7 cells, 39% in gilial cells and 11.9% in neurons was observed with mTHPC at 4 µg/mL suggesting that neurons were significantly more resistant to mTHPC-PDT than MCF-7 and glial cells.

Martinez *et al*. (137) also used the 3D non-spheroid uncompressed collagen hydrogel culture, to test the effect of PCI using $TPCS_{2a}$/$TPPS_{2a}$ (photosensitiers) and saporin

(chemotherapeutic drug) on PC3 and MatLyLu prostate carcinoma cells. In their study, only the images from a Live/dead assay were presented which showed that PCI was effective in the 3D model but no quantitative comparisons can be made with the present study. They did however note that PCI resulted in changes in cellular morphology with the cells assuming a more rounded shape post treatment.

6.3 Intracellular uptake of Dactinomycin in 2D and 3D non-spheroid cultures

Following the positive results using PCI for enhancing the cytotoxicity of dactinomycin, which has not been tested before for PCI, it was important to ascertain whether the assumptions that this drug would be suitable for PCI could be proven. Dactinomycin was originally partly because it has not been tested for PCI before but also based on its molecular weight. This relatively large drug should be taken up at least partly via endocytosis like bleomycin which has a molecular weight of approximately 1400 Da. Furthermore, since dactinomycin is fluorescent unlike bleomycin, fluorescence imaging can therefore be carried out to demonstrate endolysosomal localisation of this drug.

Intracellular uptake studies showed that dactinomycin localises within the lysosomes of the SKOV3 and HEY cells in 2D cultures and in SKOV3 3D cultures as confirmed by co-localisation with lysotracker red (Figures 44 and 45). This type of localisation within the lysosomes is important for the successful delivery of the therapeutic agent to its target site of action as $TPPS_{2a}$ localises in the membrane of the endolysosomes which causes the membrane to rupture upon the activation of the photosensitiser by light thus releasing the macromolecular agent into the cytosol.

To provide further confirmation that dactinomycin is taken up via endocytosis (an energy-dependent active uptake mechanism), the temperature dependence of uptake was examined. As shown in Figure 52, the intracellular fluorescence measurements taken from cells after incubation with dactinomycin at either 4℃ or 37 ℃, showed that the fluorescence values were higher at 37 ℃ than at 4℃. This result is consistent with endocytosis being a major route of internalisation. If uptake occurred passively via transmembrane diffusion a temperature dependent uptake should not be present. Further experiments could be carried out to investigate the particular type of endocytosis that applies to dactinomycin, but these were not pursued as part of the present work.

A similar study by Wang *et al*. (2012) (221) looked at the uptake of cell penetrating peptide porphyrin conjugate (Tat-TPP) by human squamous cancer cells (HN5) in monolayer cultures at different temperatures (4℃ and 37℃) in order to determine the temperature

dependency of the drug uptake as it is believed that endocytosis is inhibited at lower temperatures. They discovered that decreasing the incubation temperature of the cells from 37℃ to 4℃ significantly reduced cellular uptake of Tat-TPP. Such behaviour was also observed with $TPPS_{2a}$. To illustrate the value of such experiments, Garaiova *et al*. (2012) (222) also studied the effect of the same temperatures on the uptake of macromolecular Chitosan polyplexes (LCO and SBTCO) by Human Cervical cancer cells (HeLa). By using fluorescence intensity to measure polyplex binding to the cell surface, they found that incubation at 4℃ led to a substantial reduction in fluorescence levels and therefore cellular uptake of both polyplexes compared to incubation at 37℃. The results acquired by both of these groups implied that the compounds used in these studies are taken up by endocytosis indicating that this mechanism of drug uptake is temperature dependent in contrast to passive transport. In relation to our study, as both SKOV3 and HEY cells were incubated with dactinomycin at 37℃ and a high fluorescence from the drug was detected during fluorescence microscopy imaging, it is concluded that this agent was uptaken via endocytosis by the cell lines, which confirms the original hypothesis and motivation for the study. Furthermore, as the studies found that the drugs are taken up by endocytosis at 37℃ (body temperature), it gives an indication that if applied clinically, the mechanism by which the cancer cells will take up the drugs is likely to be endocytosis.

6.4 PDT/PCI in 3D spheroid cultures

For the experiments on the 3D spheroid constructs of SKOV3 and HEY cells, it was found that sizable spheroids formed 7 days post seeding and that higher concentrations of $TPPS_{2a}$ were required for the PCI studies compared to the non-spheroid constructs (0.7 µg/ml for SKOV3 cells and 0.5 µg/ml for HEY cells) (Figure 31).

Interestingly unlike the non-spheroid constructs of HEY cells which required a higher concentration of the photosensitiser compared to the SKOV3 constructs, the spheroid constructs of the HEY cells behaved oppositely requiring a lower dose of $TPPS_{2a}$ than SKOV3 spheroid constructs. In terms of saporin concentration, the SKOV3 spheroid constructs required a higher concentration of 40nM to produce a significant PCI effect compared to their non-spheroid counterparts. However, the HEY cells as spheroid constructs again showed more sensitivity to PCI treatments than the SKOV3 cells. Although a relatively long incubation period of 20 hours was used, higher photosensitiser concentrations had to be employed in the spheroids to achieve the sub-lethal PDT effect for initiating PCI. However, this does not explain the lower sensitivity of SKOV3 spheroid constructs to PCI than the HEY cells which formed generally larger spheroids and required a slightly lower photosensitiser dose. This could possibly be due to the porous sub-

structure of the HEY spheroids which enables the compounds to penetrate more efficiently albeit this was not apparent from the imaging studies. Furthermore, growth of cells in the 3D microenvironment will result in phenotype changes such as gene expression which could account for the difference in response to PCI (223). So far no systematic studies have been reported for these cell lines on phenotypic changes in 3D models, however a comparative study on changes in fibronectin expression in SKOV3 and HEY spheroids vs. 2D reported similar results for both cell lines (224).

According to Lee *et al*. (2013) (225) in terms of spheroid formation HEY and SKOV3 cells tend to form large dense aggregates and perhaps this suggests that the drug uptake is reduced in such constructs compared to the non-spheroid 3D constructs used. Furthermore, as cells grow and form spheroids, their oxygen consumption increases creating a more hypoxic condition, and this may influence the efficacy of PCI since this method requires good oxygen abundance to function effectively. The better PCI effect exhibited in the HEY cell spheroid models compared to the SKOV3 cell spheroid models throughout all illumination periods offers a promise for using PCI to treat papillary cystadenocarcinomas in ovarian cancer patients.

These results can be compared with previous studies in 3D models using photosensitisers. Although very few of these studies investigated the use of chemotherapeutics some parallels can be drawn. The results of these studies are now discussed in more detail.

In this project a significant difference was observed between the non-spheroid and spheroid cultures in terms of viability reduction after PDT. In SKOV3 and HEY cell non-spheroid constructs the viabilities were reduced to 49% and 37% respectively after 7 minutes light irradiation. However, in the spheroid constructs the viabilities were reduced to 19% and 31% respectively after 7 minutes light irradiation but required higher concentrations of $TPPS_{2a}$ to achieve this.

In a study by Chen *et al*. (2015) (182) the micro-fluid platform was used to develop a breast cancer sphere culture environment with T47D cells on a chip. The spheres were formed through the aggregation of cells in each microwell. The 3D cultures underwent incubation with photosensitiser methylene blue at 10 μM concentration for 1 hour prior to undergoing illumination for different periods of 14 seconds, 10 minutes 30 minutes and 1 hour with numerous light exposure doses of (0.1 J/cm2) (minimum) to (total 43.8 J/cm2) (maximum). 2D cultures of the T47D cell line were also seeded and treated with the same PDT conditions for comparison purposes. The results found that after 10 minutes

exposure to a light dose of 7.3 J/cm2 approximately 50% cell kill was achieved in the 2D cultures while in the 3D spheres a majority of the cells remained viable. After an illumination period of 30 minutes under an exposure dose of 21.9 J/cm2 nearly all of the cells in the 2D culture were destroyed whereas many cells within the 3D sphere still showed to be viable. Even after the longest illumination period (1 hour) and exposure to the highest light dose (43.8 J/cm2) a portion of the T47D cells located within the centre of the sphere were still viable. The larger spheres exhibited a higher level of resistance towards PDT under the same therapeutic conditions compared to the small spheres which implied that sphere size has an effect on PDT efficacy. The lower levels of oxygen within the interior of the spheroids and the more difficult penetration of the photosensitiser are both factors that contribute towards limiting the efficacy of PDT in larger spheroids. These results match those observed in the PDT studies of this project.

Another study by Rizvi *et al*. (2010) (183) concentrated on using BPD-PDT to enhance the efficacy of chemotherapy drug (carboplatin) in 3D tumour models of ovarian cancer, which comprised of micronodules of OVCAR5 human cancer cells developed on growth factor reduced (GFR) Matrigel. The models were incubated with 1.25 μmol/L BPD prior to undergoing irradiation using a 690nm fiber-coupled diode laser either before or after treatment with low dose Carboplatin 40mg/m^2. According to the results a great synergistic reduction in viability was when BPD-PDT was carried out prior to carboplatin treatment compared to monotherapies. The mean fraction viability with PDT+ carboplatin treatment was 0.45 compared to 0.80 and 0.92 observed with PDT alone and carboplatin alone respectively. However, no synergistic effect was observed between the reverse treatment order which included carboplatin followed by BPD-PDT and the monotherapies. This shows that with the application of BPD-PDT prior to carboplatin treatment a lower dose of this drug can be used thus resulting in the occurrence of few side effects. Moreover, the mono-therapies carried out in 2D indicated that the sensitivity of the OVCAR5 cells in the 2D monolayer is more than twice of that seen in the same cells in the 3D cultures; this shows the benefit of using 3D models to get a more accurate representation of therapeutic behaviours *in vivo* as seen with the other studies mentioned. The same 3D model was used by Anbil *et al*. (2013) (188) to study the effect of BPD-PDT using various concentrations of BPD. The models underwent incubation with 0.25 μM, 1 μM and 10 μM BPD for duration of 90 minutes before undergoing irradiation with a 690 nm fibre-coupled diode laser. Significant reduction in cell viability was observed in nodules which were treated with 0.25 μM BPD-PDT mostly after 72 hours and 96 hours after the treatment in comparison to nodules that were treated with 1 μM and 10 μM BPD-PDT. Interestingly the nodules that were treated with a higher concentration (10 μM) BPD-PDT produced the poorest response.

Significant reduction in cell viability was observed in nodules which were treated with 0.25 μM BPD-PDT mostly after 72 hours and 96 hours after the treatment in comparison to nodules that were treated with 1 μM and 10 μM BPD-PDT. Interestingly the nodules that were treated with a higher concentration (10 μM) BPD-PDT produced the poorest response.

Ovarian cancer spheroid growth on GFR containing Matrigel was adopted in another similar study by Evans *et al*. (2011) (180), the again using the OVCAR5 cells to examine the effect of PDT using photosensitiser 5-ethylamino-9-diethylaminobenzo[a] phenothiazinium chloride (EtNBS) on hypoxic cell populations within 3D tumour models of ovarian cancer. The spheroids underwent incubation with 500nM EtNBS for 4.5 hours to allow the photosensitiser to concentrate into the cells within the core of the spheroid. Using a light dose of 5J/cm2, EtNBS showed to selectively destruct the cells in the core of the spheroid. This indicates that EtNBS can both concentrate into as well as destroy the hypoxic cell populations that are normally hard to treat. Higher light doses resulted in cell killing across the entire model by EtNBS-PDT which showed that such therapy is effective against both hypoxic and normoxic regions of a tumour. Interestingly it was found that the uptake and cytotoxicity of EtNBS increased with expansion of spheroid size mostly due to the rise in the hypoxic populations found in the larger spheroids.

Hung *et al*. (2016) (226) however, encapsulated EtNBS in PLGA NPs in order to minimise dark toxicity of EtNBS and investigate its potential as a PDT photosensitiser in 2D and spheroid cultures of ovarian cancer developed from OVCAR5 cells. Reduced dark toxicity was observed in monolayer cultures treated with EtNBS loaded nanoparticles compared to cultures treated with free EtNBS. The uptake studies in spheroid cultures found that the PLGA-EtNBS diffused throughout the spheroids similar to the free EtNBS and the photosensitiser was released from PLGA upon exposure to laser light of 635 nm. Furthermore, PDT using PLGA- EtNBS also proved to be effective in the hypoxic cellular microenvironment within the spheroids, showing comparable efficacy to free EtNBS.

Gaio *et al.* (2016) (227) on the other hands studied the photoinduced damage by two liposomal formulations of m-THPC, Foslip® and Fospeg® compared to Foscan® in cervical cancer spheroid cultures developed from HeLa cells. Using confocal microscopy, it was revealed that m-THPC penetration was limited and mainly occurred in the external cell layers of the spheroids with Foslip® and Fospeg® showing a slightly higher accumulation compared to Foscan®. Incubation of spheroids with Foscan (8 μM) in the dark resulted in significant reduction in cell viability while the liposomal formulations did not cause dark toxicity in the spheroids. Upon treating the spheroids with PDT, the cell

viabilities were considerably reduced with all three different formulations with Foslip® causing the highest reduction in viability at each particular time point.

The results of the present study had several features in common with the studies mentioned above: the higher concentration of photosensitisers required for treating the spheroid constructs compared to the 2D and non-spheroid constructs may be a result of drug penetration problems caused by the formation of dense spheroids. However, a further factor specific to this work to consider is that the hydrogel constructs used herein contained much denser compressed collagen surrounding the cellular aggregates which could further limit penetration and drug and oxygen diffusion.

This will be an interesting area for further studies. López-Dávila *et al*. (2016) found that the efficacy of free AZD6244 (MEK1/2 inhibitor) was higher in compressed collagen hydrogels containing a colorectal cancer mass than when the drug was encapsulated into liposome formulations. The results were the opposite in the monolayer cultures of this cancer. The therapeutic effect of the nano-formulations was therefore hindered by poor diffusion through the cancer mass in 3D cultures (173).

An increase in hypoxic conditions formed with the growth of spheroids and particularly in the core of spheroids should restrict the effect of PDT and the results obtained using different oxygenation levels are now discussed. Such studies have not previously been carried out for PCI.

6.5 Oxygen consumption studies in 3D non-spheroid and spheroid and post PDT/PCI in non-spheroid 3D constructs

Imaging with a hypoxia reagent showed that oxygen consumption increases significantly with growth of cancer cells and as they form spheroids since the fluorescence observed in the day 1 constructs is considerably lower than day 7 constructs (Figure 35). This could imply that hypoxic conditions are indeed created as spheroids form thus affecting the efficiency of PDT/PCI. Lower oxygen levels were detected by Cheema *et al.* (2012) (228) in the core of a fibroblast-seeded 3D compressed collagen construct at higher seeding densities using a thin embedded probe. A localised rise in vascular endothelial growth factor (VEGF) expression was also observed in their study. Another study by Virumbrales-Munoz *et al.* (2017) (229) also reported development of hypoxic conditions in a microfluidic 3D model using the same imaging probe as Cheema *et al*. (228). The photodynamic photosensitiser $TPPS_{2a}$ requires a sufficient supply of oxygen in order to be able to produce ROS upon becoming activated and cause rupturing of endolysosomal membranes which are also necessary for PCI to be effective. The lower oxygen levels

within the spheroid constructs may limit the PDT effect, which leads to initiation of the ROS-induced intracellular drug redistribution and therefore PCI treatment efficacy (180, 230). Molecular oxygen is also consumed by the photo-oxidation reactions which occur during PDT. Seeding the cells in compressed high density collagen matrix is also another factor that contributes towards the reduction in oxygen diffusion into the construct (231), which may limit the amount of oxygen available for PCI thus leading to a poorer therapeutic response. Compressed collagen gels were found to reduce oxygen transport by ten times compared to uncompressed gels in the study by Cheema *et al.* (228).

Since oxygen can diffuse more freely from the surrounding medium in 2D cultures PDT can therefore still be effective even in hypoxic conditions (1% oxygenation) as shown in our results where as such is not the case in 3D cultures (non-spheroid and spheroid) due to limited diffusion (Figures 36-39). Price *et al.* (2013) and Moan and Sommer (1985) have explored the effect of oxygen levels on PDT in monolayer cultures using various photosensitisers (232, 233). The requirement of lower PDT dose for PCI also limits photochemical consumption of oxygen. In PDT/PCI experiments it was found that oxygen consumption increased exposure of drug treated constructs to light compared to control constructs of both ovarian cancer cell lines since the fluorescence from the hypoxia reagent became significantly more intense post treatment. This is because such treatments also consume oxygen since the singlet oxygen reacts with the tissue components so free oxygen is reduced as a result. Furthermore, it was observed that the fluorescence levels were higher 24 hours post light exposure compared to 4 hours post irradiation. All of these results stress critical importance of sufficient oxygen availability in achieving good PDT/PCI effects. As solid tumours often contain hypoxic cores, these results may be relevant to clinical studies. In an interesting study Ferguson *et al*. (2018) (234) investigated the effect of culturing cells under hyperoxia (air) over a long period on PDT. The PDT treatment results showed that cells which had been grown under hyperoxic conditions generated higher levels of mitochondrial ROS than cells which had been cultured under physioxic (2% O_2) conditions. However, no significant difference between the viabilities of cells cultured under the two conditions was observed.

6.6 Apoptosis/necrosis studies 3D non-spheroid constructs

Through staining with Annexin V-FITC and Propidium iodide it was observed that PCI treated non-spheroid constructs experienced more apoptotic cell death than PDT treated non-spheroid constructs (Figure 41) whereas a higher level of necrosis was detected in PDT treated constructs than the PCI treated constructs. A minimal level of necrosis and apoptosis was observed in the control, saporin only treated constructs as well as the

constructs which were incubated with the drug but were not exposed to light (Figure 40). Furthermore, the levels of necrosis/ apoptosis detected in the PDT/PCI treated constructs were higher 48 hours post illumination than 24 hours post illumination. Also, greater levels of necrosis/ apoptosis were detected in spheroid constructs (Figure 42) than non-spheroid constructs.

Intracellular localisation of the photosensitiser is a key factor in determining the nature of cell death as being necrotic or apoptotic (235, 236). Photosensitisers that localise in mitochondria or ER mainly stimulate apoptosis whereas localisation within the plasma membrane or lysosomes tend to promote necrosis of cells (237) (238).

Sub-lethal damage caused by PDT generally induces apoptosis (239) in comparison with cells that are treated with high dose PDT using photosensitisers that localise in the plasma membrane or lysosomes such as $TPPS_{2a}$. Saporin also functions by inducing apoptosis via mitochondrial cascade (240). PCI using saporin is therefore known to cause cell death mainly through apoptosis due to the sublethal effects of PDT as well as the use of saporin in the treatment. The increase in level of apoptosis after 48 hours post illumination compared to 24 hours could be due to apoptosis being a slower process than necrosis thus leading to more apoptosis over a longer period of time. These results are in agreement with that obtained in the study by Mathews *et al*. (2012) where $AlPcS_{2a}$ was used as a photosensitiser and cisplatin, cisplatin analog [D prostanoid, DP], doxorubicin, and bleomycin were used as chemotherapeutic agents for treating monolayer cultures of three breast cancer cell lines (MCF-7, MDA-MB-435, and MDA-MB-231) it was found that PCI treatment lead to a reduction in the percentage of viable cells, mainly through enhancing apoptotic cell death. Coupienne *et al*. (2011) (241) on the other hand showed that PDT using 5-aminolevulinic acid (5-ALA) in glioblastoma cells mainly resulted in necrotic cell death.

6.7 Cancer cell growth in tumouroid constructs

The final part of the thesis results concerned the preparation of tumouroid constructs of the HEY human ovarian cancer cell line and their treatment by both PDT and PCI. By using tumouroids it is possible to observe the effect of treatment on the morphology and spatial behaviour of cancer cells and stromal cells. PCI (photochemical internalisation of chemotherapy) was chosen as the test treatment, as PCI is known to target cancer cells but also has wider effects within the cancer tissue. Here it has been demonstrated that PCI reduces cancer invasion into the stroma and also appears to perturb cells within the stroma, with less fibroblasts, less endothelial cells and less organisation by both.

In these studies the same photosensitiser was used, $TPPS_{2a}$, and saporin was the chemotherapeutic agent. According to Figure 55, which shows images of the tumouroid constructs, the HEY cancer cells were able to proliferate and successfully invade the stroma in the area closely surrounding the central cancer mass and further into both the a-cellular and cellular stroma. This invasive behavior correlates well with another study from our laboratory using human colorectal carcinoma cells.

Magdeldin *et al*. (2017) (212) employed the same 3D culture system to develop a colorectal tumouroid construct using HT29 and HCT116 (colorectal cancer cells), HDFs (fibroblast cells) and HUVECS (endothelial cells) in order to study the mechanisms involved in cancer progression. Their results found two different mechanisms of migration whereby the HT29 cells invaded the stroma as cellular aggregates and the HCT116 cells invaded as epithelial cell sheets.

The HEY cells also appeared to invade the stroma initially as epithelial cell sheets but the cancer cells which migrated further into the stroma then coalesced and invaded as aggregates. The tumouroids created in this project consist of fully compressed cancer mass and stroma compared to the original tumouroid construct that was presented by Nyga *et al*. (2013) where only the cancer mass in the centre was compressed (174).

Other groups have used different methods to develop *in vitro* complex 3D models. For example Jaganathan *et al.* (2014) (242) created a co-culture breast cancer model consisting of breast cancer cells SUM159 and MDA-MB-231as well as fibroblast cells Hs785bst, 293T and patient derived cancer associated fibroblast cells. In their study various combinations of the breast cancer and fibroblast cells were co-cultured at different ratios in ultra-low attachment well plates prior to being exposed to magnetic levitation.

Amann *et al*. (2017) (243) on the other hand made use of the hanging drop technology to develop a tri-culture model consisting of non-small cell lung cancer (NSCLC) cell lines (A549 and Colo699) as well as a fibroblast cell line (SV 80) and two different endothelial cell lines (CC-2527 and CC-2935) with the purpose of studying the effects of anti-angiogenic drugs. According to their results endothelial cells formed small colonies in microtissues containing Colo699 cells and tube-like structures mostly in the stromal compartment of A549 containing microtissues. Also, the inhibition of proangiogenic factors using antiangiogenic drugs such as bevacizumab and nindetanib led to a significant decrease in the migration of endothelial cells into the microtissues.

6.8 PDT/PCI in tumouroid constructs

This section of the study showed that the PDT only treatment using $TPPS_{2a}$ $(0.5\mu g/mL)$ and 3 minutes of light irradiation caused a reduction in cancer cells in the central cancer mass and those invading the stroma as well as HDFs compared to the control and saporin only treated constructs (Figure 57B). In the PCI treated constructs a further destruction of the cancer cells in the central cancer mass and those invading the stroma was observed in addition to the destruction of HUVEC and HDF cells in the stroma (Figure 57D). However, PDT with $TPPS_{2a}$ $(1\mu g/mL)$ and 5 minutes of light exposure caused a significant destruction in the invading cancer mass and the HUVEC cells as well as a reduction in the number of cancer cells in the central cancer mass and the HDFs (Figure 56).

An interesting observation was that PDT and PCI application on the stroma (focusing on the fibroblast only) resulted in significant reduction in fibroblasts compared to the control construct however the effect was more severe with PDT than with PCI (Figure 59).

Since there are no previous PDT/PCI studies using tumouroid models no direct comparisons can be drawn with previous work. However, some general observations can be made since there are several studies on breast and ovarian cancer cell lines in uncompressed hydrogel models. In a PDT study by Wright *et al*. (2009) (187) uncompressed collagen 3D cultures were employed for investigating the sensitivity of neurons and glia to PDT using photosensitiser meta-tetrahydroxyphenyl chlorin (mTHPC) compared to breast carcinoma (MCF-7 cells) since some tumours can be located within or adjacent to the nervous system. In this study they observed that the cell viabilities were reduced by 48% in MCF-7 cells, 39% in glial cells and 11.9% in neurons when mTHPC was used at concentration 4 μg/mL which suggested that the neurons showed significantly more resistance towards mTHPC-PDT than MCF-7 and glial cells.

Rizvi *et al.* (2013) (244) however developed a 3D co-culture model consisting of ovarian cancer (OVAR-5 cells) and Human umbilical vascular endothelial cells (HUVECs) using the low adherence plate system to produce OVCAR-5 spheroids prior to transferring the OVCAR-5/HUVEC co-culture into GFR matrigel coated plate to examine the potential of this model for testing PDT mediated combination treatment. Interestingly this study discovered that the size of the OvCa spheroids declined as the cell density of HUVECs increased suggesting that the ratio of each cell type in such model has an influence on the interaction between the two cell types. Our study on the other hand, found that the HEY cells could effectively invade far into the stroma regardless of the presence or

absence of stromal cells and also without the size of cancer masses invading the stroma being influenced majorly.

In another interesting study Chen *et al*. (2015) (182) developed breast cancer spheres of T47D, SUM-159 and MCF-7 cells using microfluidic device to study the effect of PDT on the cancer cells. The results showed that even when using 10μM methylene blue (photosensitiser) and a light exposure dose of 43.8 J/cm^2, the cells in the centre of spheres still remained viable and the larger spheres showed more resistance to PDT treatment than the small sphere. Furthermore, this group also investigated the effect of cancer associated fibroblasts (CAFs) from primary samples on the response of the cancer cells to the treatment. For this experiment the cells were treated with media conditioned by the secretions from CAFs to mimic the effect of fibroblasts on that particular breast cancer type. It was discovered that using culture media from CAFs resulted in no significant increase in PDT resistance which suggested that fibroblast mediated resistance may not increase resistance to PDT.

The tumouroid studies in this thesis demonstrated that cancer cells invading the stroma showed more sensitivity towards PDT/PCI treatment than cancer cells in the central cancer mass. Nyga *et al*. (2013) measured the oxygen levels in various parts of a partially compressed tumouroid model and found that the oxygen levels were significantly lower in the core of the central cancer mass than in the border of the central cancer mass with the surrounding stromal environment (174). Such difference in oxygen availability within the tumouroid construct could limit the effect of PDT and PCI in the central cancer mass.

6.9 Regrowth of cancer cells in tumouroid constructs post PDT treatment

In terms of regrowth after PDT it was found that the HEY cells are able to regrow and invade the stroma 7 days post PDT treatment using $TPPS_{2a}$ ($0.5\mu g/mL$) and 3 minutes of light exposure (Figure 62). According to the study carried out by Schumann *et al*. (2015) (245) in mice a single dose of combination therapy with photosensitiser phthalocyanine (Pc) and siRNA as a DJ-1 gene suppressor resulted in full eradication of ovarian tumours (grown from A2780/AD cancer cells) without any evidence of recurrence whereas PDT only treated tumours began to regrow 16 days post treatment. Their study also explained that the ROS and heat generated after a single those of PDT could at first produce a strong response in the tumours. The further combination of the treatment with DJ-1 suppression causes a more significant therapeutic effect therefore preventing tumour regrowth.

In relation to the study presented herein, when the PDT experiment (using the same concentrations of drug and illumination period as that in the regrowth study) in tumouroids is terminated 48 hours after light illumination, it is apparent that cells within the central cancer mass are reduced in number and that the number of cells invading the stroma is also significantly reduced. However, incubating the constructs for a further 5 days led to extensive regrowth of the cancer cells, as shown in Figure 62. This suggests that a single dose of PDT can provide a strong response initially, but the cancer cells are eventually able to overcome the conditions created by PDT as the treatment loses effect if the constructs are not exposed to additional cycles of the treatment. It is possible that some cancer cells remain dormant owing to the hypoxia that develops within the tumouroids (174) that could protect the cells from PDT damage so that they can eventually invade further. The tumouroid preparation techniques employed here was slightly different as discussed in the introduction but it is likely that the tumouroids used here were also hypoxic at the centre since the surrounding stroma was also a compressed collagen hydrogel. It would be interesting in future to test how the rate of cancer cell invasion is affected by treatment of the tumouroids with multiple illumination cycles or low power densities which could counteract the effect of the pre-existing hypoxia and treatment-induced hypoxia on PDT and PCI efficacy (246).

Conclusions

PCI as a non-invasive treatment method has a potential for treating female cancers. The photosensitiser $TPPS_{2a}$ and chemotherapeutic drug dactinomycin have proven to be uptaken by cancer cells in 2D and 3D cultures. PCI using saporin and dactinomycin as chemotherapeutic drugs has proved effective in both 2D and non-spheroid 3D cultures with cultures incubated for 96 hours post illumination experiencing more cell killing than those incubated for 48 hours.

Dactinomycin is a relatively old drug in terms of its use for cancer but is still being used clinically. The new results presented here show that this agent could be ‘re-purposed’ using PCI for future clinical treatment of a wider range of tumours.

Achieving a similar cell kill in 3D non- spheroid cultures which were treated with 40nM saporin and incubated for 48 hours post illumination and cultures which were treated with half of that concentration and twice as long incubation period post illumination provides a promise for treating cancers effectively while needing a low concentration of saporin and therefore reducing the likelihood of side effects associated with saporin such as fever, myalgias, hepatotoxicity, thrombocytopenia and vascular leak syndrome from occurring. Although PCI showed effectiveness in both monolayer and 3D cultures, higher

concentrations of the photosensitiser and saporin were required for treating the spheroid constructs which may have been due to formation of dense aggregates as well as the development of hypoxic conditions within the constructs. The pre-incubation of cells with drugs prior to imbedding in 3D collagen constructs resulted in most cells remaining viable at the end of the treatment possibly due to the leaching out 24 hours after they are initially applied to the cells. PDT/PCI treatments carried out without chasing however a much higher level of cell kill in both 2D and 3D constructs compared to cultures which did undergo chasing.

Whilst PDT/PCI using the strongest parameters of the experiment (40nM saporin and 7 minutes light exposure) in monolayer cultures of ovarian cancer in hypoxic conditions (1% oxygenation) was still able to lead to a reasonable level of cell killing, in 3D non-spheroid cultures such effect was much weaker and in spheroid cultures the reductions in percentage viability were minimal. Furthermore, the ovarian cancer cells showed to consume excessive oxygen as they grew into spheroids compared to non-spheroid constructs thereby creating a more hypoxic environment. This is particularly important as tumour environment is hypoxic and oxygen abundancy is crucial for PDT/PCI to function effectively. The imaging of oxygen level consumption after PDT/PCI in non-spheroid constructs of ovarian cancer showed that oxygen consumption was higher in PDT and PCI treated constructs after exposure to light with the consumption levels steadily increasing for up to 24 hours after light irradiation. However, the level of oxygen consumption in control constructs and those treated with drugs but no light irradiation as well as constructs treated with saporin only in the presence or absence of light was very minimal.

In both 3D non-spheroid and spheroid constructs of the two ovarian cancer cell lines, PCI leads to more apoptosis than necrosis whereas PDT showed the opposite effect. The fluorescence levels corresponding to necrosis and apoptosis were more intense in spheroid cultures than non-spheroid cultures probably due to more cells being present and consequent higher integrated intensities. The level of necrosis and apoptosis was higher 48 hours post illumination than 24 hours post illumination in the PDT/PCI treated cultures particularly in the case of apoptosis. This is since apoptosis is a slower process than necrosis and occurs over a longer period and is important as saporin causes cell death via apoptosis which also explains why a bigger cytotoxic effect was observed 96 hours post illumination compared to 48 hours post illumination.

Importantly, the application of each drug without light exposure as well as the application of saporin only with or without exposure to light resulted in negligible level of necrosis and apoptosis.

Regarding the tumouroid constructs, which were more complicated to prepare, just the HEY ovarian cancer cell line was investigated. Tumouroids were prepared successfully and compared well in structure to previous published studies from our laboratory using colorectal HCT116 cells.

The cells were able to grow and invade the surrounding stromal environment successfully regardless of the presence of the stromal cells. PDT using $TPPS_{2a}$ (0.5μg/mL) and 3 minutes illumination period caused a reduction in cancer cells invading the stroma and HDFs in comparison to the control whereas PCI using the same parameters and saporin (20nM) resulted in a further destruction of the cancer cells in the central cancer mass and those invading the stroma was observed as well as destruction of HUVEC and HDF cells in the stroma. However, doubling the concentration of $TPPS_{2a}$ to (1μg/mL) and increasing the illumination period to 5 minutes for PDT treatment showed destruction in the invading cancer mass as well as the HUVEC cells and a reduction in the number of cancer cells in the central cancer mass and the HDFs therefore exerting a much stronger effect than the PDT treatment with $TPPS_{2a}$ (0.5μg/mL) and 3 minutes illumination period.

Furthermore, treatment of the constructs with $TPPS_{2a}$ (1μg/mL) and PCI with $TPPS_{2a}$ (0.5μg/mL) + Saporin (20nM) without exposure to light showed negligible toxicity as a lack of reduction in cancer or stromal cells was observed and the cells maintained their normal shapes looked comparable to the controls.

Regarding the regrowth of cancer cells post treatment with PDT, it was shown that in PDT treated constructs where $TPPS_{2a}$ ($0.5\mu g/mL$) in addition to 3 minutes of light illumination were applied, the cancer cells were able to regrow and invade the stroma 7 days after the treatment.

Using the complex tumouroid constructs has the benefit of allowing other components and cells found in the stroma of the tumour to be included in the model and for their response to the treatment as well as the effect of their presence on the response of the cancer cells on the treatment to be examined. Other approaches can also be used for testing PDT treatment in tumour models as has been demonstrated by Zhang *et al*. (2015) (247) who used the relatively in-expensive Zebrafish tumour models to test nanoparticle-mediated PDT.

As HEY cells are derived from papillary cystadenocarcinoma which is known as one of the most common types of ovarian cancer, it will be interesting to examine how this cell line and other cell lines respond to the PCI treatment *in vivo*.

Future work

To expand on the current research as part of future work, confocal microscopy could be used to study more accurately the intracellular uptake of the photosensitiser in non-spheroid 3D constructs as well as the growth of cancer cells in different dimensions of the tumouroid. Furthermore, conjugates of photosensitiser and drug can be used to allow them both to be delivered into the cell at the same time.

The penetration and distribution of anti-cancer drugs in the constructs is also crucial to study as a higher concentration of the drug may be required for various constructs (ie non-spheroid vs. spheroid). The cytotoxin can be fluorescently labelled for such study, however such conjugation may affect the diffusion properties of the drug.

To increase the complexity of the tumouroid constructs and better replicate the *in vivo* environment extracellular matrix proteins such as laminin and fibrillin can be incorporated into the collagen matrix. Moreover, cancer associated fibroblasts can be used in the stroma as they aid cancer progression and again mimic *in vivo* cancer microenvironment better than the currently used HDFs.

As Dactinomycin has shown to be an efficacious drug requiring a low concentration for PCI studies, it would be important to see how effective this cytotoxin behaves in more complex constructs such as the spheroid and tumouroid constructs. Furthermore, as this is the first time such drug is being used for PCI studies, it would be interesting to examine its effect in *in vivo* models.

Correlation of the 3D results with *in vivo* experimental tumour models using the same tumour lines would be very useful and it would then be possible to ascertain whether the different cellular sensitivities to PCI elicited in 3D models are replicated *in vivo*.

Publications and Presentations

Published articles

L. Mohammad- Hadi, A.J. MacRobert, M. Loizidou, E. Yaghini, Photodynamic therapy in 3D cancer models and utilisation of nanodelivery systems. Nanoscale. 2018;10(4):1570-81, (Impact factor 7.3).

L. Mohammad- Hadi, E. Yaghini, K. Stamati, M. Loizidou, A.J. MacRobert, Therapeutic enhancement of a cytotoxic agent using Photochemical internalisation in 3D compressed collagen constructs of ovarian cancer. Acta Biomaterialia Journal (2018), (In press), (Impact factor 6.3).

Papers in preparation for publication

L. Mohammad- Hadi, E. Yaghini, M. Loizidou, A.J. MacRobert, Repurposing a chemotherapeutic drug for Photochemical internalisation treatment of 3D compressed collagen ovarian cancer construct.

L. Mohammad- Hadi, E. Yaghini, K. Stamati, M. Loizidou, A.J. MacRobert, Photochemical internalisation in tumouroid constructs of ovarian cancer.

Conference presentations

L. Mohammad- Hadi, E. Yaghini, M. Loizidou, A.J. MacRobert, Photochemical internalisation in 3D compressed collagen models of breast and ovarian cancer, (July 2016)- Tissue and cell engineering society annual conference (TCES), London, Poster presentation.

L. Mohammad- Hadi, E. Yaghini, M. Loizidou, A.J. MacRobert, Photochemical internalisation in 3D compressed collagen models of ovarian cancer, (September 2017)- 17th Congress of the European Society for Photobiology (ESP), Pisa, Oral presentation.

L. Mohammad- Hadi, E. Yaghini, M. Loizidou, A.J. MacRobert, Photochemical internalisation as an effective drug delivery method in 3D compressed collagen ovarian cancer models, (May 2018)- ASPIC conference, Lisbon, Poster presentation.

L. Mohammad- Hadi, E. Yaghini, M. Loizidou, A.J. MacRobert, Photochemical internalisation in 3D tumouroid constructs of ovarian cancer, (August 2018)- British Society of Nanomedicine (BSNM)

References

1. Bistoni G, Farhadi J. Anatomy and physiology of the breast. Farhadieh RD, editor. Wiley Online Library; 2015.

2. Rahman M, Mohammed S. Breast cancer metastasis and the lymphatic system. Oncol Lett. 2015;10(3):1233-9.

3. National Health Service. Breast Lumps: National Health Service; 2018 (cited 2018 Dec 10). Available from: https://www.nhs.uk/conditions/breast-lump/

4. Williams CJ, Erickson GF. Morphology and Physiology of the Ovary. In: De Groot LJ, Chrousos G, Dungan K, Feingold KR, Grossman A, Hershman JM, et al., editors. Endotext. South Dartmouth (MA)2000.

5. Clement PB. Anatomy and Histology of the Ovary. R.J K, editor: Springer Science; 1987.

6. Morton D, Albertine K, Foreman B. The Big Picture: Gross Anatomy. Albertine KH, editor: The McGraw-Hill Companies; 2011.

7. National Health Service UK. Osteoporosis (Internet): National Health Service UK; 2016 (Cited 2018 Jul 12). Available from: https://www.nhs.uk/conditions/osteoporosis/

8. Cancer Research UK. Ovarian cancer (Internet): Cancer research UK; 2016 (Cited 2018 Jul 12). Available from: https://www.cancerresearchuk.org/about-cancer/ovarian-cancer?ds_kids=p1717488291&adc=cpc

9. Stany MP, Hamilton CA. Benign disorders of the ovary. Obstet Gynecol Clin North Am. 2008;35(2):271-84, ix.

10. Nationl Health Service UK. Polycystic ovary syndrome (Internet): National Health Service UK; 2016 (Cited 2018 Jul 12). Available from: https://www.nhs.uk/conditions/polycystic-ovary-syndrome-pcos/

11. World Health Organisation. Breast Cancer (Internet): World Health Organisation; 2018 (Cited 2018 Jul 12). Available from: http://www.who.int/cancer/prevention/diagnosis-screening/breast-cancer/en/

12. Moller H, Henson K, Luchtenborg M, Broggio J, Charman J, Coupland VH, et al. Short-term breast cancer survival in relation to ethnicity, stage, grade and receptor status: national cohort study in England. Br J Cancer. 2016;115(11):1408-15.

13. Iyer R, Ring A. Breast cancer survivorship: key issues and priorities of care. Br J Gen Pract. 2017;67(656):140-1.

14. Torre LA, Siegel RL, Ward EM, Jemal A. Global Cancer Incidence and Mortality Rates and Trends-An Update. Cancer Epidemiol Biomarkers Prev. 2016;25(1):16-27.

15. Cancer Research UK. Breast cancer statistics (Internet): Cancer Research UK; 2016 (Cited 2018 Jul 12). Available from: https://www.cancerresearchuk.org/health-professional/cancer-statistics/statistics-by-cancer-type/breast-cancer

16. Munro AJ. Comparative cancer survival in European countries. Br Med Bull. 2014;110(1):5-22.

17. Sharma G. N DR, Sanadya J, Sharma P, Sharma K.K. VARIOUS TYPES AND MANAGEMENT OF BREAST CANCER: AN OVERVIEW. J Adv Pharm Technol Res. 2010;1(2):109-26.

18. Cancer Research UK. Ovarian cancer statistics (Internet): Cancer Research UK; 2016 (Cited 2018 Jul 12). Available from: https://www.cancerresearchuk.org/health-professional/cancer-statistics/statistics-by-cancer-type/ovarian-cancer

19. Sundar S, Neal RD, Kehoe S. Diagnosis of ovarian cancer. BMJ. 2015;351:h4443.

20. Cancer Research UK. Breast Cancer risk factors Cancer Research (Internet): Cancer Research UK; 2018 (Cited 2018 Jul 12). Available from: https://www.cancerresearchuk.org/health-professional/cancer-statistics/statistics-by-cancer-type/breast-cancer/risk-factors

21. Stefan N.T SS, Ovidiu C.D, Vasile S, Silvia S, Irina N. Surgical Treatment in Ovarian Cancer - Complete or Optimal Surgery? ARS Medica Tomitana. 2018;24(2):60-5.

22. Raja FA, Chopra N, Ledermann JA. Optimal first-line treatment in ovarian cancer. Ann Oncol. 2012;23 Suppl 10:x118-27.

23. Partridge AH, Burstein HJ, Winer EP. Side effects of chemotherapy and combined chemohormonal therapy in women with early-stage breast cancer. J Natl Cancer Inst Monogr. 2001(30):135-42.

24. Simpkins F, Garcia-Soto A, Slingerland J. New insights on the role of hormonal therapy in ovarian cancer. Steroids. 2013;78(6):530-7.

25. Colleoni M, Giobbie-Hurder A. Benefits and adverse effects of endocrine therapy. Ann Oncol. 2010;21 Suppl 7:vii107-11.

26. Dolmans DE, Fukumura D, Jain RK. Photodynamic therapy for cancer. Nat Rev Cancer. 2003;3(5):380-7.

27. Banerjee SM, MacRobert AJ, Mosse CA, Periera B, Bown SG, Keshtgar MRS. Photodynamic therapy: Inception to application in breast cancer. Breast. 2017;31:105-13.

28. Azzouzi AR, Vincendeau S, Barret E, Cicco A, Kleinclauss F, van der Poel HG, et al. Padeliporfin vascular-targeted photodynamic therapy versus active surveillance in men with low-risk prostate cancer (CLIN1001 PCM301): an open-label, phase 3, randomised controlled trial. Lancet Oncol. 2017;18(2):181-91.

29. Mallidi S, Anbil S, Bulin AL, Obaid G, Ichikawa M, Hasan T. Beyond the Barriers of Light Penetration: Strategies, Perspectives and Possibilities for Photodynamic Therapy. Theranostics. 2016;6(13):2458-87.

30. Abrahamse H HM. New photosensitizers for photodynamic therapy. Biochem J 2016;473(4):347-64.

31. Agostinis P, Berg K, Cengel KA, Foster TH, Girotti AW, Gollnick SO, et al. Photodynamic therapy of cancer: an update. CA Cancer J Clin. 2011;61(4):250-81.

32. Hopper C. Photodynamic therapy: a clinical reality in the treatment of cancer. Lancet Oncol. 2000;1:212-9.

33. Nyst H, Tan, I., Stewart, F. and Balm, A. Is photodynamic therapy a good alternative to surgery and radiotherapy in the treatment of head and neck cancer? Photodiagnosis and Photodynamic Therapy. 2009;6(1):3-11.

34. Brown SB, Brown EA, Walker I. The present and future role of photodynamic therapy in cancer treatment. Lancet Oncol. 2004;5(8):497-508.

35. Misra R, Acharya S, Sahoo SK. Cancer nanotechnology: application of nanotechnology in cancer therapy. Drug Discov Today. 2010;15(19-20):842-50.

36. Acedo P, Stockert JC, Canete M, Villanueva A. Two combined photosensitizers: a goal for more effective photodynamic therapy of cancer. Cell Death Dis. 2014;5:e1122.

37. O'Connor AE, Gallagher WM, Byrne AT. Porphyrin and nonporphyrin photosensitizers in oncology: preclinical and clinical advances in photodynamic therapy. Photochem Photobiol. 2009;85(5):1053-74.

38. Slastnikova TA, Rosenkranz AA, Lupanova TN, Gulak PV, Gnuchev NV, Sobolev AS. Study of efficiency of the modular nanotransporter for targeted delivery of photosensitizers to melanoma cell nuclei in vivo. Dokl Biochem Biophys. 2012;446:235-7.

39. Kessel D. Apoptosis and associated phenomena as a determinants of the efficacy of photodynamic therapy. Photochem Photobiol Sci. 2015;14(8):1397-402.

40. Kessel D, Oleinick NL. Photodynamic therapy and cell death pathways. Methods Mol Biol. 2010;635:35-46.

41. Marchal S, Fadloun, A., Maugain, E., D'Hallewin, M., Guillemin, F. and Bezdetnaya, L. Necrotic and apoptotic features of cell death in response to Foscan® photosensitization of HT29 monolayer and multicell spheroids. Biochemical Pharmacology. 2005;69(8):1167-76.

42. Kessel D. Autophagic death probed by photodynamic therapy. Autophagy. 2015;11(10):1941-3.

43. Ion RM. ChemInform Abstract: Photodynamic Therapy (PDT): A Photochemical Concept with Medical Applications. ChemInform. 2008;39(49).

44. Juarranz A, Jaen P, Sanz-Rodriguez F, Cuevas J, Gonzalez S. Photodynamic therapy of cancer. Basic principles and applications. Clin Transl Oncol. 2008;10(3):148-54.

45. Hempstead J, Jones DP, Ziouche A, Cramer GM, Rizvi I, Arnason S, et al. Low-cost photodynamic therapy devices for global health settings: Characterization of battery-powered LED performance and smartphone imaging in 3D tumor models. Sci Rep. 2015;5:10093.

46. Kushibiki T, Tajiri T, Tomioka Y, Awazu K. Photodynamic therapy induces interleukin secretion from dendritic cells. Int J Clin Exp Med. 2010;3(2):110-4.

47. Ding H, Yu H, Dong Y, Tian R, Huang G, Boothman DA, et al. Photoactivation switch from type II to type I reactions by electron-rich micelles for improved photodynamic therapy of cancer cells under hypoxia. J Control Release. 2011;156(3):276-80.

48. Rajesh S, Koshi E, Philip K, Mohan A. Antimicrobial photodynamic therapy: An overview. J Indian Soc Periodontol. 2011;15(4):323-7.

49. Josefsen LB, Boyle RW. Photodynamic Therapy and the Development of Metal-Based Photosensitisers. Metal-Based Drugs. 2008;2008:1-23.

50. Triesscheijn M, Baas P, Schellens JH, Stewart FA. Photodynamic therapy in oncology. Oncologist. 2006;11(9):1034-44.

51. Oseroff A, Blumenson L, Wilson B, Mang T, Bellnier D, Parsons, J, et al. A dose ranging study of photodynamic therapy with porfimer sodium (Photofrin®) for treatment of basal cell carcinoma. Lasers Surg Med. 2006;38(5):417-26.

52. Usuda J, Kato H, Okunaka T, Furukawa K, Tsutsui H, Yamada K, et al. Photodynamic therapy (PDT) for lung cancers. J Thorac Oncol. 2006;1(5):489-93.

53. Vo-Dinh T. Biomedical photonics handbook n.d.

54. Allison RR, Downie GH, Cuenca R, Hu XH, Childs CJ, Sibata CH. Photosensitizers in clinical PDT. Photodiagnosis Photodyn Ther. 2004;1(1):27-42.

55. Tanaka M, Kataoka H, Mabuchi M, Sakuma S, Takahashi S, Tujii R, et al. Anticancer effects of novel photodynamic therapy with glycoconjugated chlorin for gastric and colon cancer. Anticancer Res. 2011;31(3):763-9.

56. Yamashita K, Hagiya Y, Nakajima M, Ishizuka M, Tanaka T, Ogura S. The effects of the heme precursor 5-aminolevulinic acid (ALA) on REV-ERBalpha activation. FEBS Open Bio. 2014;4:347-52.

57. Wachowska M, Muchowicz A, Firczuk M, Gabrysiak M, Winiarska M, Wańczyk M, et al. Aminolevulinic Acid (ALA) as a Prodrug in Photodynamic Therapy of Cancer. Molecules. 2011;16(12):4140-64.

58. Montcel B, Mahieu-Williame L, Armoiry X, Meyronet D, Guyotat J. Two-peaked 5-ALA-induced PpIX fluorescence emission spectrum distinguishes glioblastomas from low grade gliomas and infiltrative component of glioblastomas. Biomed Opt Express. 2013;4(4):548-58.

59. Yano T, Hatogai K, Morimoto H, Yoda Y, Kaneko K. Photodynamic therapy for esophageal cancer. Ann Transl Med. 2014;2(3):29.

60. Yang DF, Lee JW, Chen HM, Hsu YC. Topical methotrexate pretreatment enhances the therapeutic effect of topical 5-aminolevulinic acid-mediated photodynamic therapy on hamster buccal pouch precancers. J Formos Med Assoc. 2014;113(9):591-9.

61. Ye X, Yin H, Lu Y, Zhang H, Wang H. Evaluation of Hydrogel Suppositories for Delivery of 5-Aminolevulinic Acid and Hematoporphyrin Monomethyl Ether to Rectal Tumors. Molecules. 2016;21(10).

62. Wan MT, Lin JY. Current evidence and applications of photodynamic therapy in dermatology. Clin Cosmet Investig Dermatol. 2014;7:145-63.

63. Rodriguez L, de Bruijn HS, Di Venosa G, Mamone L, Robinson DJ, Juarranz A, et al. Porphyrin synthesis from aminolevulinic acid esters in endothelial cells and its role in photodynamic therapy. J Photochem Photobiol B. 2009;96(3):249-54.

64. De Visscher S, Dijkstra P, Tan I, Roodenburg J, Witjes M. mTHPC mediated photodynamic therapy (PDT) of squamous cell carcinoma in the head and neck: A systematic review. Oral Oncology. 2013;49(3):192-210.

65. Qumseya BJ, David W, Wolfsen HC. Photodynamic Therapy for Barrett's Esophagus and Esophageal Carcinoma. Clin Endosc. 2013;46(1):30-7.

66. Hopper C, Kubler A, Lewis H, Tan IB, Putnam G. mTHPC-mediated photodynamic therapy for early oral squamous cell carcinoma. Int J Cancer. 2004;111(1):138-46.

67. Meier D, Campanile C, Botter SM, Born W, Fuchs B. Cytotoxic efficacy of photodynamic therapy in osteosarcoma cells in vitro. J Vis Exp. 2014(85).

68. Jerjes W, Hamdoon Z, Hopper C. Photodynamic therapy in the management of potentially malignant and malignant oral disorders. Head Neck Oncol. 2012;4:16.

69. Olivo M, Bhuvaneswari R, Lucky S, Dendukuri N, Soo-Ping Thong P. Targeted Therapy of Cancer Using Photodynamic Therapy in Combination with Multi-faceted Anti-Tumor Modalities. Pharmaceuticals. 2010;3(5):1507-29.

70. Josefsen LB, Boyle RW. Photodynamic therapy: novel third-generation photosensitizers one step closer? Br J Pharmacol. 2008;154(1):1-3.

71. Huang Z. A review of progress in clinical photodynamic therapy. Technol Cancer Res Treat. 2005;4(3):283-93.

72. Yoon I, Li JZ, Shim YK. Advance in photosensitizers and light delivery for photodynamic therapy. Clin Endosc. 2013;46(1):7-23.

73. Ormond AB, Freeman HS. Dye Sensitizers for Photodynamic Therapy. Materials. 2013;6(3):817-40.

74. Bhatta AK, Keyal U, Wang XL. Photodynamic therapy for onychomycosis: A systematic review. Photodiagnosis Photodyn Ther. 2016;15:228-35.

75. Poriel C, Kessel D, Vicente MG. Stability of tin etiopurpurin. Photochem Photobiol. 2005;81(1):149-53.

76. Muehlmann LA, Ma BC, Longo JP, Almeida Santos Mde F, Azevedo RB. Aluminum-phthalocyanine chloride associated to poly(methyl vinyl ether-co-maleic anhydride) nanoparticles as a new third-generation photosensitizer for anticancer photodynamic therapy. Int J Nanomedicine. 2014;9:1199-213.

77. Chatterjee DK, Fong LS, Zhang Y. Nanoparticles in photodynamic therapy: an emerging paradigm. Adv Drug Deliv Rev. 2008;60(15):1627-37.

78. Bamrungsap S, Zhao Z, Chen T, Wang L, Li C, Fu T, et al. Nanotechnology in therapeutics: a focus on nanoparticles as a drug delivery system. Nanomedicine. 2012;7(8):1253-71.

79. Bazak R, Houri M, Achy SE, Hussein W, Refaat T. Passive targeting of nanoparticles to cancer: A comprehensive review of the literature. Mol Clin Oncol. 2014;2(6):904-8.

80. Mohammad-Hadi L, MacRobert AJ, Loizidou M, Yaghini E. Photodynamic therapy in 3D cancer models and the utilisation of nanodelivery systems. Nanoscale. 2018;10(4):1570-81.

81. Yin R, Wang M, Huang YY, Huang HC, Avci P, Chiang LY, et al. Photodynamic therapy with decacationic [60]fullerene monoadducts: effect of a light absorbing electron-donor antenna and micellar formulation. Nanomedicine. 2014;10(4):795-808.

82. Bakry R, Vallant RM, Najam-ul-Haq M, Rainer M, Szabo Z, Huck CW, et al. Medicinal applications of fullerenes. Int J Nanomedicine. 2007;2(4):639-49.

83. Mroz P, Tegos GP, Gali H, Wharton T, Sarna T, Hamblin MR. Photodynamic therapy with fullerenes. Photochem Photobiol Sci. 2007;6(11):1139-49.

84. Aqel A, Yusuf K, Al-Othman ZA, Badjah-Hadj-Ahmed AY, Alwarthan AA. Effect of multi-walled carbon nanotubes incorporation into benzyl methacrylate monolithic columns in capillary liquid chromatography. Analyst. 2012;137(18):4309-17.

85. Madani SY, Naderi N, Dissanayake O, Tan A, Seifalian AM. A new era of cancer treatment: carbon nanotubes as drug delivery tools. Int J Nanomedicine. 2011;6:2963-79.

86. Zhu W, Duan H, Bolton K. Diameter and chirality changes of single-walled carbon nanotubes during growth: an ab-initio study. J Nanosci Nanotechnol. 2009;9(2):1222-5.

87. Shao L, Gao Y, Yan F. Semiconductor quantum dots for biomedicial applications. Sensors (Basel). 2011;11(12):11736-51.

88. Juzenas P, Chen W, Sun YP, Coelho MA, Generalov R, Generalova N, et al. Quantum dots and nanoparticles for photodynamic and radiation therapies of cancer. Adv Drug Deliv Rev. 2008;60(15):1600-14.

89. Thomas A, Nair PV, Thomas KG. InP Quantum Dots: An Environmentally Friendly Material with Resonance Energy Transfer Requisites. J Phys Chem C. 2014;118(7):3838- 45.

90. Yaghini E, Turner HD, Le Marois AM, Suhling K, Naasani I, MacRobert AJ. In vivo biodistribution studies and ex vivo lymph node imaging using heavy metal-free quantum dots. Biomaterials. 2016;104:182-91.

91. Yaghini E, Seifalian AM, MacRobert AJ. Quantum dots and their potential biomedical applications in photosensitization for photodynamic therapy. Nanomedicine (Lond). 2009;4(3):353-63.

92. Wang C, Cheng L, Liu Z. Upconversion nanoparticles for potential cancer theranostics. Ther Deliv. 2011;2(10):1235-9.

93. Jin J, Xu Z, Zhang Y, Gu YJ, Lam MH, Wong WT. Upconversion nanoparticles conjugated with Gd(3+) -DOTA and RGD for targeted dual-modality imaging of brain tumor xenografts. Adv Healthc Mater. 2013;2(11):1501-12.

94. Ang LY, Lim ME, Ong LC, Zhang Y. Applications of upconversion nanoparticles in imaging, detection and therapy. Nanomedicine (Lond). 2011;6(7):1273-88.

95. Sibani SA, McCarron PA, Woolfson AD, Donnelly RF. Photosensitiser delivery for photodynamic therapy. Part 2: systemic carrier platforms. Expert Opin Drug Deliv. 2008;5(11):1241-54.

96. Firczuk M, Winiarska M, Szokalska A, Jodlowska M, Swiech M, Bojarczuk K, et al. Approaches to improve photodynamic therapy of cancer. Front Biosci (Landmark Ed). 2011;16:208-24.

97. Li L, Huh KM. Polymeric nanocarrier systems for photodynamic therapy. Biomater Res. 2014;18:19.

98. Paszko E, Ehrhardt C, Senge MO, Kelleher DP, Reynolds JV. Nanodrug applications in photodynamic therapy. Photodiagnosis Photodyn Ther. 2011;8(1):14-29.

99. Debele TA, Peng S, Tsai HC. Drug Carrier for Photodynamic Cancer Therapy. Int J Mol Sci. 2015;16(9):22094-136.

100. Wang F, Li C, Cheng J, Yuan Z. Recent Advances on Inorganic Nanoparticle-Based Cancer Therapeutic Agents. Int J Environ Res Public Health. 2016;13(12).

101. Zhang X. Gold Nanoparticles: Recent Advances in the Biomedical Applications. Cell Biochem Biophys. 2015;72(3):771-5.

102. Valentine RM, Wood K, Brown CT, Ibbotson SH, Moseley H. Monte Carlo simulations for optimal light delivery in photodynamic therapy of non-melanoma skin cancer. Phys Med Biol. 2012;57(20):6327-45.

103. Chester A, Martellucci S, Verga Scheggi A. Laser systems for photobiology and photomedicine. New York: Plenum Press. 2012.

104. Huang Z, Xu H, Meyers AD, Musani AI, Wang L, Tagg R, et al. Photodynamic therapy for treatment of solid tumors--potential and technical challenges. Technol Cancer Res Treat. 2008;7(4):309-20.

105. Porteous MS, Rowe DJ. Adjunctive Use of the Diode Laser in Non-Surgical Periodontal Therapy: Exploring the Controversy. Journal of Dental Hygiene. 2014;88(2):78-86.

106. Santosa V, Limantara L. PHOTODYNAMIC THERAPY: NEW LIGHT IN MEDICINE WORLD. Indo J Chem. 2008;8(2):279-91.

107. Hamblin MR, Mroz P. Advances in photodynamic therapy: Boston: Artech House; 2008.

108. Mallidi S, Mai Z, Rizvi I, Hempstead J, Arnason S, Celli J, et al. In vivo evaluation of battery-operated light-emitting diode-based photodynamic therapy efficacy using tumor volume and biomarker expression as endpoints. Journal of Biomedical Optics. 2015;20(4):048003.

109. Kinhikar R, Chaudhari S, Kadam S, Dhote D, Deshpande D. Dosimetric validation of new semiconductor diode dosimetry system for intensity modulated radiotherapy. J Cancer Res Ther. 2012;8(1):86-90.

110. Opel DR, Hagstrom E, Pace AK, Sisto K, Hirano-Ali SA, Desai S, et al. Light-emitting Diodes: A Brief Review and Clinical Experience. J Clin Aesthet Dermatol. 2015;8(6):36-44.

111. Parker S. The use of diffuse laser photonic energy and indocyanine green photosensitiser as an adjunct to periodontal therapy. BDJ. 2013;215(4):167-71.

112. Geddes C. Metal-enhanced fluorescence.1st ed: Hoboken, N.J: Wiley; 2010.

113. Barret E, Durand M. Technical aspects of focal therapy in localized prostate cancer. 1st ed.2015.

114. Shafirstein G, Battoo A, Harris K, Baumann H, Gollnick SO, Lindenmann J, et al. Photodynamic Therapy of Non-Small Cell Lung Cancer. Narrative Review and Future Directions. Ann Am Thorac Soc. 2016;13(2):265-75.

115. Simone CB 2nd, Cengel KA. Definitive surgery and intraoperative photodynamic therapy: a prospective study of local control and survival for patients with pleural dissemination of non-small cell lung cancer. Proc SPIE Int Soc Opt Eng. 2014;8931.

116. Oliveira J, Monteiro E, Santos J, Silva J D, Almeida L, Santos L L. A first in human study using photodynamic therapy with Redaporfin in advanced head and neck cancer. Journal of Clinical Oncology. 2017;35(15).

117. Zou ZY, Yuan CL, Huang H, Zhao B, Hu XL. [Influence of IL-2 on proliferation of cultured human pituitary adenoma cells and its mechanism]. Xi Bao Yu Fen Zi Mian Yi Xue Za Zhi. 2005;21(6):778-81.

118. Wilson JJ, Jones H, Burock M, Smith D, Fraker DL, Metz J, et al. Patterns of recurrence in patients treated with photodynamic therapy for intraperitoneal carcinomatosis and sarcomatosis. Int J Oncol. 2004;24(3):711-7.

119. Li X, Ferrel GL, Guerra MC, Hode T, Lunn JA, Adalsteinsson O, et al. Preliminary safety and efficacy results of laser immunotherapy for the treatment of metastatic breast cancer patients. Photochem Photobiol Sci. 2011;10(5):817-21.

120. Hahn SM, Fraker DL, Mick R, Metz J, Busch TM, Smith D, et al. A phase II trial of intraperitoneal photodynamic therapy for patients with peritoneal carcinomatosis and sarcomatosis. Clin Cancer Res. 2006;12(8):2517-25.

121. Banerjee SM, Malhotra A, El-Sheikh S, Tsukagoshi D, Tran-Dang M, Mosse A, Parker S, Davidson TI, Williams NR, Bown S, Keshtgar MR. Photodynamic therapy for the treatment of primary breast cancer: Preliminary results of a phase I/IIa clinical trial. Cancer Research. 2017;77(4).

122. Gottesman MM. Mechanisms of cancer drug resistance. Annu Rev Med. 2002;53:615-27.

123. Berg K, Folini M, Prasmickaite L, Selbo PK, Bonsted A, Engesaeter B Ø, et al. Photochemical internalization: a new tool for drug delivery. Curr Pharm Biotechnol. 2007;8(6):362-72.

124. Wang JT GF, Eggleston IM, Bown SG, MacRobert AJ. Photochemical internalisation of a macromolecular protein toxin using a cell penetrating peptide-photosensitiser conjugate. J Control Release. 2012;157(2):305-13.

125. Berg K, Weyergang A, Prasmickaite L, Bonsted A, Hogset A, Strand MT, et al. Photochemical internalization (PCI): a technology for drug delivery. Methods Mol Biol. 2010;635:133-45.

126. Martinez de Pinillos Bayona A, Moore CM, Loizidou M, MacRobert AJ, Woodhams JH. Enhancing the efficacy of cytotoxic agents for cancer therapy using photochemical internalisation. International Journal of Cancer. 2015;138(5):1049-57.

127. Weyergang A, Berstad ME, Bull-Hansen B, Olsen CE, Selbo PK, Berg K. Photochemical activation of drugs for the treatment of therapy-resistant cancers. Photochem Photobiol Sci. 2015;14(8):1465-75.

128. Fu A, Tang R, Hardie J, Farkas ME, Rotello VM. Promises and pitfalls of intracellular delivery of proteins. Bioconjug Chem. 2014;25(9):1602-8.

129. Mathews MS, Vo V, Shih EC, Zamora G, Sun CH, Madsen SJ, et al. Photochemical internalization-mediated delivery of chemotherapeutic agents in human breast tumor cell lines. J Environ Pathol Toxicol Oncol. 2012;31(1):49-59.

130. Yaghini E, Dondi R, Tewari KM, Loizidou M, Eggleston IM, MacRobert AJ. Endolysosomal targeting of a clinical chlorin photosensitiser for light-triggered delivery of nano-sized medicines. Sci Rep. 2017;7(1):6059.

131. Meng F, Cheng R, Deng C, Zhong Z. Intracellular drug release nanosystems. Materialstoday 2012;15(10):436-42.

132. Stahl P, Schwartz AL. Receptor-mediated endocytosis. J Clin Invest. 1986;77(3):657-62.

133. Salatin S, Yari Khosroushahi A. Overviews on the cellular uptake mechanism of polysaccharide colloidal nanoparticles. J Cell Mol Med. 2017;21(9):1668-86.

134. Berg K, Weyergang A, Vikdal M, Norum O J, Berstad M, Selbo P. Photochemical internalization (PCI), a technology for site-specific drug delivery. Recent advances. Photodiagnosis and Photodynamic Therapy. 2011;8(2):156.

135. Berg K, Moan J. Lysosomes as photochemical targets. International Journal of Cancer. 1994;59(6):814-22.

136. Prasmickaite L, Hogset A, Selbo PK, Engesæter BØ, Hellum M, Berg K. Photochemical disruption of endocytic vesicles before delivery of drugs: a new strategy for cancer therapy. Br J Cancer. 2002;86(4):652-7.

137. Martinez de Pinillos Bayonaa A, Woodhams JH, Pye H, Hamoudia RA, Moore CM, MacRobert AJ. Efficacy of photochemical internalisation using disulfonated chlorin and porphyrin photosensitisers: An in vitro study in 2D and 3D prostate cancer models. Cancer Letters. 2017;393:68-75.

138. Selbo PK, Weyergang A, Bonsted A, Bown SG, Berg K. Photochemical internalization of therapeutic macromolecular agents: a novel strategy to kill multidrug-resistant cancer cells. J Pharmacol Exp Ther. 2006;319(2):604-12.

139. Berg K, Dietze A, Kaalhus O, Hogset A. Site-specific drug delivery by photochemical internalization enhances the antitumor effect of bleomycin. Clin Cancer Res. 2005;11(23):8476-85.

140. Polito L, Bortolotti M, Mercatelli D, Battelli MG, Bolognesi A. Saporin-S6: a useful tool in cancer therapy. Toxins (Basel). 2013;5(10):1698-722.

141. Errico Provenzano A, Posteri R, Giansanti F, Angelucci F, Flavell SU, Flavell DJ, et al. Optimization of construct design and fermentation strategy for the production

of bioactive ATF-SAP, a saporin based anti-tumoral uPAR-targeted chimera. Microb Cell Fact. 2016;15(1):194.

142. Nicolay NH, Ruhle A, Perez RL, Trinh T, Sisombath S, Weber KJ, et al. Mesenchymal stem cells are sensitive to bleomycin treatment. Sci Rep. 2016;6:26645.

143. Rosenblum MG, Cheung LH, Liu Y, Marks J W. Design, Expression, Purification, and Characterization, in Vitro and in Vivo, of an Antimelanoma Single-chain Fv Antibody Fused to the Toxin Gelonin. Cancer Research. 2003;63(14).

144. Yuan X, Lin X, Manorek G, Howell SB. Challenges associated with the targeted delivery of gelonin to claudin-expressing cancer cells with the use of activatable cell penetrating peptides to enhance potency. BMC Cancer. 2011;11(1):61.

145. Lilletvedt M THH, Høgset A, Høgset A, Nardo L, Kristensen S. Physicochemical characterization of the photosensitizers TPCS 2aand TPPS2a 1. Spectroscopic evaluation of drug - Solvent interactions. Pharmazie. 2010;65(8):588-95.

146. Yacoub TJ, Reddy AS, Szleifer I. Structural effects and translocation of doxorubicin in a DPPC/Chol bilayer: the role of cholesterol. Biophys J. 2011;101(2):378-85.

147. Antoni D, Burckel H, Josset E, Noel G. Three-dimensional cell culture: a breakthrough in vivo. Int J Mol Sci. 2015;16(3):5517-27.

148. Chen J, Wang J, Zhang Y, Chen D, Yang C, Kai C, et al. Observation of ovarian cancer stem cell behavior and investigation of potential mechanisms of drug resistance in three-dimensional cell culture. J Biosci Bioeng. 2014;118(2):214-22.

149. Kucinska M, Murias M, Nowak-Sliwinska P. Beyond mouse cancer models: Three-dimensional human-relevant in vitro and non-mammalian in vivo models for photodynamic therapy. Mutat Res. 2017;773:242-62.

150. van Duinen V, Trietsch SJ, Joore J, Vulto P, Hankemeier T. Microfluidic 3D cell culture: from tools to tissue models. Curr Opin Biotechnol. 2015;35:118-26.

151. Huh D, Hamilton GA, Ingber DE. From 3D cell culture to organs-on-chips. Trends Cell Biol. 2011;21(12):745-54.

152. Shin CS, Kwak B, Han B, Park K. Development of an in vitro 3D tumor model to study therapeutic efficiency of an anticancer drug. Mol Pharm. 2013;10(6):2167-75.

153. Celli JP, Rizvi I, Blanden AR, Massodi I, Glidden MD, Pogue BW, et al. An imaging-based platform for high-content, quantitative evaluation of therapeutic response in 3D tumour models. Sci Rep. 2014;4:3751.

154. Gu L, Mooney DJ. Biomaterials and emerging anticancer therapeutics: engineering the microenvironment. Nat Rev Cancer. 2016;16(1):56-66.

155. Ricketts K, Cheema U, Nyga A, Castoldi A, Guazzoni C, Magdeldin T, et al. A 3D In Vitro Cancer Model as a Platform for Nanoparticle Uptake and Imaging Investigations. Small. 2014;10(19):3954-61.

156. Kimlin LC, Casagrande G, Virador VM. In vitro three-dimensional (3D) models in cancer research: an update. Mol Carcinog. 2013;52(3):167-82.

157. Weiswald LB, Bellet D, Dangles-Marie V. Spherical cancer models in tumor biology. Neoplasia. 2015;17(1):1-15.

158. Kutys ML, Doyle AD, Yamada KM. Regulation of cell adhesion and migration by cell-derived matrices. Exp Cell Res. 2013;319(16):2434-9.

159. Evans C. Three-dimensional in vitro cancer spheroid models for photodynamic therapy: strengths and opportunities. 2015.

160. Charoen K, Fallica B, Colson Y, Zaman M, Grinstaff M. Embedded multicellular spheroids as a biomimetic 3D cancer model for evaluating drug and drug-device combinations. Biomaterials. 2014;35(7):2264-71.

161. Till U, Gibot L, Vicendo P, Rols M, Gaucher M, Violleau F, Mingotaud A. Crosslinked polymeric self-assemblies as an efficient strategy for photodynamic therapy on a 3D cell culture. RSC Adv. 2016;6(74):69984-98.

162. Hinger D, Navarro F, Käch A, Thomann J, Mittler F, Couffin A, Maake C. (2016). Photoinduced effects of m-tetrahydroxyphenylchlorin loaded lipid nanoemulsions on multicellular tumor spheroids. Journal of Nanobiotechnology. 2016;14(1).

163. Mehta G, Hsiao A, Ingram M, Luker G, Takayama S. Opportunities and challenges for use of tumor spheroids as models to test drug delivery and efficacy. Journal of Controlled Release. 2012;164(2):192-204.

164. Herrmann D, Conway JR, Vennin C, Magenau A, Hughes WE, Morton JP, et al. Three-dimensional cancer models mimic cell-matrix interactions in the tumour microenvironment. Carcinogenesis. 2014;35(8):1671-9.

165. Fitzpatrick LE, McDevitt TC. Cell-derived matrices for tissue engineering and regenerative medicine applications. Biomater Sci. 2015;3(1):12-24.

166. Geraldo S, Simon A, Elkhatib N, Louvard D, Fetler L, Vignjevic D. Do cancer cells have distinct adhesions in 3D collagen matrices and in vivo? European Journal of Cell Biology. 2012;91(11-12):63-81.

167. Geckil H, Xu F, Zhang X, Moon S, Demirci U. Engineering hydrogels as extracellular matrix mimics. Nanomedicine. 2010;5(3):469-84.

168. Zhu J, Marchant RE. Design properties of hydrogel tissue-engineering scaffolds. Expert Rev Med Devices. 2011;8(5):607-26.

169. Nyga A, Cheema U, Loizidou M. 3D tumour models: novel in vitro approaches to cancer studies. J Cell Commun Signal. 2011;5(3):239-48.

170. Cheema U, Yang SY, Mudera V, Goldspink GG, Brown RA. 3-D in vitro model of early skeletal muscle development. Cell Motil Cytoskeleton. 2003;54(3):226-36.

171. Brown R, Wiseman M, Chuo C, Cheema U, Nazhat S. Ultrarapid Engineering of Biomimetic Materials and Tissues: Fabrication of Nano- and Microstructures by Plastic Compression. Advanced Functional Materials. 2005;15(11):1762-70.

172. Paszek MJ, Zahir N, Johnson KR, Lakins JN, Rozenberg GI, Gefen A, et al. Tensional homeostasis and the malignant phenotype. Cancer Cell. 2005;8(3):241-54.

173. López-Dávila V MT, Welch H, Dwek MV, Uchegbu I, Loizidou M. Efficacy of DOPE/DC-cholesterol liposomes and GCPQ micelles as AZD6244 nanocarriers in a 3D colorectal cancer in vitro model. nanomedicine. 2016;11(4):331-44.

174. Nyga A, Loizidou M, Emberton M, Cheema U. A novel tissue engineered three-dimensional in vitro colorectal cancer model. Acta Biomater. 2013;9(8):7917-26.

175. Asti A, Gioglio L. Natural and synthetic biodegradable polymers: different scaffolds for cell expansion and tissue formation. Int J Artif Organs. 2014;37(3):187-205.

176. Dhandayuthapani B, Yoshida Y, Maekawa T, Kumar D. Polymeric Scaffolds in Tissue Engineering Application: A Review. International Journal of Polymer Science. 2011;2011:1-19.

177. Perez-Castillejos R. Replication of the 3D architecture of tissues. Materials Today. Materials Today. 2010;13(1-2):32-41.

178. van Straten D, Mashayekhi V, de Bruijn HS, Oliveira S, Robinson DJ. Oncologic Photodynamic Therapy: Basic Principles, Current Clinical Status and Future Directions. Cancers (Basel). 2017;9(2).

179. Hung H, Klein O, Peterson S, Rokosh S, Osseiran S, Nowell N, Evans C. PLGA nanoparticle encapsulation reduces toxicity while retaining the therapeutic efficacy of EtNBS-PDT in vitro. Scientific Reports. 2016;6:33234.

180. Evans CL, Abu-Yousif AO, Park YJ, Klein OJ, Celli JP, Rizvi I, et al. Killing hypoxic cell populations in a 3D tumor model with EtNBS-PDT. PLoS One. 2011;6(8):e23434.

181. Rizvi I, Anbil S, Alagic N, Celli J, Zheng LZ, Palanisami A, et al. PDT dose parameters impact tumoricidal durability and cell death pathways in a 3D ovarian cancer model. Photochem Photobiol. 2013;89(4):942-52.

182. Chen YC, Lou X, Zhang Z, Ingram P, Yoon E. High-Throughput Cancer Cell Sphere Formation for Characterizing the Efficacy of Photo Dynamic Therapy in 3D Cell Cultures. Sci Rep. 2015;5:12175.

183. Rizvi I, Celli JP, Evans CL, Abu-Yousif AO, Muzikansky A, Pogue BW, et al. Synergistic enhancement of carboplatin efficacy with photodynamic therapy in a three-dimensional model for micrometastatic ovarian cancer. Cancer Res. 2010;70(22):9319-28.

184. Rowlands CJ, Wu J, Uzel S, G.M. Klein O, Evans C L, So PTC. 3D-resolved targeting of photodynamic therapy using temporal focusing. Laser Physics letters. 2015;11(11):doi: 10.1088/612-2011/11/11/115605.

185. Aggarwal N, Santiago AM, Kessel D, et al. Photodynamic therapy as an effective therapeutic approach in MAME models of inflammatory breast cancer. Breast Cancer Res Treat 2015;154(2):251-62.

186. O'Rourke C, Hopper C, MacRobert AJ, Phillips JB, Woodhams JH. Could clinical photochemical internalisation be optimised to avoid neuronal toxicity? Int J Pharm. 2017;528(1-2):133-43.

187. Wright KE, Liniker E, Loizidou M, Moore C, Macrobert AJ, Phillips JB. Peripheral neural cell sensitivity to mTHPC-mediated photodynamic therapy in a 3D in vitro model. Br J Cancer. 2009;101(4):658-65.

188. Anbil S, Rizvi I, Celli JP, Alagic N, Pogue BW, Hasan T. Impact of treatment response metrics on photodynamic therapy planning and outcomes in a three-dimensional model of ovarian cancer. J Biomed Opt. 2013;18(9):098004.

189. Huygens A, Huyghe D, Bormans G, Verbruggen A, Kamuhabwa AR, Roskams T, et al. Accumulation and photocytotoxicity of hypericin and analogs in two- and three-dimensional cultures of transitional cell carcinoma cells. Photochem Photobiol. 2003;78(6):607-14.

190. Huang H, Yu B, Zhang P, Huang J, Chen Y, Gasser G, Ji L, Chao H. Highly Charged Ruthenium(II) Polypyridyl Complexes as Lysosome-Localized Photosensitizers for Two-Photon Photodynamic Therapy. Angew Chem, Int Ed. 2015;54(47):14049– 52.

191. Liu J, Chen Y, Li G, Zhang P, Jin C, Zeng L, Ji L, Chao H. Ruthenium(II) polypyridyl complexes as mitochondria-targeted two-photon photodynamic anticancer agents. Biomaterials. 2015;56:140-53.

192. Qiu K, Wang J, Song C, Wang L, Zhu H, Huang H, et al. Crossfire for Two-Photon Photodynamic Therapy with Fluorinated Ruthenium (II) Photosensitizers. ACS Appl Mater Interfaces. 2017;9(22):18482-92.

193. Yang Y, Yang X, Zou J, Jia C, Hu Y, Du H, Wang H. Evaluation of photodynamic therapy efficiency using an in vitro three-dimensional microfluidic breast cancer tissue model. Lab Chip. 2015;15(3):735-44.

194. Zhang P, Huang H, Huang J, Chen H, Wang J, Qiu K, et al. Noncovalent Ruthenium(II) Complexes-Single-Walled Carbon Nanotube Composites for Bimodal Photothermal and Photodynamic Therapy with Near-Infrared Irradiation. ACS Appl Mater Interfaces. 2015;7(41):23278-90.

195. Liu J, Liu K, Feng L, Liu Z, Xu L. Comparison of nanomedicine-based chemotherapy, photodynamic therapy and photothermal therapy using reduced graphene oxide for the model system. Biomaterials Science 2017;5(2):331-40.

196. Gaio E, Scheglmann D, Reddi E, Moret F. Uptake and photo-toxicity of Foscan®, Foslip® and Fospeg® in multicellular tumor spheroids. Journal of Photochemistry and Photobiology B: Biology. 2016;161:244-52.

197. Lee J, Kim J, Jeong M, Lee H, Goh U, Kim H, et al. Liposome-based engineering of cells to package hydrophobic compounds in membrane vesicles for tumor penetration. Nano Lett. 2015;15(5):2938-44.

198. Xiao Z, Hansen CB, Allen TM, Miller GG, Moore RB. Distribution of photosensitizers in bladder cancer spheroids: implications for intravesical instillation of photosensitizers for photodynamic therapy of bladder cancer. J Pharm Pharm Sci. 2005;8(3):536-43.

199. Wang Y, Xie Y, Li J, Peng ZH, Sheinin Y, Zhou J, et al. Tumor-Penetrating Nanoparticles for Enhanced Anticancer Activity of Combined Photodynamic and Hypoxia-Activated Therapy. ACS Nano. 2017;11(2):2227-38.

200. Arentsen HC, Falke J, Hogset A, Oosterwijk E, Alfred Witjes J. The effect of photochemical internalization of bleomycin in the treatment of urothelial carcinoma of the bladder: an in vitro study. Urol Oncol. 2014;32(1):49 e1-6.

201. Sultan AA, Jerjes W, Berg K, Hogset A, Mosse CA, Hamoudi R, et al. Disulfonated tetraphenyl chlorin (TPCS2a)-induced photochemical internalisation of bleomycin in patients with solid malignancies: a phase 1, dose-escalation, first-in-man trial. Lancet Oncol. 2016;17(9):1217-29.

202. Weyergang A, Selbo PK, Berstad ME, Bostad M, Berg K. Photochemical internalization of tumor-targeted protein toxins. Lasers Surg Med. 2011;43(7):721-33.

203. Norum OJ, Gaustad J, Angell-Petersen E, Rofstad EK, Peng Q, Giercksky KE, Berg K. Photochemical internalization of bleomycin is supe-rior to photodynamic therapy due to the therapeutic effect in the tumorperiphery. Photochem Photobiol. 2009b;85:740-9.

204. Lilletvedt M, Tonnesen HH, Hogset A, Sande SA, Kristensen S. Evaluation of physicochemical properties and aggregation of the photosensitizers TPCS2a and TPPS2a in aqueous media. Pharmazie. 2011;66(5):325-33.

205. Bull-Hansen B, Berstad MB, Berg K, Cao Y, Skarpen E, Fremstedal AS, et al. Photochemical activation of MH3-B1/rGel: a HER2-targeted treatment approach for ovarian cancer. Oncotarget. 2015;6(14):12436-51.

206. Selbo PK, Weyergang A, Eng MS, Bostad M, Mælandsmo GM, Høgset A, Berg K. Strongly amphiphilic photosensitizers are not substrates of the cancer stem cell marker ABCG2 and provides specific and efficient light-triggered drug delivery of an EGFR-targeted cytotoxic drug. J Control Release. 2012;159(2):197-203.

207. Olsen CE, Weyergang A, Edwards VT, Berg K, Brech A, Weisheit S, Høgset A, Selbo PK. Development of resistance to photodynamic therapy (PDT) in human breast cancer cells is photosensitizer-dependent: Possible mechanisms and approaches for overcoming PDT-resistance. Biochem Pharmacol. 2017;144:63-77.

208. Spring BQ, Rizvi I, Xu N, Hasan T. The role of photodynamic therapy in overcoming cancer drug resistance. Photochem Photobiol Sci. 2015;14(8):1476-91.

209. Lou PJ, Lai PS, Shieh MJ, Macrobert AJ, Berg K, Bown SG. Reversal of doxorubicin resistance in breast cancer cells by photochemical internalization. Int J Cancer. 2006;119(11):2692-8.

210. Bostad M, Berg K, Høgset A, Skarpen E, Stenmark H, Selbo PK. Photochemical internalization (PCI) of immunotoxins targeting CD133 is specific and highly potent at femtomolar levels in cells with cancer stem cell properties. J Control Release. 2013;168(3):317-26.

211. Magdeldin T, Lopez-Davila V, Villemant C, Cameron G, Drake R, Cheema U, et al. The efficacy of cetuximab in a tissue-engineered three-dimensional in vitro model of colorectal cancer. J Tissue Eng. 2014;5:2041731414544183.

212. Magdeldin T, Lopez-Davila V, Pape J, Cameron GW, Emberton M, Loizidou M, et al. Engineering a vascularised 3D in vitro model of cancer progression. Sci Rep. 2017;7:44045.

213. Mathews MS, Blickenstaff JW, Shih EC, Zamora G, Vo V, Sun CH, et al. Photochemical internalization of bleomycin for glioma treatment. J Biomed Opt. 2012;17(5):058001.

214. Z Shen, Qin X, Yan M, Li R, Chen G, Zhang J, Chen W. Cancer-associated fibroblasts promote cancer cell growth through a miR-7-RASSF2-PAR-4 axis in the tumor microenvironment. Oncotarget. 2017;8(1).

215. Martinez de Pinillos Bayona A, Woodhams JH, Pye H, Hamoudi RA, Moore CM, MacRobert AJ. Efficacy of photochemical internalisation using disulfonated chlorin and porphyrin photosensitisers: An in vitro study in 2D and 3D prostate cancer models. cancer Lett. 2017;393:68-75.

216. Berg K, Madslien K, Bommer JC, Oftebro R, Winkelman JW, Moan J. Light induced relocalization of sulfonated meso-tetraphenylporphines in NHIK 3025 cells and effects of dose fractionation. Photochem Photobiol. 1991;53(2):203-10.

217. Fretz MM, Hogset A, Koning GA, Jiskoot W, Storm G. Cytosolic delivery of liposomally targeted proteins induced by photochemical internalization. Pharm Res. 2007;24(11):2040-7.

218. Khan S, Aspe JR, Asumen MG, Almaguel F, Odumosu O, Acevedo-Martinez S, De Leon M, Langridge WHR, Wall NR. Extracellular, cell-permeable survivin inhibits apoptosis while promoting proliferative and metastatic potential. British Journal of Cancer. 2009;100(7):1073–86.

219. Fingrut O, Flescher E. Plant stress hormones suppress the proliferation and induce apoptosis in human cancer cells. Leukemia. 2002;16(4):608-16.

220. Selbo PK, Rosenblum MG, Cheung LH, Zhang W, Berg K. Multi-modality therapeutics with potent anti-tumor effects: photochemical internalization enhances delivery of the fusion toxin scFvMEL/rGel. PLoS One. 2009;4(8):e6691.

221. Wang JT, Giuntini F, Eggleston IM, Bown SG, MacRobert AJ. Photochemical internalisation of a macromolecular protein toxin using a cell penetrating peptide-photosensitiser conjugate. Journal of Controlled Release. 2012;157(2):305-13.

222. Garaiova Z, Strand SP, Reitan NK, Lelu S, Storset SO, Berg K, et al. Cellular uptake of DNA-chitosan nanoparticles: the role of clathrin- and caveolae-mediated pathways. Int J Biol Macromol. 2012;51(5):1043-51.

223. Paullin T, Powell C, Menzie C, Hill R, Cheng F, Martyniuk CJ, et al. Spheroid growth in ovarian cancer alters transcriptome responses for stress pathways and epigenetic responses. PLoS One. 2017;12(8):e0182930.

224. Powell CD, Paullin TR, Aoisa C, Menzie CJ, Ubaldini A, Westerheide SD. The Heat Shock Transcription Factor HSF1 Induces Ovarian Cancer Epithelial-Mesenchymal Transition in a 3D Spheroid Growth Model. PLoS One. 2016;11(12):e0168389.

225. Lee JM, Mhawech-Fauceglia P, Lee N, Parsanian LC, Lin YG, Gayther SA, et al. A three-dimensional microenvironment alters protein expression and chemosensitivity of epithelial ovarian cancer cells in vitro. Lab Invest. 2013;93(5):528-42.

226. Hung HI, Klein OJ, Peterson SW, Rokosh SR, Osseiran S, Nowell NH, Evans CL. PLGA nanoparticle encapsulation reduces toxicity while retaining the therapeutic efficacy of EtNBS-PDT in vitro. Sci Rep. 2016;6: 33234.

227. Gaio E, Scheglmann D, Reddi E, Moret F. Uptake and photo-toxicity of Foscan®, Foslip® and Fospeg® in multicellular tumor spheroids. J Photochem Photobiol B. 2016;161:244- 52.

228. Cheema U, Rong Z, Kirresh O, Macrobert AJ, Vadgama P, Brown RA. Oxygen diffusion through collagen scaffolds at defined densities: implications for cell survival in tissue models. J Tissue Eng Regen Med. 2012;6(1):77-84.

229. Virumbrales-Munoz M, Ayuso JM, Olave M, Monge R, de Miguel D, Martinez-Lostao L, et al. Multiwell capillarity-based microfluidic device for the study of 3D tumour tissue-2D endothelium interactions and drug screening in co-culture models. Sci Rep. 2017;7(1):11998.

230. Alemany-Ribes M, Garcia-Diaz M, Busom M, Nonell S, Semino CE. Toward a 3D cellular model for studying in vitro the outcome of photodynamic treatments: accounting for the effects of tissue complexity. Tissue Eng Part A. 2013;19(15-16):1665-74.

231. Cheema U, Brown RA, Alp B, MacRobert AJ. Spatially defined oxygen gradients and vascular endothelial growth factor expression in an engineered 3D cell model. Cell Mol Life Sci. 2008;65(1):177-86.

232. Price M, Heilbrun L, Kessel D. Effects of the oxygenation level on formation of different reactive oxygen species during photodynamic therapy. Photochem Photobiol. 2013;89(3):683-6.

233. Moan J, Sommer S. Oxygen dependence of the photosensitizing effect of hematoporphyrin derivative in NHIK 3025 cells. Cancer Res. 1985;45(4):1608-10.

234. Ferguson DCJ, Smerdon GR, Harries LW, Dodd NJF, Murphy MP, Curnow A, et al. Altered cellular redox homeostasis and redox responses under standard oxygen cell culture conditions versus physioxia. Free Radic Biol Med. 2018;126:322-33.

235. Oliveira CS, Turchiello R, Kowaltowski AJ, Indig GL, Baptista MS. Major determinants of photoinduced cell death: Subcellular localization versus photosensitization efficiency. Free Radic Biol Med. 2011;51(4):824-33.

236. Jeon KW. International Review of Cell and Molecular Biology, 2012.

237. Chiaviello A, Postiglione I, Palumbo G. Targets and mechanisms of photodynamic therapy in lung cancer cells: a brief overview. Cancers (Basel). 2011;3(1):1014-41.

238. Benov L. Photodynamic therapy: current status and future directions. Med Princ Pract. 2015;24 Suppl 1:14-28.

239. Almeida RD, Manadas BJ, Carvalho AP, Duarte CB. Intracellular signaling mechanisms in photodynamic therapy. Biochim Biophys Acta. 2004;1704:1704:59–86.

240. Sikriwal D, Ghosh P, Batra JK. Ribosome inactivating protein saporin induces apoptosis through mitochondrial cascade, independent of translation inhibition. The International Journal of Biochemistry & Cell Biology. 2008;40(12):2880-8.

241. Coupienne I, Fettweis G, Rubio N, Agostinis P, Piette J. 5-ALA-PDT induces RIP3-dependent necrosis in glioblastoma. Photochem Photobiol Sci. 2011;10(12):1868-78.

242. Jaganathan H, Gage J, Leonard F, Srinivasan S, Souza GR, Dave B, Godin B. Three-Dimensional In Vitro Co-Culture Model of Breast Tumor using Magnetic Levitation. Sci Rep. 2014;4:doi:10.1038/srep06468.

243. Amann A, Zwierzina M, Koeck S, Gamerith G, Pechriggl E, Huber JM, et al. Development of a 3D angiogenesis model to study tumour - endothelial cell interactions and the effects of anti-angiogenic drugs. Sci Rep. 2017;7(1):2963.

244. Hasan I, Anbil S, Celli JP, Alagic N, Massodi I, Hasan T. Modeling stromal determinants of 3D tumor growth to inform PDT-mediated combination treatments. SPIE. 2013;8568:doi: 10.1117/12.2010678.

245. Schumann C, Taratula O, Khalimonchuk O, Palmer AL, Cronk LM, Jones CV, et al. ROS-induced nanotherapeutic approach for ovarian cancer treatment based on the combinatorial effect of photodynamic therapy and DJ-1 gene suppression. Nanomedicine. 2015;11(8):1961-70.

246. Curnow A, Haller JC, Bown SG. Oxygen monitoring during 5-aminolaevulinic acid induced photodynamic therapy in normal rat colon. Comparison of continuous and fractionated light regimes. J Photochem Photobiol B. 2000;58(2-3):149-55.

247. Zhang J, Liang YC, Lin X, Zhu X, Yan L, Li S, et al. Self-Monitoring and Self-Delivery of Photosensitizer-Doped Nanoparticles for Highly Effective Combination Cancer Therapy in Vitro and in Vivo. ACS Nano. 2015;9(10):9741-56.